AN ABSTRACT OF THE THESIS OF

Michael J. Love for the degree of Doctor of Philosophy in Physics presented on September 3, 1993.

Title: Computer Simulation of Phase Transitions in Zirconia

Redacted for privacy

Abstract approved: _____ H.J.F.Jansen

Experimental data on the structural phase changes in zirconia are summarized. The computational techniques of molecular dynamics are reviewed and equations of motion are formulated which allow the study of phase changes as a function of temperature and pressure.

The molecular dynamics program **NPT** which was written for this purpose is described. This program performs numerical integration of the classical equations of motions in atomistic simulations which allow a varying cell size and shape. The simulations produce time averages which are related to thermodynamic ensemble averages.

Routines used to calculated the interatomic forces are implemented for potentials which vary as the inverse power of the separation distance between atoms. Calculation of Coulomb forces is done with the Ewald method and with a multipole method. The two methods are shown to be analytically equivalent and the precision and speed of the two routines are compared.

Results generated by the program **NPT** are presented for energy minimization of crystal structures and for dynamic simulations.

A number of different minimum-energy structures for soft-sphere potentials are found. Simulations are performed for several soft-sphere structures and dynamic properties are established. Structural phases changes are observed in two cases.

A potential derived from ab initio calculations for monoclinic zirconia is tested.

Computer Simulation of
Phase Transitions in Zirconia

by

Michael J. Love

A THESIS

submitted to

Oregon State University

in partial fulfillment of
the requirements for the
degree of

Doctor of Philosophy

Completed September 3, 1993

Commencement June 1994

APPROVED:

Redacted for privacy

Professor of Physics in charge of major

Redacted for privacy

Head of Department of Physics

Redacted for privacy

Dean of Graduate School

Date thesis is presented September 3, 1993

Typed by Michael J. Love

Table of Contents

1 Introduction 1

2 Structure of Zirconia Crystals 3
- 2-1 General 3
- 2-2 Monoclinic and Tetragonal I Phases 3
- 2-3 Tetragonal I and Cubic Phases 4
- 2-4 Tetragonal II (Orthorhombic I) Phase 4
- 2-5 Orthorhombic II Phase 5
- 2-6 Tetragonal III Phase 6
- 2-7 Summary 6

3 Computer Simulations of Atomic Systems 8
- 3-1 Atomic Models for Phase Transitions 8
- 3-2 Periodic Boundary Conditions 9
- 3-3 Statistical Ensembles 10
- 3-4 Molecular Dynamics at Constant Temperature 11
- 3-5 Molecular Dynamics at Constant Pressure 14
- 3-6 NPT Molecular Dynamics 16

4 Interatomic Force Calculations 23
- 4-1 Electrostatic Forces 23
- 4-2 The Ewald Method 25
- 4-3 Planewise Summation Methods 27
- 4-4 Numerical Accuracy of Algorithms 34

5 Program Description 42
- 5-1 General Description 42
- 5-2 Program Structure 46
- 5-3 Integration Subroutines 48
- 5-4 Energy and Force Calculations 49
- 5-5 Hardware 50

6 Results and Summary 52
6-1 Effective Potentials for Zirconia 52
6-2 Soft-sphere Ionic Crystals 53
6-3 Simulation of a Monoclinic Crystal 70
6-4 Discussion 79
6-5 Summary 82

Bibliography 84

Appendix A: NPT dynamics 88
A-1 Derivation of the Equations of Motion 88
A-2 Equivalence to NPT Ensemble 90

Appendix B: Stress Tensor Calculations 93

Appendix C: The Ewald Method of Lattice Summations 97
C-1 Derivation of the Total Energy Sum 97
C-2 Ewald Force Summations 102

Appendix D: Multipole Summations 104
D-1 Derivation of the Multipole Expansion 104
D-2 Coulomb Energy and Force Summations 105
D-3 Planewise Summations 110

Appendix E: Planewise Sums for r^{-4} and r^{-6} 113

Appendix F: Error Approximations for Numerical Calculations 118
F-1 Short-range Energy 118
F-2 Ewald Energy Sums 119
F-3 Multipole Expansions 120
F-4 Planewise Summation 123

Appendix G: Short-Range Energy and Forces 124

LIST OF FIGURES

Figure		Page
1.	Phase diagram for zirconia	7
2.	Distribution functions for particle momenta before (a) and after (b) resetting virtual momenta to zero	21
3.	Two equivalent unit cells for tetragonal ZrO_2	24
4.	Addition of compensating charges which result in zero dipole moments for the unit cells of Figure 3	31
5.	Computer run times for various numbers of atoms per unit cell	41
6.	Typical input file for program **NPT**	43
7.	Main flow diagram for program **NPT**	45
8.	Charge density contours for monoclinic zirconia: (a) O_I atoms; (b) Zr atoms; (c) O_{II} atoms; (d) location of sections in crystal	54
9.	Crystal structure and pair correlations for $\beta \geq 0.8$.	56
10.	Crystal structure and pair correlations for $\beta = 0.78$.	57
11.	Crystal structure and pair correlations for $\beta = 0.73$.	58
12.	Crystal structure and pair correlations for $\beta = 0.48$.	59
13.	Crystal structure and pair correlations for $\beta = 0.414$.	60
14.	β =0.52, T=1000K, P=0: (a) momentum distribution; (b) oxygen-oxygen pair correlations	65
15.	β =0.52, T=1000K, P=0: (a) volume; (b) unit cell lattice vector components	66
16.	β =0.52, T=1000K, P=0: averages of dynamic variables	67
17.	Low-temperature pair correlations for $\beta = 0.48$ at (a) zero external pressure and (b) 30 GPa external pressure	68
18.	β =0.52 at 2000K and zero pressure: (a) volume; (b) unit cell lattice vector components	69
19.	Pair correlations for the static monoclinic crystal: (a) Zr-Zr; (b) Zr-O	72
20.	Momentum distributions for the monoclinic crystal: (a) 300K; (b) 2000K	73

21. Total energies for the monoclinic crystal: (a) kinetic energy; (b) potential energy 74

22. Lattice parameters for the monoclinic crystal: (a) volume; (b) unit cell lattice vector components 75

23 Virtual variables for the monoclinic crystal: (a) virtual time variable s; (b) associated momentum p_s 76

24. Pair correlations for the monoclinic crystal at 300K: (a) Zr-Zr; (b) Zr-O 77

25. Pair correlations for the monoclinic crystal at 2000K: (a) Zr-Zr; (b) Zr-O 78

LIST OF TABLES

Table		Page
1.	Lattice parameters for zirconia phases	6
2.	Truncation errors for short-range energy sums	34
3.	Truncation errors for Ewald energy sums	35
4.	Truncation errors for radial short-range energy sums	36
5.	Truncation errors for the multipole expansion	37
6.	Truncation errors for the planewise summation: $\frac{c_z}{a} = 1$	39
7.	Truncation errors for the planewise summation: $\frac{c_z}{a} \neq 1$	40
8.	Parameters for error tolerances for multipole and Ewald methods	41
9.	Crystal structures for soft-sphere potentials	62
10.	Dynamic simulation results for soft-sphere potentials	64
11.	NPT simulation results for zirconia potential	79

Computer Simulation of

Phase Transitions in Zirconia

Chapter 1

Introduction

Zirconia (ZrO_2, zirconium oxide) is a ceramic material which occurs naturally as the mineral baddeleyite. Commercially available as both a natural and manufactured product, major applications include uses in alumina-zirconia abrasives, refractory products, ceramic coloring agents, and PZT piezoelectric materials[1].

The high melting temperature and corrosion resistance of zirconia are attractive properties for general use as a ceramic material, but applications have been limited until recently by the unusual temperature dependence of the crystal structure. At room temperature, zirconia crystals are monoclinic. Between approximately 1000C and 2300C the structure is tetragonal, and between 2300C and the melting temperature of 2750C zirconia has a cubic structure. During cooling from the tetragonal to monoclinic phase, an abrupt volume expansion occurs and the resultant stresses reduce any large crystals to a granular or powder form.

Recent interest in zirconia has been stimulated by the discovery of additives which stabilize zirconia crystals in their high-temperature structures and an economical process for producing large crystals[2]. Stabilized zirconia is an excellent ionic conductor of oxygen, and new applications include uses in oxygen sensors[3], high temperature fuel cells[4] and hydrogen production by water dissociation[5]. Cubic zirconia is also popular as a synthetic gemstone.

Another recent application of zirconia takes advantage of the tetragonal-monoclinic transformation by using zirconia microcrystals as a toughening agent for other ceramic materials. It has been found that the microcrystals transform during microcracking in such a way as to inhibit further crack propagation; this phenomenon has led to recent investigations into the 'transformation toughening' properties of zirconia[6,7].

Interest in these and other properties of zirconia has resulted in a number of experimental and theoretical studies regarding the nature of the crystalline structures and the mechanisms for the phase transitions. The structures of the low pressure phases are well defined and a number of high pressure phases have been described. Theoretical work includes band structure

calculations[8,9,10] for static crystal structures as well as thermodynamic[11] and crystallographic analyses[12,13] of the phase transitions.

Practical studies of structural phase transitions at finite pressure and temperature are now possible with dynamical simulations at the atomic scale. An appropriate set of interatomic potentials is determined and nonlinear equations of motion are used to generate thermodynamic averages which correspond to given external conditions. The subject of this thesis is the development and implementation of appropriate methods and computational techniques for the study of the phase transitions in zirconia by dynamical simulation with simple interatomic forces.

Chapter 2

Structure of Zirconia Crystals

2-1 General

Studies of zirconia at high temperatures and at high pressures have yielded at least six distinct crystal structures. The monoclinic, tetragonal I, and cubic structures found at low pressure are well defined. In addition, high pressure phases form at approximately 4,15 and 32 GPa. The most probable structures at these pressures appear to be tetragonal II (orthorhombic I), orthorhombic II, and tetragonal III, respectively; the two high pressure tetragonal phases are distinct from each other and from the low temperature tetragonal I phase. The existence of these high pressure phases is well documented but the exact atomic structure has not yet been well established. A summary of experimental evidence for the various phases is given in the following sections.

While the variety of phases may make the formulation of a single set of interatomic forces insufficient for a detailed reproduction of the entire phase diagram, it may be hoped that a relatively simple set of forces will be capable of producing the general features of the experimental structure and phase transitions and that further refinement of the potential will lead to more realistic models.

The detail given here is intended as a guide for measuring the the success of the simple forces and computational methods used in this study to simulate atomic zirconia.

2-2 Monoclinic and Tetragonal I Phases

The crystal structure of monoclinic zirconia was established in 1959 by McCullough and Trueblood[14], based on projection data from natural crystal fragments which did not appear to contain the twinning common to natural crystals. Their proposed structure has since been confirmed and refined through x-ray single crystal diffraction[15], x-ray powder diffraction[16], and neutron diffraction[17] experiments. The space group is $P2_1/c$ with twelve atoms in the unit cell. The zirconia atoms are coordinated by seven oxygen atoms. The oxygen atoms form approximate planes. The atoms in these planes are coordinated by either three or four zirconium atoms, with

neighboring planes containing oxygen atoms with different coordination numbers.

Phase equilibrium studies by Baun[18] found that the tetragonal phase first appears on heating around 1000C, and the last trace of the monoclinic phase disappears around 1180C. On cooling the monoclinic phase appears around 970C with the last of the tetragonal phase disappearing at 750C. Later studies confirmed the hysteresis in the phase transition and a monoclinic-tetragonal transition temperature of 1170C, while the reverse transformation was found to be 850C to 975C depending on crystallite size[19]. Smaller crystallites have lower transition temperatures, and in the extreme case (crystallites less than 300 Angstroms) the tetragonal form may be retained at room temperature[20]. The volume increase from the tetragonal to the monoclinic structure is about 3%.

2-3 Tetragonal I and Cubic Phases

The tetragonal and cubic high temperature phases were described by Teufer[21] and Smith and Kline[22] from high temperature x-ray diffraction data and were later refined by Adelbert and Traverse[23] in neutron diffraction experiments over the temperature range of 1295C to 2410C in neutral and reducing atmospheres. The cubic phase has the fluorite structure with space group Fm3m and three atoms in the unit cell. The tetragonal structure is closely related to the cubic structure but the oxygen atoms are displaced from their fluorite positions and the unit cell shows an expansion along the axis parallel to these displacements. The space group of the tetragonal form is $P4_2/nmc$ with six atoms per unit cell. Neither high temperature crystal structure is retained at room temperature after quenching.

The tetragonal-cubic transition was found to be 2300C in a neutral atmosphere and 2050C in a reducing atmosphere. A mixed phase containing both tetragonal and cubic crystal structures was found in samples of oxygen-deficient zirconia. Similar results for the presence of a mixed phase in nonstoichiometric crystals have also been obtained by metallographic and high temperature x-ray experiments[24].

The melting temperature of pure ZrO_2 has been measured at 2710 ± 15C[25], with a reduction in melting temperature and a mixed liquid-cubic phase for oxygen-deficient samples[24].

2-4 Tetragonal II (Orthorhombic I) Phase

In situ measurements of zirconia at high pressures were obtained by Block et al.[26] in 1985

using optical polarizing microscopy of single crystals and x-ray powder diffraction studies. They found a phase transition to a tetragonal structure which begins at 3.8GPa and is complete at 8.3GPa. The volume change for the monoclinic to tetragonal II transition (mc-ttrII) was measured at -3.8%, comparable to the mc-ttrI volume change of -3.0%. At room temperature the phase boundary is given as 3.3GPa for increasing pressure and 2.8GPa for decreasing pressure. The hysteresis of 0.5GPa is relatively constant up to the mc-ttrI-ttrII triple point, which occurs around 600C with increasing pressure and 535C with decreasing pressure.

In a later report[27], the same authors found that annealing of the high pressure phase at 350C and 8GPa results in the retention of the phase after quenching. In this paper the most probable structure is revised to an orthorhombic cell (orthoI) with space group Pbcm, in agreement with x-ray measurements of Kudoh et al[28,29]. Both the ttrII and orthoI unit cells contain twelve atoms and lattice parameters for the two cells are very similar.

In an article published almost simultaneously with Block's later report, Alzyab et al.[30] used DAC techniques coupled with high pressure Raman scattering and found a gradual phase transition beginning at 3.6GPa and complete at 4.1GPa. Their data led them to conclude that this high pressure phase is tetragonal, probably with D_{2d} or C_{4v} symmetry.

Further studies may resolve the question of whether the symmetry of the high pressure phase found above 4GPa should be properly considered as tetragonal or orthorhombic. Despite this uncertainty, the transition temperatures, hysteresis range and approximate unit cell dimension are all fairly well established.

2-5 Orthorhombic II Phase

A phase transition from the tetragonal II structure to a higher pressure orthorhombic phase was also found by Block et al[26]. The structure of this phase is that of cotunnite ($PbCl_2$), with twelve atoms per unit cell. The coordination number of the zirconium atoms in this phase is nine, in contrast to coordination numbers of eight for the tetragonal II and seven for the monoclinic phases. The orthorhombic (orthoII) phase appeared at 16.6GPa and the last of the ttrII phase disappeared at 22.0GPa. The phase transition was found to be accompanied by a volume change of -6.8%. The orthoII structure was not found to be quenchable in this study. A later report by Ohtaka and Kume[31] found that the orthoII phase can be retained at low pressures if samples were sufficiently annealed; this data was used to construct an orthoI(ttrII)- orthoII phase boundary at approximately 20GPa.

2-6 Tetragonal III Phase

A recent study by Arashi et al.[32] used x-ray diffraction and micro-Raman scattering experiments to investigate the phases of zirconia up to 60GPa. They found evidence of a transformation from the orthoII phase to a tetragonal phase (ttrIII) at pressures over 35GPa and concluded that the most probable symmetry for this new phase is $P4/m_1,P4_2/n$, P4/mmm, or P4/mbm. This phase is distinguished from that found earlier by Alzyab et al. The volume change for this transition is -3.8%, making ttrIII the densest of the zirconia polymorphs. The proposed symmetry groups suggest that the coordination number of zirconium atoms in this phase is eight.

2-7 Summary

Lattice parameters and volumes for the various phases are given in Table 1. A partial phase diagram is shown in Figure 1.

structure (*units*)	*a* (Å)	*b* (Å)	*c* (Å)	*β* (*deg.*)	*volume* (Å^3)	*temp.* (°*C*)	*press.* (*GPa*)
monoclinic[17]	5.151	5.212	5.317	99.2	140.9	20	
tetragonal I[23]	5.144		5.269		139.4	1160	
cubic[23]	5.269				146.3	2410	
tetragonal II[26]	5.009		5.237		131.4		8.3
orthorhombic I[29]	5.036	5.255	5.086		134.6	600	6.0
orthorhombic II[26]	3.29	5.62	6.34		117.2		21.6
tetragonal III[32]	4.52		5.01		102.4		55

Table 1: Lattice parameters for zirconia phases.

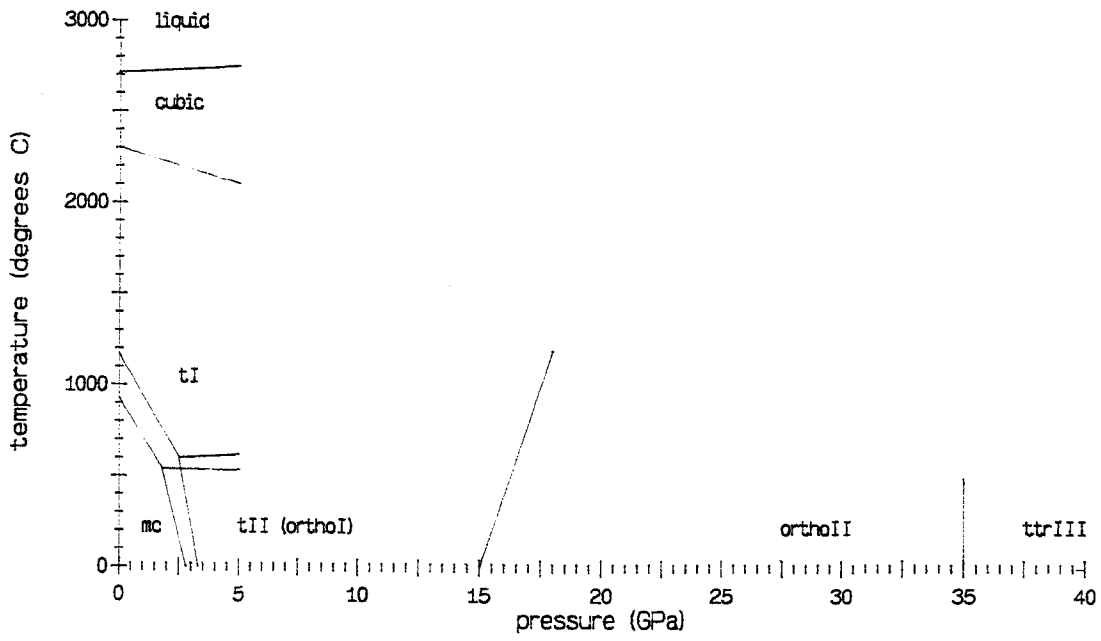

Figure 1: Phase diagram for zirconia. Data is from references 19, 25, 26, and 31-33.

Chapter 3

Computer Simulations of Atomic Systems

3-1 Atomic Models for Phase Transitions

Structural phases are described by the relative positions of the atomic nuclei for the various species of atoms within a material. Since the forces which determine the atomic positions are quantum mechanical in nature, an accurate description of atomic motion could in principle be formulated on the basis of the time evolution of the combined nuclear and electronic state vector. In practice, such a description is impractical because of the computational burden involved; from a theoretical viewpoint, this method is excessively complicated. Since the properties under study are characterized by a relatively small number of physical parameters, the most useful atomic models contain a similarly small number of parameters. While approximations and methods have been developed towards this end, the construction of a realistic model for the study of the properties of materials is generally limited by the number of particles in the system of interest, the computer resources available, and the efficiency of the numerical calculations.

Dynamical properties present a particular challenge for atomic models, and a number of approximations are in general use for the study of atomic motion. The most common of these is the adiabatic or Born-Oppenheimer approximation. The electrons are expected to reach an equilibrium state on a time scale that is relatively short compared to that of the nuclear motion, and in the adiabatic approximation the electrons are taken to be in the ground state at all times. This allows a separation of the nuclear and electronic wave functions. The electronic ground state is calculated by considering the nuclei as static point charges and the nuclear forces are calculated from the electronic state through the Hellmann-Feynman theorem. As a result, the forces on the nuclei are determined by the nuclear positions and models may be constructed which make no direct reference to the electronic wave functions. This simplification is generally considered to be justified in structural models although it does not allow for the possibility of electron-phonon interactions or forces which are fundamentally quantum mechanical in nature, such as the Van der Waals interaction.

In many cases an analytic potential for the atomic nuclei is formulated by adopting a physically reasonable form and fitting parameters to experimental data or static quantum calculations performed for nuclear positions near an equilibrium configuration. Other methods have been

developed which require more or less empirical or fitted data. Examples are the techniques of Carr and Parrinello[34], which minimize a set of electronic wave functions concurrently with the evolution of the nuclear positions, and the embedded atom method of Daw and Baskes[35], which uses density functional theory to generate forces from the overlap of fixed atomic charge densities. Intermediate approaches have also been implemented; an example is the Gordon-Kim model[36], in which the overlap of electronic charge densities is used only to determine short range pairwise forces between atoms.

The choice of method for generating realistic interatomic forces is made by considering the material under study and the computational burden involved. Ionic and dielectric materials are subject to long range forces, and the accurate calculation of these forces may preclude the choice of any but the simplest of short range forces. In materials with strong covalent bonding, pairwise forces may be insufficient to reproduce the experimental structure and three-body potentials are utilized. Realistic results for systems with defects have also been found to require many-body potentials such as those of the embedded atom method or the classical potentials of Finnis and Sinclair[37].

Zirconia shows a mixture of ionic and covalent character[9], and is commonly considered to contain Zr^{4+} and O^{2-} atoms. While this is an oversimplification, it is apparent from band structure and atomic charge density calculations[38] that zirconia is at least partially ionic in character. This observation will be taken as a starting point for the development of a classical potential for this system.

3-2 Periodic Boundary Conditions

The bulk properties of a material may be found by cluster calculations, in which the properties are computed for larger and larger systems until numerical convergence is obtained. Alternatively, a bulk material may be divided into a large number of identical computational cells, each cell containing the same number and type of atoms. With the assumption of periodic boundary conditions, the configuration and momenta of the atoms within each cell are identical to those of the corresponding atoms in every other cell, and the number of independent atoms is reduced to the number found in a single cell. By taking the number of cells to be infinite, the motion of the independent atoms is made to simulate a system which has no surface. This is expected to give realistic results for numbers of atoms which are small compared to those in cluster calculations.

Since the motion of equivalent atoms in each cell is assumed to be the same, the choice

of the particular unit cell should be immaterial provided that the cell contains exactly one of each of the independent atoms. This implies that a cell may be equally well described by any of several sets of unit cell edge vectors and that the choice of the origin for the unit cell or the replacement of any single atom by an equivalent atom in an adjacent computational cell should not affect the equations of motion.

If consistency with periodic boundary conditions is required, this places some constraint on the form of the potentials which may be used. In summations of potential terms from an infinite lattice, the sum must be absolutely convergent in order to obtain unambiguous results. The effect of this constraint on the Coulomb potential is discussed at length in the following chapter.

In some cases, the use of periodic boundary conditions may affect the atomic forces even though the equations of motion are invariant with regard to the choice of computational cell. As an example, total angular momentum is not generally conserved in periodic systems. The rate of change of angular momentum for a system of particles within a cell depends on the orientation of the particles relative to the cell, since the separations between atoms in adjacent cells depends on the cell orientation. Such effects may be difficult or impossible to eliminate, and interpretation of the results of simulations using periodic boundary conditions must take such effects into account.

3-3 Statistical Ensembles

The determination of macroscopic properties from interatomic potentials is made through the application of statistical thermodynamics. Once a classical (or quantum mechanical) Hamiltonian is obtained, the ensemble averages may by determined for systems in the presence of external constraints such as constant temperature, pressure, or volume. There are currently two techniques in common use: the Monte Carlo method[39], in which atomic coordinates and momenta are generated randomly and averages are weighted according to the appropriate thermodynamic distribution function; and molecular dynamics (MD), which follows the motion of the individual atoms by numerical integration.

Time averages in molecular dynamics are equated to ensemble averages through the ergodic theorem. This theorem relies upon the assumption that the points in phase space sampled by the system as it evolves in time are representative of the entire phase space available to the system. In many cases this assumption is unjustified, and molecular dynamics simulations cannot be considered to be equivalent to the associated ensemble. While Monte Carlo methods do not have this shortcoming, they are somewhat less intuitive for systems with continuous variables and are

less applicable to systems which are not in equilibrium. The importance of such considerations to the phase transitions in zirconia is not entirely clear, although features such as the hysteresis in the monoclinic-tetragonal transformation suggest that non-equilibrium dynamics may be involved. For these reasons, the method of molecular dynamics has been utilized in this study.

A number of developments have been made in the theory of molecular dynamics in recent years. In the original formulation, a fixed number of particles is confined to a fixed volume and the Lagrangian or Hamiltonian equations of motion conserve the energy of the system. This formulation is interpreted as a microcanonical ensemble. In view of the equivalence of different types of ensembles in the thermodynamic limit, this single ensemble is sufficient to generate any of the macroscopic properties of the material. Even so, the constraint of constant volume and the difficulty of establishing a given internal temperature make this ensemble very inconvenient for the study of phase transitions which occur as a result of changing temperature and pressure.

A method of generating averages corresponding to ensembles other than the microcanonical was introduced in 1980 by Anderson[40]. The introduction of an extended Hamiltonian which includes kinetic and potential terms due to a 'virtual' volume variable makes it possible to produce time averages which correspond to isobaric-isoenthalpic ensemble averages while preserving the deterministic and conservative properties of the usual microcanonical formulation. Extensions of this technique by Parrinello and Rahman[41] to unit cells with varying shape allow the simulation of systems which undergo structural transitions at fixed pressure. Introduction of a 'virtual' time variable by Nosé[42] provided a method for generating canonical averages at a given temperature. These are the basic techniques implemented here in order to investigate the phase diagram of zirconia. Since their advent, these 'new' molecular dynamics methods have been successfully applied to the study of phase transitions in a variety of materials, including Ag_2S[43] and AgI[44], two materials which display structurally dependent ionic conductivity similar to that found in zirconia.

3-4 Molecular Dynamics at Constant Temperature

The Hamiltonian for N particles in a microcanonical ensemble is generally of the form

$$H = \sum_{i=1}^{N} \frac{p_i^2}{2m_i} + \Phi(\vec{r}_i)$$

where the potential Φ is a function of the coordinates of the particles only. In order to obtain equations of motion which give time averages equal to the canonical ensemble averages for this Hamiltonian, Nosé postulated the Lagrangian[42]

$$L = \sum_{i=1}^{N} \frac{m_i}{2} s^2 \dot{\vec{r}}^2 - \Phi(\vec{r}_i) + \frac{Q}{2}\dot{s}^2 - (f+1)kT_{eq}ln(s)$$

with the corresponding 'extended' Hamiltonian given by

$$\vec{p}_{i(v)} = \frac{\partial L}{\partial \dot{\vec{r}}_i} = m_i s^2 \dot{\vec{r}}_i$$

$$p_s = -\frac{\partial L}{\partial \dot{s}} = Q\dot{s}$$

$$H = \sum_{i=1}^{N} \frac{p_{i(v)}^2}{2m_i s^2} + \Phi(\vec{r}_i) + \frac{p_s^2}{Q} + (f+1)kT_{eq}ln(s)$$

In these equations, s is a 'virtual' variable, and p_s is the momentum conjugate to s. The subscript 'v' (for 'virtual') is added to the particle momenta to distinguish them from the 'real' momenta in the original Hamiltonian; the canonical momenta averages are obtained from the virtual equations of motion if p_i is identified as $s^{-1}p_{i(v)}$. With the time scaled according to $dt^{(r)} = s^{-1}dt$, the appropriate value for the constant $(f+1)$ is 3N, the number of degrees of freedom for the original system. The equations of motion for the original variables are then (dropping the superscript from the time differentials)

$$\frac{d\vec{q}_i}{dt} = \frac{\vec{p}_i}{m_i}$$

$$\frac{d\vec{p}_i}{dt} = \frac{\partial \Phi}{\partial \vec{q}_i} - \frac{p_s}{Q}\vec{p}_i$$

$$\frac{ds}{dt} = \frac{sp_s}{Q}$$

$$\frac{dp_s}{dt} = \sum_{i=1}^{N} \frac{p_i^2}{2m_i} - 3NkT_{eq}$$

The virtual variables and the extended Hamiltonian alter the equations of motion for the momenta by the addition of a frictional term. The kinetic energy of the system is driven towards T_{eq} through the coupling between the real and virtual momenta.

The time averages of functions of $\vec{p}_i$ and $\vec{r}_i$ are proved by Nosé to be equal in the ergodic limit to the canonical ensemble averages. This is done by calculating the partition function and ensemble averages for the extended system. Hoover[45] has since shown that the canonical distribution is a stationary solution of the equation governing conservation of probability in the extended system. This implies that a canonical distribution will be maintained by the particles in such a system. The two derivations are similar in content, both showing that in at least some sense Nosé's equations of motion are consistent with a canonical ensemble.

Nosé's proof of the equality of time averages and canonical ensemble averages is particularly interesting because it is exact not only in the thermodynamic limit but also for small numbers of particles. This has resulted in numerical and analytic studies specifically concerned with the application of Nosé's equation to small systems.

In applications to very simple systems, H.J.F. Jansen[46] has demonstrated that the behavior of free particles is unphysical, and the behavior of harmonic oscillators is dependent on the initial conditions and the value of the virtual mass Q. For small Q or initial conditions far from equilibrium the averages will not be those of a canonical distribution and the motion of the particles may include accelerations which are not only unphysical but also numerically unstable. In general, Nosé's equations cannot be considered to model a classical heat bath, and in particular this method is not applicable to calculations of phonon energies.

Hoover and others[45,47,48] have investigated the behavior of the one-dimensional harmonic oscillator for various initial conditions and virtual masses. For conditions which produce chaotic motion an approximately canonical distribution is obtained, while other starting conditions produce marginal or completely unphysical motion.

These results suggest that the ergodic theorem is not well satisfied for systems with small numbers of particles. Larger systems generally exhibit a correspondly greater amount of disordered behavior, and the chaotic conditions required to produce a canonical distribution are more easily met. Still, instabilities may be introduced if the equilibrium temperature is reset in order to simulate a rise or fall in the temperature of the system.

In the past few years different sets of equations of motion have been found which also give canonical averages in the ergodic limit. Jellinek[49] in particular has shown how to generate many different dynamics which are consistent with the canonical distribution, along with the suggestion that the averages obtained for a particular case may be tested by applying a different dynamics to the same system and comparing the results. Bulgac and Kusnezov[50] argue that Nosé's formulation does not decouple the coordinate and momentum distribution functions, and propose an extended system with an additional virtual variable used to scale the coordinates. Their method is shown to result in distribution functions for the one-dimensional harmonic oscillator which are much closer to the canonical distributions than those obtained with Nosé's formulation.

The progress in obtaining more reliable equations of motion is encouraging, but at present these new methods are still largely untested. Nosé's method, despite its shortcomings, is still useful for the simulation of systems at a given equilibrium temperature. The average of the kinetic energy in a system will be driven toward the set temperature regardless of the initial conditions;

whether this results in a system with canonical distribution functions must be determined for each particular case.

3-5 Molecular Dynamics at Constant Pressure

Anderson[40] introduced an extended Hamiltonian which allows the volume of a molecular dynamics unit cell to vary isotropically in response to a given pressure, and showed that the ensemble averages obtained with this Hamiltonian are equal (to order 1/N) to the averages for an isobaric-isoenthalpic (NPH) ensemble with the same external pressure. Parrinello and Rahman[41] generalized Anderson's Hamiltonian to obtain equations of motion which allow the shape of the unit cell as well as the volume to vary in response to a given hydrostatic pressure. The Lagrangian proposed for this purpose by Parrinello and Rahman is

$$L = \sum_{i=1}^{N} \frac{m_i}{2} \dot{\vec{q}}_i^T h^T h \dot{\vec{q}}_i - \Phi(\vec{r}) + \frac{W}{2} Tr(\dot{h}^T \dot{h}) - P_{ext} det(h)$$

In this equation the components of the unit cell vectors $\vec{a}$,$\vec{b}$, and $\vec{c}$ are column vectors comprising the 3x3 matrix h, h^T is the transpose of h and the determinant of h is the volume of the unit cell. The components of h are treated as virtual variables along with the vectors $\vec{q}_i$. The relationships between the real and virtual variables are

$$\vec{r}_i = h\vec{q}_i = \begin{pmatrix} a_x & b_x & c_x \\ a_y & b_y & c_y \\ a_z & b_z & c_z \end{pmatrix} \begin{pmatrix} \xi_i \\ \eta_i \\ \zeta_i \end{pmatrix}$$

$$\vec{p}_i = m_i h \dot{\vec{q}}_i$$

The components of the vector $\vec{q}_i$ describe the position of the i^{th} particle within the unit cell. ξ_i,η_i,and ζ_i are the displacements of this particle along the vectors $\vec{a}$,$\vec{b}$,and $\vec{c}$, respectively. If the center of the unit cell is taken as the origin, the position of any particle within the unit cell will be described by a vector $\vec{q}_i$ with component values between 0.5 and -0.5.

The correspondence between the real and virtual momenta is determined by applying the ergodic theorem to the Hamiltonian expressed in 'virtual' variables and identifying the resulting ensemble average as an isobaric-isoenthalpic ensemble average for a classical Hamiltonian expressed in 'real' variables. It may also be noted that the direct substitution $\vec{p}_i = m_i \dot{\vec{r}}_i$ would be inconsistent with periodic boundary conditions, since the momenta defined in this manner would not necessarily be equal for equivalent atoms in different unit cells.

When periodic boundary conditions are imposed, the potential is generally a function of the unit cell dimensions as well as the particle coordinates. In this case the equations of motion may be written

$$\dot{\vec{r}}_i = \frac{\vec{p}_i}{m_i} + \dot{h}h^{-1}\vec{r}_i$$

$$\dot{\vec{p}}_i = -\frac{\partial\Phi(\vec{r},h)}{\partial\vec{r}_i} - h^{T-1}\dot{h}^T\vec{p}_i \equiv \vec{f}_i - h^{T-1}\dot{h}^T\vec{p}_i$$

$$\dot{h} = \frac{p_h}{W}$$

$$\begin{aligned} \dot{p_h} &= \left\{\sum_{i=1}^{N}\frac{1}{m_i}\vec{p}_i\vec{p}_i^T + \sum_{i=1}^{N}\vec{f}_i\vec{r}_i^T - \mathcal{P}_{ex}det(h) + f_h h^T\right\}h^{T-1} \\ &\equiv \{\mathcal{P} - \mathcal{P}_{ex}\}\,det(h)h^{T-1} \end{aligned}$$

$$\mathcal{P}_{ex} \equiv \begin{pmatrix} P_{ex} & 0 & 0 \\ 0 & P_{ex} & 0 \\ 0 & 0 & P_{ex} \end{pmatrix}$$

$$(f_h)_{\alpha\beta} \equiv -\frac{\partial\Phi(\vec{r},h)}{\partial h_{\alpha\beta}}$$

The equations for $\vec{r}_i$ and $\vec{p}_i$ are equivalent to those derived previously by Hoover et.al.[51] for the study of externally driven nonequilibrium phenomena. In addition, the unit cell matrix h is driven by the difference between the external stress tensor $\mathcal{P}_{ex}$ and the microscopic stress tensor $\mathcal{P}$.

Ray and Rahman[52] show that these equations of motion generate a thermodynamically consistent isoenthalpic-isobaric (NPH) ensemble. They also show that the physical stress tensor $\mathcal{P}_{ex}$ necessary to hold the unit cell matrix h constant in a microcanonical EhN ensemble with fixed unit cell dimensions is equal to the average of the microscopic stress tensor $\mathcal{P}$. The 'h' in the EhN ensemble denotes a constant unit cell matrix h; in the more usual EVN microcanonical ensemble, the volume is held constant and the unit cell is generally presumed to be cubic.

The equilibrium condition for the unit cell dimensions when the components of h are allowed to vary is

$$\langle W\dot{p}_h\rangle = 0 = \langle(\mathcal{P} - \mathcal{P}_{ex})det(h)h^{T-1}\rangle \equiv \langle(\mathcal{P} - \mathcal{P}_{ex})A\rangle$$

or

$$\langle\mathcal{P}A\rangle = \mathcal{P}_{ex}\langle A\rangle$$

In these equations, brackets denote a time average and A is the area tensor. If h is well defined at equilibrium, then this equilibrium condition is the same as the relation between internal

and external stress tensors in the fixed-cell EhN ensemble. This equivalence provides a simple method for verifying the cell dimensions obtained with the NPH ensemble and a given external pressure. If the cell dimensions are fixed at their average values, then a simulation in the EhN ensemble at the same temperature should result in components of the microscopic stress tensor which are equal to the corresponding components of the given external pressure tensor used in the NPH simulation.

Suggested modifications to the Parrinello-Rahman equations have mainly focused on the form of the kinetic energy term for the virtual variables:

$$K_{v(PR)} = \frac{1}{2} W Tr(\dot{h}^T \dot{h})$$

As pointed out by Ray[53], this expression leads to equations of motion which do not reduce to those of Anderson's model for a cubic molecular dynamics cell and a single virtual volume variable. A virtual kinetic energy expression which does agree in this case is given by

$$K_{v(R)} = \frac{1}{2} c Tr(\dot{h}^T h h^T \dot{h}^T h \dot{h})$$

Cleveland[54] shows that $K_{v(PR)}$ is not invariant with respect to replacement of one set of unit cell vectors with another equivalent set of vectors. A virtual kinetic energy term which does have the required invariance as well as reducing to Anderson's model in the isotropic limit is given as

$$K_{v(C)} = \frac{1}{2} w (det(h))^2 Tr(\dot{h} h^{-1} h^{T-1} \dot{h}^T)$$

If either $K_{v(R)}$ or $K_{v(C)}$ is used instead of $K_{v(PR)}$ as the virtual kinetic energy term in the Parrinello-Rahman Lagrangian, the equations of motion for $\ddot{\vec{r}}_i$ and $\dot{\vec{p}}_i$ are left unchanged, while the expressions for $\dot{p}_h$ and $\dot{h}$ include a number of new terms which are functions of h and p_h only.

3-6 NPT Molecular Dynamics

The following Lagrangian has been implemented for the study of pressure and temperature induced phase transitions in zirconia:

$$\begin{aligned} L &= \sum_{i=1}^{N} m_i s^2 \dot{\vec{q}}_i^T h^T h \dot{\vec{q}}_i - \Phi(h\vec{q}, h) \\ &\quad + \frac{Q}{2}\dot{s}^2 - 3N k_B T_{ex} ln(s) + \frac{W}{2} Tr(\dot{h}^T \dot{h}) - P_{ex} det(h) \end{aligned}$$

The relations between the real and virtual variables and the equations of motion are

$$\vec{r}_i = h\vec{q}_i \equiv \begin{pmatrix} a_x & b_x & c_x \\ 0 & b_y & c_y \\ 0 & 0 & c_z \end{pmatrix} \begin{pmatrix} \xi \\ \eta \\ \zeta \end{pmatrix}$$

$$\vec{p}_i = sm_i h\dot{\vec{q}}_i$$

$$\dot{\vec{r}}_i = \frac{\vec{p}_i}{m_i} + \frac{s}{W} p_h h^{-1} \vec{r}_i$$

$$\begin{aligned} \dot{\vec{p}}_i &= -\frac{\partial \Phi(\vec{r}, h)}{\partial \vec{r}_i} - \frac{p_s}{Q}\vec{p}_i - \frac{s}{W} h^{T-1} p_h^T \vec{p}_i \\ &\equiv \vec{f}_i - \frac{p_s}{Q}\vec{p}_i - \frac{s}{W} h^{T-1} p_h^T \vec{p}_i \end{aligned}$$

$$\dot{s} = \frac{s}{Q} p_s$$

$$\dot{p}_s = \sum_{i=1}^{N} \frac{p_i^2}{m_i} - 3Nk_B T_{ex}$$

$$\dot{h} = \frac{s}{W} p_h$$

$$\begin{aligned} \dot{p}_h &= s\left[\sum_{i=1}^{N} \left(\frac{1}{m_i}\vec{p}_i \vec{p}_i^T + \vec{f}_i \vec{r}_i^T\right) - \frac{\partial \Phi(\vec{r}, h)}{\partial h} h^T - \mathcal{P}_{ex} det(h)\right] h^{T-1} \\ &\equiv s\left[\mathcal{P} - \mathcal{P}_{ex}\right] A \end{aligned}$$

The time average of any function of $\vec{p}_i$ and $\vec{r}_i$ is equal, in the ergodic limit, to the isobaric-isothermal (NPT) ensemble average for a system described by the Hamiltonian

$$H = \sum_{i=1}^{N} \frac{p_i^2}{m_i} + \Phi(\vec{r}, h).$$

A proof of this equivalence and the derivation of the equations of motions are given in Appendix A.

Similar Lagrangians for the simulation of NPT dynamics have been formulated by Nosé[55] for the case of isotropic volume changes and by Ferrario and Ryckaert[56] for rigid molecules. These formulations vary most noticeably in the manner in which the rotation of the computational cell

is suppressed. If the Lagrangian of Parrinello and Rahman is used in simulations, it is possible for the cell to rotate as a whole. There is no physical significance to this rotation, and it may be reduced or eliminated by introducing constraints which reduce the number of independent variables in the matrix h from nine to six. Nosé accomplished this by symmetrizing h with a coordinate rotation at the beginning of the simulation; the cell was seen to remain approximately symmetrical and the cell rotation was small compared to that found with h unsymmetrized. Ferrario and Ryckaert proposed a simpler scheme, in which the cell vector $\vec{a}$ is fixed along the x-axis and $\vec{b}$ is constrained to lie in the x-y plane. This procedure offers some computational advantages due to the reduced number of variables in the force equations, and this is the method used in implementing the Lagrangian presented above.

The validity of either procedure for suppressing rotation is easily tested, since the average values of h may be used to simulate an NhT ensemble and the internal pressure tensor computed in this ensemble may be compared directly to the fixed external pressure set in the NPT simulation. The relation between internal NhT and external NPT pressures will also be affected by the choice of the form of the kinetic energy term in the Lagrangian. If good agreement is obtained, it may be concluded that the particular formulation used is consistent with NPT ensemble dynamics. With this in mind, the methods which are the simplest to implement have been chosen. The kinetic energy term is that of Parrinello and Rahman, and in the matrix h the elements a_y,a_z, and b_z are set to zero.

In the expressions for the components of the microscopic stress tensor $\mathcal{P}$, the term $\frac{\partial\Phi(\vec{r},h)}{\partial h}$ contains partial derivatives of the potential with respect to each of the nine components of h. However, if a_y, a_z, and b_z are set to zero, the potential is no longer a function of these variables, and partial derivatives cannot be evaluated with respect to these variables. By utilizing the symmetry of the stress tensor, the terms in question can be eliminated. The components of $\mathcal{P}$ are then

$$
\begin{aligned}
\mathcal{P}_{xx}det(h) &= \sum_{i=1}^{N}\frac{p_{ix}^2}{m_i}+\sum_{i=1}^{N}f_{ix}x_i-\frac{\partial\Phi(\vec{r},h)}{\partial a_x}a_x-\frac{\partial\Phi(\vec{r},h)}{\partial b_x}b_x-\frac{\partial\Phi(\vec{r},h)}{\partial c_x}c_x \\
\mathcal{P}_{yy}det(h) &= \sum_{i=1}^{N}\frac{p_{iy}^2}{m_i}+\sum_{i=1}^{N}f_{iy}y_i-\frac{\partial\Phi(\vec{r},h)}{\partial b_y}b_y-\frac{\partial\Phi(\vec{r},h)}{\partial c_y}c_y \\
\mathcal{P}_{zz}det(h) &= \sum_{i=1}^{N}\frac{p_{iz}^2}{m_i}+\sum_{i=1}^{N}f_{iz}z_i-\frac{\partial\Phi(\vec{r},h)}{\partial c_z}c_z \\
\mathcal{P}_{xy}det(h) &= \sum_{i=1}^{N}\frac{p_{ix}p_{iy}}{m_i}+\sum_{i=1}^{N}f_{ix}y_i-\frac{\partial\Phi(\vec{r},h)}{\partial b_x}b_y-\frac{\partial\Phi(\vec{r},h)}{\partial c_x}c_y \\
&= \mathcal{P}_{yx}det(h)
\end{aligned}
$$

$$\begin{aligned}
\mathcal{P}_{xz}det(h) &= \sum_{i=1}^{N} \frac{p_{ix}p_{iz}}{m_i} + \sum_{i=1}^{N} f_{ix}z_i - \frac{\partial \Phi(\vec{r},h)}{\partial c_x} c_z \\
&= \mathcal{P}_{zx}det(h) \\
\mathcal{P}_{yz}det(h) &= \sum_{i=1}^{N} \frac{p_{iy}p_{iz}}{m_i} + \sum_{i=1}^{N} f_{iy}z_i - \frac{\partial \Phi(\vec{r},h)}{\partial c_y} c_z \\
&= \mathcal{P}_{zy}det(h)
\end{aligned}$$

A general expression for the rate of change of the total angular momentum of the particles can also be derived once $\mathcal{P}$ is shown to be symmetric. This expression for the torque is:

$$\begin{aligned}
\vec{N} &= \sum_{i=i}^{N} \vec{r}_i \times \vec{f}_i \\
&= \vec{a} \times \frac{\partial \Phi(\vec{r},h)}{\partial \vec{a}} + \vec{b} \times \frac{\partial \Phi(\vec{r},h)}{\partial \vec{b}} + \vec{c} \times \frac{\partial \Phi(\vec{r},h)}{\partial \vec{c}}
\end{aligned}$$

Derivations for expressions involving the microscopic stress tensor are given in Appendix B.

As a check on the validity of the proposed Lagrangian, and as a first approximation to a model potential for zirconia, simulations were run for four zirconium and eight oxygen atoms interacting through a Born-Landé type potential:

$$\Phi(\vec{r},h) = \frac{1}{2} \sum_{\alpha\beta\gamma} \sum_{i,j=1}^{N} {}' \left\{ \frac{Z_i Z_j e^2}{\mid \vec{r}_i - \vec{R}_{\alpha\beta\gamma} - \vec{r}_j \mid} + \frac{C}{\mid \vec{r}_i - \vec{R}_{\alpha\beta\gamma} - \vec{r}_j \mid^{10}} \right\} - \Phi_{surf}$$

In this expression $\vec{R}_{\alpha\beta\gamma} \equiv \alpha\vec{a}+\beta\vec{b}+\gamma\vec{c}$; α, β, and γ are integers running from $+\infty$ to $-\infty$; the prime on the last summation indicates omission of the terms for which $i = j$ and $\alpha = \beta = \gamma = 0$; and Φ_{surf} is a correction to the Coulomb potential necessary for convergence of the lattice sum. This last term is included implicitly if the Ewald summation method is used to calculate the Coulomb forces. The constant C was set to obtain an equilibrium volume approximately equal to that of monoclinic zirconia at low temperatures. Details regarding the calculation of the lattice sums and the methods used in the simulations are given in later chapters; the results given here are presented simply to evaluate the equivalence of the calculated time averages and the associated NPT ensemble averages.

This system was brought to equilibrium at 300K and zero pressure. The pressure was then raised to 0.1, 1 and 10 GPa, with the temperature held constant at 300K. With the pressure held at 10 GPa, the temperature was raised to 1000K and then to 5000K in 1000K increments. Finally, the temperature and pressure were reduced directly to the starting conditions of 300K and zero pressure.

With the exception of the final run, the results found were in good agreement with expected results. The cell vectors described a cubic shape in the starting configuration and this shape was retained throughout the simulation to an accuracy of a few tenths of a percent, again with the exception of the final run. In the following discussion, the results for all of the runs except the last are summarized, and the last run is then considered separately.

With increasing pressure, the volume decreased from 143.5 to 140.9 $Å^3$. As the temperature increased the cell expanded more or less linearly to a maximum volume of 158.9 $Å^3$ at 5000K. The diagonal elements of the internal pressure tensor were within two or three percent of the set external pressure for temperatures below 3000K and a set external pressure of 10 GPa; with lower pressures and higher temperatures the fluctuations were relatively large and the figures were not quite as consistent. The off-diagonal elements were less than one percent of the external pressure at high pressure and low temperature, and the general behavior with other conditions was similar to that of the diagonal elements.

The average kinetic energy gave an internal 'temperature' which agreed with the set external temperature to an accuracy of one percent or better throughout the simulation. The momentum distribution was compared to an ideal Maxwell-Boltzmann distribution for each set of external parameters. Agreement was generally good, but some variations were noted. In cases of obvious deviations from the ideal distribution, the virtual momenta were set to zero and the simulation was restarted; this resulted in some improvement in the distribution. Examples of distributions before and after resetting the virtual momenta are shown in Figure 2.

At 1000K and 10 GPa, the components of the cell vectors were replaced with their average values and held constant during the following run. The average value of each diagonal internal pressure element was found to be within one percent of the value of the external pressure used to establish the average cell dimensions. The averages of each of the off-diagonal elements remained at less than one percent of the diagonal value.

In the final run, the system exhibited extremely nonphysical behavior. While the real momenta were quickly reduced to zero, the velocities remained high, and the kinetic energies of the virtual cell variables increased by several orders of magnitude. The cell itself expanded so quickly that it would be fair to say that it exploded. Since numerical accuracy was completely lost in this run, it is difficult to draw any real conclusions from this data except to note that in this case the simulation failed. This failure during rapid changes in external temperature is consistent with results previously obtained for very small systems[46].

Provided that changes in temperature are introduced gradually, the equations of motion appear to provide a reasonable simulation of an NPT ensemble. The agreement between the pres-

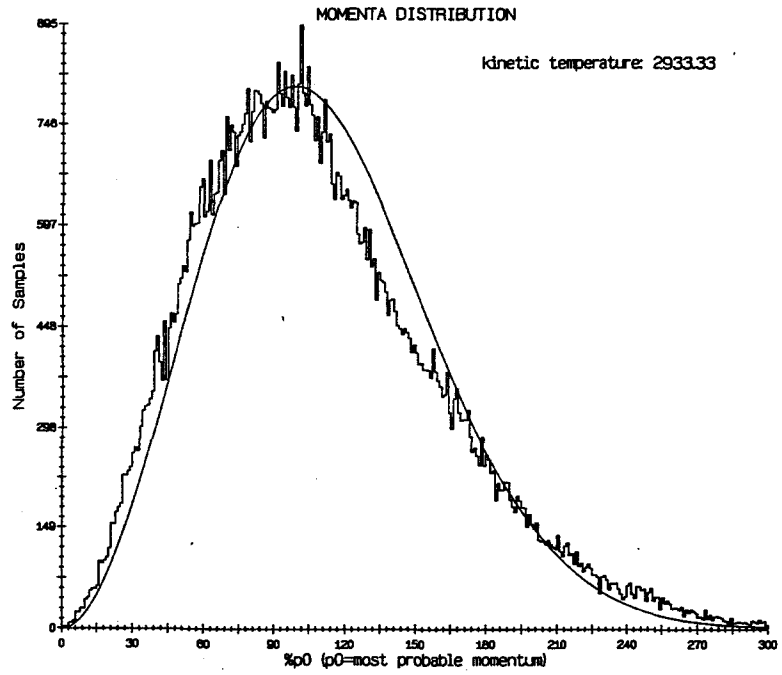

(a)

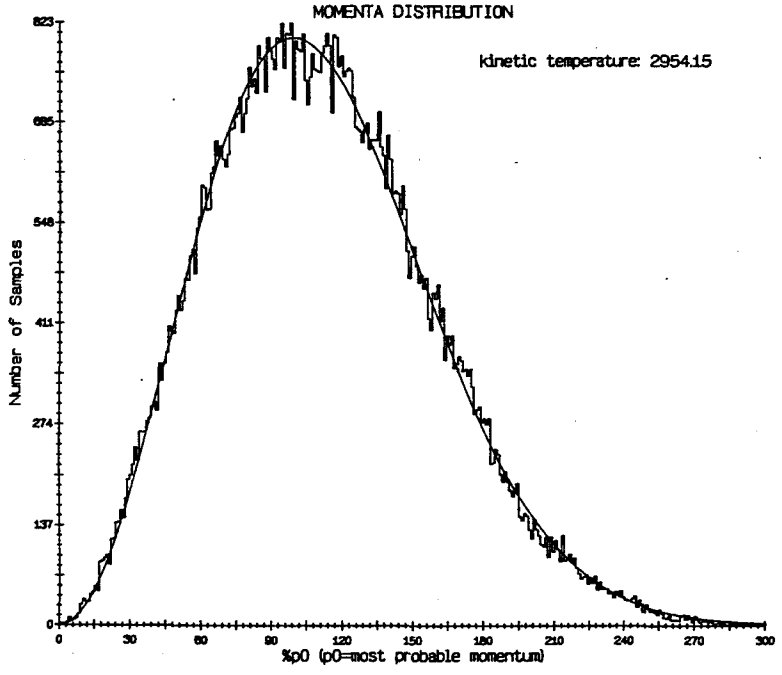

(b)

Figure 2: Distribution functions for particle momenta before (a) and after (b) resetting virtual momenta to zero.

sure obtained for NPT and EhN ensembles is quite good, particularly at lower temperatures. At higher temperatures, this situation can be expected to improve for systems with larger numbers of particles and correspondingly smaller fluctuations.

The momentum distribution produces a good approximation to the canonical Maxwell-Boltzmann distribution in most cases, although it is sometimes necessary to reduce the kinetic energy of the virtual variables in a rather ad hoc way to achieve this agreement.

According to the ergodic theorem, the average kinetic energy should be 0.5kT for each of the virtual variables. In general, this is not found to be the case. Typical values for the virtual kinetic energies may be orders of magnitude above or below the ergodic value, and while it may be that these averages will be obtained if the run times are extremely long, for reasonable simulation times this is not the case. In some cases, energy appeared to circulate between the virtual momenta in a cyclic fashion.

In contrast to the nonergodic behavior of the virtual momenta, stable values were reached rather quickly for the kinetic energy of the real system, the components of the microscopic pressure tensor, and the magnitudes of the cell vector components. This suggests that equilibrium for these quantities is reached despite the failure of the ergodic assumption in other respects. For this reason, the equations of motion are expected to give reasonable results for NPT simulations provided the momentum distribution is monitored and brought into correspondence with the canonial distribution when deviations are objectionably large.

While the simulation techniques are judged to be reasonable, the atomic potential used in this preliminary study is obviously inadequate and a more realistic potential must be used to model the phase transitions.

Chapter 4

Interatomic Force Calculations

4-1 Electrostatic Forces

When periodic boundary conditions are employed, a molecular dynamics computational cell containing N atoms may be considered to be a unit cell with an N-point basis in a crystal lattice. The calculations of long-range Coulomb interactions can then be performed with techniques developed for the evaluation of electrostatic energies and forces within crystals. While essentially all molecular dynamics simulations which include long-range ionic interactions have used the Ewald method[57] to calculate the Coulomb energy and forces, alternative methods offer some computational advantages. A method for performing Coulomb lattice sums using multipole techniques is developed and implemented as part of this work, and results are contrasted with those of the Ewald method.

The necessity for special procedures to obtain lattice sums for the Coulomb potential is due not only to the extremely slow convergence of the lattice sums but also to the ambiguous results obtained from straightforward summations. The cause of this ambiguity can be found by examination of a simple lattice summation for the energy per unit cell due to N charged particles within an MD computational cell. This energy may be written:

$$E = \frac{1}{2} \sum_{\alpha=-\infty}^{\infty} \sum_{\beta=-\infty}^{\infty} \sum_{\gamma=-\infty}^{\infty} \sum_{i=1}^{N} \sum_{j=1}^{N}{}' \frac{q_i q_j}{\mid \vec{r}_i - \vec{R}_{\alpha\beta\gamma} - \vec{r}_j \mid}$$

where $\vec{R}_{\alpha\beta\gamma} \equiv \alpha\vec{a}+\beta\vec{b}+\gamma\vec{c}$; $\vec{a}$, $\vec{b}$, and $\vec{c}$ are Bravais lattice vectors; and the prime on the summation over lattice indices now indicates omission of the terms for which $i = j$ and $\alpha = \beta = \gamma = 0$.

Using this expression to approximate the energy by evaluation of a finite number of terms leads to contradictions with the periodic boundary conditions which have been postulated for the MD cell. In the usual case of a cell in which the total charge is zero, the energy sum has a finite limit. However, if the cell has a nonzero dipole moment there will be a constant electric field component throughout the MD cell. Because of this, the potential at a point on one face of the cell will differ from that at a point translated through the cell along a Bravais lattice vector to the opposite face. The existence of a non-zero dipole moment also makes the constant electric field component dependent on the choice of the unit cell. An example of how this may occur is

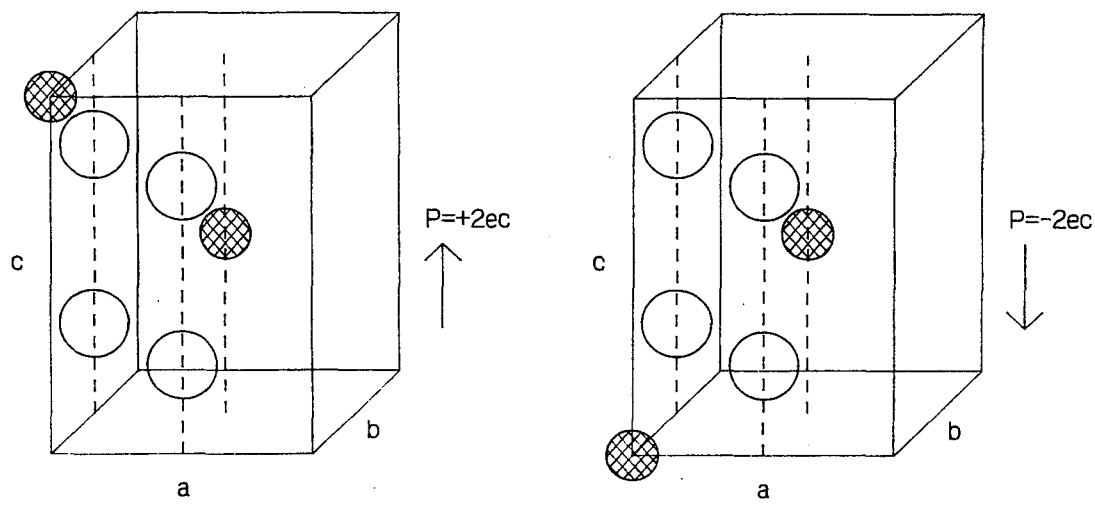

Figure 3: Two equivalent unit cells for tetragonal ZrO_2. Cross-hatched circles are Zr^{4+} atoms and open circles are O^{--} atoms. P is the dipole moment of the unit cell.

illustrated in Figure 3. Two different, equivalent choices for the unit cell of tetragonal zirconia are shown along with the net dipole moment for the cell. It is seen that the dipole moment can be made to change sign simply by redefining the locations of the atoms on the corners of the cell. If the derivative of the energy sum is calculated for each of these cells, then each sum will contain terms describing an electric field parallel to the dipole moment of the associated unit cell, and even though the cells are physically equivalent the electric fields for the two cases will differ in sign.

The presence of a constant electric field component in an MD simulation due to a nonzero dipole moment in the unit cell tends to accelerate each charged particle in a direction parallel to the dipole moment of the cell until a particle leaves the cell. Applying periodic boundary conditions, there is an identical particle displaced by a Bravais lattice vector which simultaneously enters the cell through the opposite face. When the entering ion is included in the multipole moments of the cell instead of the exiting ion, the unit cell is effectively redefined. The configuration of the unit cell could change, for example, from one of those shown in Figure 3 to the other in the course of the simulation. When this happens, the electric field inside the cell changes

discontinuously. Since the particles in an MD cell are not taken to have any particular symmetry, a dipole moment is generally present and discontinuities in the electric field and therefore the forces is the general rule.

The dependence of the energy sum on the dipole moment of the unit cell is well known. In addition to early studies on the effect of the order of summation of terms on the energy totals[58], the development of fast summation techniques for the Coulomb energy of ionic lattices has led to methods which can give different total energy values for the same unit cell. The Ewald method and the planewise summation method[59] (PSM), for example, yield different values if the unit cell has a net dipole moment.

4-2 The Ewald Method

The potential due to a lattice of positive point charges is obtained in the Ewald method by surrounding the point charges with equal positive and negative Gaussian charge distributions and a uniform volume charge. The point charges plus the negative Gaussian distributions and the positive Gaussian distributions plus the negative volume charges are then summed separately, with the convergence of the positive Gaussian-volume charge lattice sum improved by performing the sum in reciprocal space. Both sums converge, in contrast to the simple Coulomb lattice sum. The reason for this is that the Ewald sum does not evaluate the lattice sum for positive point charges alone, but rather evaluates the sum for the point charges plus a uniform negative background charge. When the energy of a collection of positive and negative point charges in the unit cell of a neutral crystal is calculated using the Ewald potential, the background charges cancel and so the energy sum is generally taken to be due to the point charges alone.

The total dipole moment of the Ewald unit cell is always zero, since each point charge plus volume charge has a dipole moment of zero irrespective of the position of the associated point charge. The absolute convergence of the Ewald energy sum resulting from the zero dipole moment leads to periodicity of the potential within the cell and to invariance of the forces in a given cell regardless of the exact choice of unit cell.

The difference between results obtained from the Ewald method and the simple Coulomb lattice sum can be clarified by replacing the infinite lattice summation in the Ewald method with a summation over a very large but finite lattice. By inspecting the surface of the finite crystals, it can be seen that the volume charges cancel each other exactly only if the net dipole moment of the unit cell is zero. If the dipole moment is nonzero, then there will be a net surface charge on the exterior of the crystal. A derivation of the Ewald energy sum which describes the surface

charges explicitly is given in Appendix C. Expressions for the forces calculated from the Ewald energy are also given in are given in Appendix C.

The absolute convergence properties of the Ewald method make this method a reasonable one for dynamical simulations. While the system under study must now be taken as that of a Coulomb system plus a specified surface charge, the lack of physical currents in a neutral crystal implies that there must be, in general, surface conditions which result in the cancellation of any constant forces predicted by the simple Coulomb sum. The Ewald method thus produces forces which are both mathematically unambiguous and physically realistic for crystals which do not have an intrinsic dipole moment.

A drawback of the Ewald method for computing Coulomb forces presents itself when simulations containing large numbers of particles are considered. For an MD cell containing N atoms, the number of Ewald sums required to calculate the forces is proportional to N^2.

The terms which are summed in an Ewald energy calculation are rather complicated, particularly the direct sum. A force calculation requires the calculation and summation of terms which are even more complicated. The speed of convergence can be improved in a simple way by adjusting the free parameter α in the Ewald sums so that the direct and reciprocal sums converge at the same rate. Nijboer and de Wette[60] have shown that this will occur if $\alpha = \sqrt{\pi}/\mathrm{L}$, where L is the length of a cubic cell edge. Sangster and Dixon[61] show that the reciprocal sum can be reformulated so that the number of terms is proportional to N rather than N^2, and the free parameter can then be adjusted to increase the number of reciprocal space terms and decrease the number of direct space terms required to obtain a given degree of convergence. The optimum value of α will be that which minimizes the overall computational time. An implementation of both the original and modified Ewald methods[62] indicates that the techniques suggested by Sangster and Dixon can increase the speed of computation by a factor of about two or three.

The Ewald method was extended by Nijboer and deWette[60] to include cases in which the interactions are proportional to any negative power of the separation distance. Williams[63] later extended these methods to allow multiple atoms in a unit cell. These techniques give formulas which can be used to perform fast summation of potentials and forces which would otherwise converge very slowly, such as the r^{-4} dipole-charge interaction commonly encountered in ionic models and the r^{-6} Van der Waals or dispersion interaction. These formulas become progressively more complicated as the reciprocal power increases, and it is common to use a cutoff radius to calculate these potentials rather than utilize the rapidly converging formulations.

4-3 Planewise Summation Methods

In the planewise summation method, two-dimensional lattice sums are first obtained for lattice points in the planes defined by two of the lattice vectors and the contributions from each plane are then summed along the third lattice vector. A Fourier transform is applied to the two-dimensional sums, which allows the third sum to be performed analytically. The result is a lattice sum which requires summation over only two reciprocal lattice indices.

Planewise summation was first developed by Nijboer and de Wette[59] for dipole lattices and crystals with monoclinic and higher symmetry. They later extended the method[64] to summation of multipole lattices of all orders and used the multipole summations to calculate an electrostatic potential for ionic lattices. The method was extended to multipole lattices in triclinic crystals by Massidda[65]. Massidda and Hernando also developed a formulation for the direct use of the planewise summation method to obtain the electrostatic potential[66].

The planewise summation method offers some computational advantages over the Ewald method. The lattice summation is performed over two indices rather than three, there is only a reciprocal space sum and not a direct sum, and the individual terms in the sum are generally simpler to calculate than those in an Ewald sum.

A disadvantage of both Ewald and direct planewise summation methods is that the number of calculations is proportional to N^2. An additional disadvantage of the planewise method is the dependence of the potential on the choice of the planes in the crystal and inconsistency with periodic boundary conditions when the dipole moment of the unit cell is nonzero.

An alternative to the direct planewise method is the separation of the potential into multipoles which can then be summed individually. By using procedures similar to those of the fast multipole method of Greengard and Rokhlin[67], algorithms can be written which require a number of calculations proportional to N.

The multipole expansion of the Coulomb potential contains the same indeterminacy and dipole dependence of the simple Coulomb sum, so for dynamical simulations it is necessary to modify the potential in such a way that periodic boundary conditions are maintained regardless of the choice of unit cell. It is possible to accomplish this by separating the indeterminate part of the multipole expansion into contributions due to surface charges and a separate lattice sum which is absolutely convergent. This is the same separation that is included implicitly in the Ewald method. In the following derivation of a periodic multipole potential, the two methods will be shown to be equivalent.

In order to expand the Coulomb potential in multipole moments, it is necessary to define a

sphere about the origin of the MD cell and restrict the application of the multipole expansion to those terms in the lattice sums which come from cells with centers outside the sphere. This radius must be greater than the longest diagonal of the MD cell to insure the validity of the multipole expansion. The cells inside the sphere are hereafter referred to as 'near-neighbors'. When a multipole expansion which separates the lattice sums from the particle locations is used[64], the energy sum becomes

$$E = \frac{1}{2} \sum_{\alpha\beta\gamma=nn} \sum_{i=1}^{n} \sum_{j=1}^{n}{}' \frac{q_i q_j}{\mid \vec{r}_i - \vec{R}_{\alpha\beta\gamma} - \vec{r}_j \mid}$$

$$+\frac{1}{2} \sum_{\alpha\beta\gamma\neq nn} \sum_{i=1}^{n} \sum_{j=1}^{n} q_i q_j \sum_{k=0}^{\infty} \sum_{n=-k}^{k} \sum_{l=0}^{\infty} \sum_{m=-l}^{l}$$

$$c_{kn;lm} r_i^l Y_{lm}^*(\hat{r}_i) r_j^k Y_{kn}^*(\hat{r}_j) \frac{Y_{k+l,n+m}(\hat{R}_{\alpha\beta\gamma})}{R_{\alpha\beta\gamma}^{k+l+1}}$$

$$c_{kn;lm} \equiv \frac{(-1)^l (k+l-m-n)!}{(k+n)!(l+m)!}$$

Here the unnormalized spherical harmonics are defined as

$$Y_{lm}(\hat{r}) = P_l^{|m|}(cos\theta) e^{im\phi}$$

A derivation of this equation is provided for reference in Appendix D. With the multipole moments of the MD cell defined as

$$Q_{lm} \equiv \sum_{i=1}^{n} q_i r_i^l Y_{lm}(\hat{r}_i)$$

and the first term defined as E_{nn}, the energy can be written as

$$E = E_{nn} + \frac{1}{2} \sum_{kn} \sum_{lm} c_{kn;lm} Q_{lm}^* Q_{kn}^* \sum_{\alpha\beta\gamma\neq nn} \frac{Y_{k+l,n+m}(\hat{R}_{\alpha\beta\gamma})}{R_{\alpha\beta\gamma}^{k+l+1}}$$

The lattice sums can be calculated separately for each combination of k+l and n+m. For $k + l \geq 4$, these sums are absolutely convergent[68] and can be calculated by the PSM without ambiguity. The indeterminancy in the total energy is contained in the lattice sums with $k+l < 4$, and since these sums are at best conditionally convergent other methods must be used for their evaluation.

In all cases but one, terms in the sum which contain combinations of k and l with $k+l < 4$ can be shown to be zero. This is the case for any combinations with k or l equal to zero, since charge neutrality of the MD cell insures that $Q_{00} = 0$. The inversion symmetry of the Bravais lattice in combination with the parity of spherical harmonics of odd order leads to zero contributions from all odd-valued combinations, including k+l equal to 1 or 3. The only non-zero terms with $k + l < 4$ are those with k=1 and l=1. The strength of this term is determined by

the collective dipole moment of the charges in the MD cell. As expected, if the dipole moment is zero, then Q_{1m} is zero and there is no indeterminancy is the overall sum.

In order to evaluate the term with k=l=1 and nonzero dipole moment, a set of point charges of arbitrary magnitude can be added and subtracted at the center of the face of each cell in the lattice. The energy in the MD cell due to these added point charges is zero, which in this case may be written

$$0 = \frac{1}{2} \sum_{\alpha\beta\gamma=-M}^{M} \sum_{i=1}^{N} q_i \sum_{j=a,b,c} \{ \frac{\tilde{q}_j}{\mid \vec{r}_i - \vec{R}_{\alpha\beta\gamma} - \frac{\vec{i}}{2} \mid} - \frac{\tilde{q}_j}{\mid \vec{r}_i - \vec{R}_{\alpha\beta\gamma} - \frac{\vec{i}}{2} \mid} \}$$

or

$$\begin{aligned} 0 = & \frac{1}{2} \sum_{\alpha\beta\gamma=-M}^{M} \sum_{i=1}^{N} q_i \sum_{j=a,b,c} \frac{\tilde{q}_j}{\mid \vec{r}_i - \vec{R}_{\alpha\beta\gamma} - \frac{\vec{i}}{2} \mid} \\ & - \frac{1}{2} \sum_{\alpha=-M+1}^{M+1} \sum_{\beta\gamma=-M}^{M} \sum_{i=1}^{N} q_i \frac{\tilde{q}_a}{\mid \vec{r}_i - \vec{R}_{\alpha\beta\gamma} + \frac{\vec{a}}{2} \mid} \\ & - \frac{1}{2} \sum_{\beta=-M+1}^{M+1} \sum_{\alpha\gamma=-M}^{M} \sum_{i=1}^{N} q_i \frac{\tilde{q}_b}{\mid \vec{r}_i - \vec{R}_{\alpha\beta\gamma} + \frac{\vec{b}}{2} \mid} \\ & - \frac{1}{2} \sum_{\gamma=-M+1}^{M+1} \sum_{\alpha\gamma=-M}^{M} \sum_{i=1}^{N} q_i \frac{\tilde{q}_c}{\mid \vec{r}_i - \vec{R}_{\alpha\beta\gamma} + \frac{\vec{c}}{2} \mid} \end{aligned}$$

In these equations, $\vec{a}$, $\vec{b}$, and $\vec{c}$ are the unit cell lattice vectors. By combining the contributions from the positive and negative charges at each common lattice point, a single lattice sum plus a number of surface terms are created:

$$\begin{aligned} 0 = & \frac{1}{2} \sum_{\alpha\beta\gamma=-M}^{M} \sum_{i=1}^{N} q_i \sum_{j=a,b,c} \{ \frac{\tilde{q}_j}{\mid \vec{r}_i - \vec{R}_{\alpha\beta\gamma} - \frac{\vec{i}}{2} \mid} - \frac{\tilde{q}_j}{\mid \vec{r}_i - \vec{R}_{\alpha\beta\gamma} + \frac{\vec{i}}{2} \mid} \} \\ & - \frac{1}{2} \sum_{i=1}^{N} q_i \sum_{\beta\gamma=-M}^{M} \{ \frac{\tilde{q}_a}{\mid \vec{r}_i - \vec{R}_{M+1\beta\gamma} + \frac{\vec{a}}{2} \mid} - \frac{\tilde{q}_a}{\mid \vec{r}_i - \vec{R}_{-M\beta\gamma} + \frac{\vec{a}}{2} \mid} \} \\ & - \frac{1}{2} \sum_{i=1}^{N} q_i \sum_{\alpha\gamma=-M}^{M} \{ \frac{\tilde{q}_b}{\mid \vec{r}_i - \vec{R}_{\alpha M+1\gamma} + \frac{\vec{b}}{2} \mid} - \frac{\tilde{q}_b}{\mid \vec{r}_i - \vec{R}_{\alpha -M\gamma} + \frac{\vec{b}}{2} \mid} \} \\ & - \frac{1}{2} \sum_{i=1}^{N} q_i \sum_{\alpha\beta=-M}^{M} \{ \frac{\tilde{q}_c}{\mid \vec{r}_i - \vec{R}_{\alpha\beta M+1} + \frac{\vec{c}}{2} \mid} - \frac{\tilde{q}_c}{\mid \vec{r}_i - \vec{R}_{\alpha\beta -M} + \frac{\vec{c}}{2} \mid} \} \end{aligned}$$

The last three terms contain point charges spaced uniformly on the surfaces of the finite crystal. Representing these terms by $-E_{surf}$ and performing a multipole expansion on the terms in the lattice which are not near neighbors,

$$0 = \frac{1}{2} \sum_{\alpha\beta\gamma=nn} \sum_{i=1}^{N} q_i \sum_{j=a,b,c} \{ \frac{\tilde{q}_j}{\mid \vec{r}_i - \vec{R}_{\alpha\beta\gamma} - \frac{\vec{j}}{2} \mid} - \frac{\tilde{q}_j}{\mid \vec{r}_i - \vec{R}_{\alpha\beta\gamma} + \frac{\vec{j}}{2} \mid} \} - Esurf$$

$$+ \frac{1}{2} \sum_{kn} \sum_{lm} c_{kn;lm} Q^*_{lm} \{ \sum_{j=a,b,c} \tilde{q}_j (\frac{r_j}{2})^k (Y^*_{kn}(\hat{j}) - Y^*_{kn}(-\hat{j})) \}$$

$$\times \sum_{\alpha\beta\gamma \neq nn} \frac{Y_{k+l,n+m}(\hat{R}_{\alpha\beta\gamma})}{R^{k+l+1}_{\alpha\beta\gamma}}$$

Referring to the first term in this equation as $\tilde{E}_{nn}$ and the expression in brackets in the multipole term as $\tilde{Q}^*_{kn}$, this equation becomes:

$$0 = \tilde{E}_{nn} - E_{surf} + \frac{1}{2} \sum_{kn} \sum_{lm} c_{kn;lm} Q^*_{lm} \tilde{Q}^*_{kn} \sum_{\alpha\beta\gamma \neq nn} \frac{Y_{k+l,n+m}(\hat{R}_{\alpha\beta\gamma})}{R^{k+l+1}_{\alpha\beta\gamma}}$$

Values for $\tilde{q}_a$, $\tilde{q}_b$, and $\tilde{q}_c$ are determined by setting $\tilde{Q}_{1m} = -Q_{1m}$.The resulting values for the compensating charges are

$$\tilde{q}_a = -\sum_{i=1}^{N} q_i \xi_i$$

$$\tilde{q}_b = -\sum_{i=1}^{N} q_i \eta_i$$

$$\tilde{q}_c = -\sum_{i=1}^{N} q_i \zeta_i$$

where q_i is the ionic charge of the i^{th} atom and ξ_i, η_i, and ζ_i are the fractional displacements within the unit cell along the $\vec{a}$, $\vec{b}$, and $\vec{c}$ directions, respectively. Compensating charges for the unit cells of Figure 3 are shown in Figure 4.

In an orthorhombic lattice the compensating charges are proportional to the dipole moments of the unit cell. In triclinic lattices the values are proportional to the projection of the total dipole moment along the lattice vectors. Using these values for the compensating charges, the dipole moment for the MD cell can be equated to an expression containing terms which represent a surface charge, a near neighbor sum, and lattice sums which are all absolutely convergent.

$$\frac{1}{2} \sum_{m=-1}^{1} \sum_{n=-1}^{1} c_{1n;1m} Q^*_{1m} Q^*_{1n} \sum_{\alpha\beta\gamma \neq nn} \frac{Y_{2,n+m}(\hat{R}_{\alpha\beta\gamma})}{R^{k+l+1}_{\alpha\beta\gamma}}$$

$$= \tilde{E}_{nn} + \frac{1}{2} \sum_{lm} \sum_{kn} c_{kn;lm} Q^*_{lm} \tilde{Q}^*_{kn} \sum_{\alpha\beta\gamma \neq nn} \frac{Y_{k+l,n+m}(\hat{R}_{\alpha\beta\gamma})}{R^{k+l+1}_{\alpha\beta\gamma}}$$

$$- E_{surf}$$

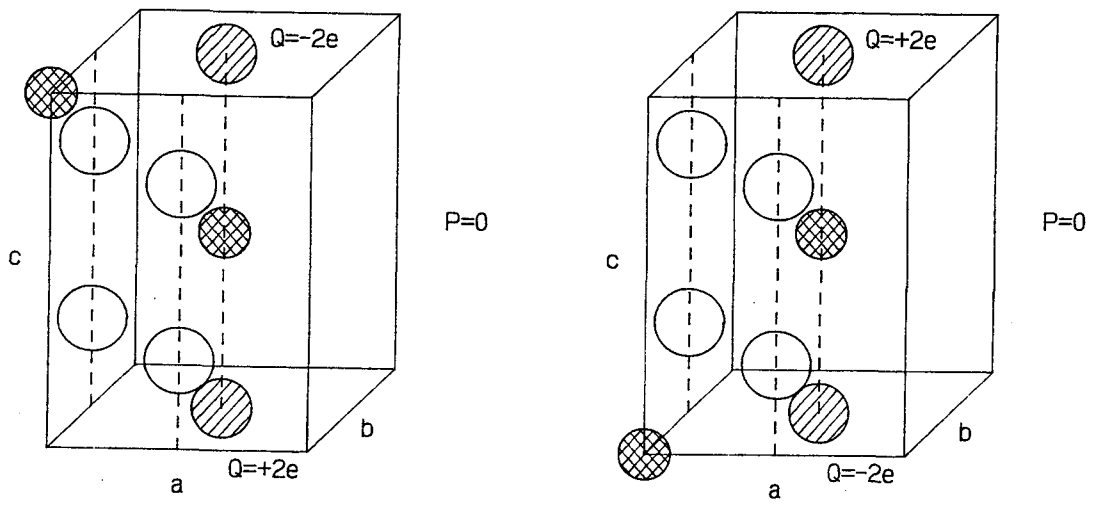

Figure 4: Addition of compensating charges which result in zero dipole moments for the unit cells of Figure 3. Parallel hatched circles are the compensating charges.

Here the sums on the RHS are restricted to values of k and l for which $k+l \geq 4$. When this expression is inserted into the original Coulomb sum, the required form for the total electrostatic energy is obtained.

$$E = E_{nn} + \tilde{E}_{nn} - E_{surf}$$

$$+\frac{1}{2}\sum_{lm}\sum_{kn} c_{kn;lm} Q^*_{lm}(Q^*_{kn} + \tilde{Q}^*_{kn}) \sum_{\alpha\beta\gamma \neq nn} \frac{Y_{k+l,n+m}(\hat{R_{\alpha\beta\gamma}})}{R^{k+l+1}_{\alpha\beta\gamma}}$$

The distance from the original MD cell to the surface charges can be taken to be very large compared to the cell dimensions. In this limit the point charges at the summation limits can be well approximated as surface charges with values $\rho_a = \tilde{q}_a/A_{bc}$, $\rho_b = \tilde{q}_b/A_{ac}$ and $\rho_c = \tilde{q}_c/A_{ab}$. A_{ab} is the area of the MD cell face defined by lattice vectors $\vec{a}$ and $\vec{b}$. A_{ac} and A_{bc} are defined similarly.

If the energy of the system is taken as

$$E_{mp} \equiv E + E_{surf}$$

then all of the lattice sums are absolutely convergent and the forces generated by E_{mp} are periodic

with the lattice. Because of this, the value of the energy is not affected by the definition of the unit cell. In fact, E_{mp} is the same as the Ewald energy if the same lattice limits are used in both cases. The Ewald energy may also be considered as the simple Coulomb energy plus a surface term, with the magnitude of the the surface charge distribution exactly equal to that obtained for the multipole method (Appendix C). For lattice sums taken over the same limits, the surface charge distributions generated by each method are identical.

The computation of lattice sums for interaction potentials inversely porportional to higher powers of the separation distance is somewhat problematic. Direct extension of the planewise method yields expressions which are difficult to sum analytically or which contain slowly converging series. Expressions for planewise sums for potentials varying as r^{-4} and r^{-6} are given in Appendix E.

It would be possible to tabulate the integrals in the r^{-4} and r^{-6} formulations in order to speed the computation of these sums. The formulas in these cases are absolutely convergent, so no special considerations are required in their use. Performance in an algorithm could be expected to be competitive with that of the Ewald-type summations, with the number of calculations proportional to N^2 in either case.

Incorporation of interaction potentials of the form r^{-n} into a multipole method presents even more difficulties. The multipole separation used for the Coulomb potential cannot be used for the higher power terms; since these terms do not satisfy Laplace's equation they cannot be constructed from linear combinations of the solutions to that equation. The multipole character of the summations could be preserved by separating the lattice sums and particle coordinates through application of a three-dimensional Taylor series expansion. The lattice sums so obtained are found to be derivatives of the direct lattice sums for r^{-n} evaluated at the origin. These sums could in principle be evaluated with a number of operations proportional to N by the planewise summation as outlined above and then differentiated to obtain the terms which would be included in the multipole sums.

A more intuitive approach to including the higher-power terms can be found by considering these terms in light of their physical origins. The r^{-4} term is generally considered to be a charge-dipole interaction, while the r^{-6} terms usually arise from an induced dipole-dipole interaction. If each atom is assigned a polarizability, then the dipole moment induced in each atom will be proportional to the electric field at that atom. The field at each atom is obtained as part of the force calculation. The charge-dipole interaction could then be calculated directly for near neighbors and through an additional multipole sum for the long-range contributions. The corrections to the electric field at each atom would in turn cause corrections in the atomic dipole

moments, and the procedure would be repeated until self-consistency is obtained. At each step the only corrections are to the multipole moments of the unit cell; the lattice sums remain unchanged throughout the self-consistency routine.

The direct calculation of dipole interactions through the multipole method has a number of advantages. All of the electrostatic forces due to dipole interactions are included automatically. The r^{-4} and r^{-6} potentials, for instance, need not be considered separately. Using fast multipole techniques, it is possible to construct algorithms which include all of the electrostatic forces to any required degree of accuracy with a number of calculations proportional to N. The short-range forces would be calculated in the last step of the fast multipole procedure and would also require a number of calculations proportional to N. The method could readily be extended to include quadrupole and higher order interactions if required. A deficiency of this method is that it does not allow for the faithful modelling of materials with intrinsic dipole moments or interactions such as the Van der Waals force which are implicitly quantum mechanical in nature.

The multipole expressions for energy and force have been incorporated in a rather simple way into an algorithm for molecular dynamics simulations. The near neighbor interactions are calculated directly, and the planewise summation method is used to calculate the lattice sums for the long-range Coulomb interactions. The resulting algorithm includes a number of calculations proportional to N^2 due to the near neighbor terms. The terms in these calculations are simpler than those of the Ewald summation, and total run time is expected to be less for systems containing moderately large numbers of atoms. The number of multipole calculations is proportional to N but it is also proportional to the fourth power of the highest order multipole index included in the sums. If the full procedure of the fast multipole method is implemented, each stage of the procedure reduces the number of near neighbor calculations by a factor of eight and increases the number of multipole calculations by the same factor. Trial implementation of a one-stage fast multipole algorithm indicated that for several hundred atoms the fast multipole routine increased the run time. There are many approaches to improving the speed of the fast multipole algorithm but these are beyond the scope of this work. Energy and force calculations using the planewise summation method are given in Appendix D.

Both the Ewald method and the planewise summation method have been incorporated into algorithms for calculating the long-range energy and forces. Analytically, the two methods produce identical numerical results when applied to a given MD cell. The choice of which to use in dynamical simulations may be made by considering the speed and accuracy of the algorithms for each of these methods.

4-4 Numerical Accuracy of Algorithms

Computation of energies and forces in molecular dynamics simulations are limited in precision by the numerical accuracy of the algorithms. The accuracy is determined by the choice of parameters used in calculating the interactions due to short-range forces as well as those used in the long-range Coulomb interactions. The various types of numerical errors are discussed in this section, and the parameters necessary to achieve a given relative error are obtained. Derivations of the various expressions for the fractional errors are given in Appendix F. The short-range forces are assumed here to be proportional to r^{-10}.

For a short-range potential proportional to r^{-10} the associated energy per unit cell is:

$$E_{sr} = \frac{1}{2} \sum_{\alpha\beta\gamma=-\infty}^{\infty} \sum_{ij=1}^{N}{}' \frac{C_{10}}{| \vec{r}_i - \vec{R}_{\alpha\beta\gamma} - \vec{r}_j |^{10}}$$

In a numerical computation, the sums over the lattice are finite and the expression for the total energy contains a truncation error. If the sums are evaluated for all lattice parameters with an absolute value less than or equal to a given positive integer value, the truncation error can be written:

$$\delta_{sr} = E_{sr} - \frac{1}{2} \sum_{\alpha\beta\gamma=-M}^{M} \sum_{ij=1}^{N}{}' \frac{C_{10}}{| \vec{r}_i - \vec{R}_{\alpha\beta\gamma} - \vec{r}_j |^{10}}$$

A approximate expression for the fractional error with a given value for the lattice limit M is:

$$\epsilon_M \equiv \frac{\delta}{E} \approx \frac{24}{2^{10}} \frac{1}{7M^7}$$

The estimated error bounds for various values of M are given in Table 2, along with the actual errors calculated for NaCl and tetragonal and monoclinic zirconia.

M	$\epsilon_M(est.)$	$NaCl$	$ZrO_2(ttr)$	$ZrO_2(mc)$
1	$3x10^{-5}$	$2x10^{-4}$	$1x10^{-4}$	$6x10^{-6}$
2	$2x10^{-6}$	$4x10^{-6}$	$2x10^{-6}$	$9x10^{-8}$
3	$2x10^{-7}$	$3x10^{-7}$	$2x10^{-7}$	$7x10^{-9}$

Table 2: Truncation errors for short-range energy sums.

Ewald summations include a free parameter α which is set to $\alpha = \sqrt{\pi}/a$, a being the lattice constant. This definition of α is used for all calculations described here, with the result

that for non-cubic cells the rate of convergence depends on the ratios of the lattice constants. The fractional truncation error for the Ewald sum is estimated as:

$$\epsilon_M \approx e^{-\pi(\frac{b}{a})^2(3+5+\cdots+(2M+1))} \quad M \geq 1$$

In this approximation a is the largest lattice constant and b is the smallest. Error estimates and calculated errors for lattice sums computed with the Ewald method are listed in table 3.

M	$\epsilon_M(\frac{b}{a}=1)$	$\frac{1}{2}$	$\frac{1}{4}$	$NaCl$	$ZrO_2(ttr)$	$ZrO_2(mc)$
1	10^{-4}	10^{-2}	10^{-1}	$1x10^{-5}$	$8x10^{-4}$	$1x10^{-4}$
2	10^{-11}	10^{-5}	10^{-3}	$5x10^{-12}$	$5x10^{-9}$	$6x10^{-9}$
3	10^{-20}	10^{-10}	10^{-5}	$2x10^{-20}$	$1x10^{-14}$	$2x10^{-16}$

Table 3: Truncation errors for Ewald energy sums.

In dynamical simulations, a fractional error of 10^{-4} in the forces is generally considered to be acceptable. Due to the convergence of the Ewald sum, this accuracy can usually be obtained with M=2, M=1 being marginally acceptable for cubic crystals. In most cases, the accuracy of the calculations will be much better than the estimate. For the crystals listed in the tables, the error for $M = 2$ is $\approx 10^{-8}$ for the Ewald sums and $\approx 10^{-5}$ for the short-range sums. The short-range energy is estimated to be approximately 10% of the total energy, so the short-range error relative to the total for M=2 is $\epsilon_{sr} \approx 10^{-6}$.

A multipole calculation for the energy in the MD cell will include truncation errors for both the short-range and Coulomb energies. The multipole expansion is valid for cells with centers more than the maximum MD cell diagonal from the the origin, but if this distance is used as a cutoff radius the multipole terms will converge very slowly. For maximum efficiency, the number of direct calculations within a given cutoff radius must be weighed against the number of terms in the multipole expansion which are required to achieve a given accuracy.

The accuracy of the short-range energy sums is directly determined by the cutoff radius. An estimate for the fractional short-range truncation error is:

$$\epsilon_{sr} \approx \frac{4\pi}{7 \cdot 2^{10}}(\frac{a}{R})^7$$

R is the cutoff radius and a is an average lattice constant. Estimated and calculated errors are listed in table 4 for various values of the cutoff radius. In this and the following tables, the parameter n is defined as $n \equiv R/r_o$, with r_o equal to the maximum MD cell diagonal. The value $r_o = \sqrt{3}a$ is used to calculate the estimated values.

n	$\epsilon_n(est.)$	$NaCl$	$ZrO_2(ttr)$	$ZrO_2(mc)$
1.5	$2.2x10^{-6}$	$4x10^{-6}$	$9x10^{-6}$	$2.5x10^{-7}$
2.0	$2.9x10^{-7}$	$5x10^{-7}$	$8x10^{-7}$	$1.7x10^{-8}$
2.5	$6.1x10^{-8}$	$7x10^{-8}$	$1x10^{-7}$	$2.4x10^{-9}$

Table 4: Truncation errors for radial short-range energy sums.

The error estimates for a spherical lattice sum are directly related to those for the cubic sum used with the Ewald method. Values for n= 1.5, 2.0 and 2.5 in table 4 are approximately the same as those for M=2, 3, and 4, respectively, in table 2.

In all cases, the short-range sums within the cutoff radius have a fractional error of $\approx 10^{-5}$ or less. For simulations in which the short-range energy is expected to approximately a tenth of the total energy, the short-range error is expected to be less than $\approx 10^{-6}$. For a multipole method in which Coulomb and short-range energy and forces are calculated directly for all lattice points within a given radius, accuracy of short-range contributions with any practical cutoff radius will be sufficient unless a relative precision of $\approx 10^{-7}$ or less is required. In most cases, the truncations errors in the multipole sums will determine the overall accuracy of the calculations.

The truncation error for the multipole expansion is:

$$\delta_{mp} \equiv \frac{1}{\mid \vec{r}_i - \vec{R}_{\alpha\beta\gamma} - \vec{r}_j \mid} - \sum_{k=0}^{\mu} \sum_{n=-k}^{k} \sum_{l=0}^{\mu-k} \sum_{m=-l}^{l} c_{kn;lm} Q^*_{kn} Q^*_{lm} \frac{Y_{k+l,n+m}(\hat{R}_{\alpha\beta\gamma})}{R^{k+l+1}_{\alpha\beta\gamma}}$$

The magnitude of the error is determined by the value of μ, the highest multipole index retained in the sums, and also by the cutoff radius, since this radius determines the minimum value of $\vec{R}_{\alpha\beta\gamma}$. An approximate expression for the fractional truncation error for the expansion is:

$$\epsilon_\mu \equiv \frac{\mid \delta_\mu \mid}{\mid \vec{r}_i - \vec{R}_{\alpha\beta\gamma} - \vec{r}_j \mid^{-1}} \approx (\frac{n+1}{n-1}) n^{-(\mu+1)}$$

The parameter n in this expression is again the ratio of the cutoff radius to the maximum MD cell diagonal. Estimated values for ϵ_μ with $n = \frac{3}{2}$ and $n = 2$ are shown in table 5.

The contribution from cells outside the cutoff radius is around one percent of the total Coulomb energy for all of the examples given. The magnitude of this contribution falls off very slowly as the cutoff radius is increased, so in estimates of the multipole truncation error the multipole energy is taken to be one percent of the total Coulomb energy.

Additional numerical errors in the multipole sums arise from the computation of the lattice sums using the planewise summation. This method uses Fourier transforms to replace multipole

n	μ	$\epsilon_\mu(est.)$	$NaCl$	$ZrO_2(ttr)$	$ZrO_2(mc)$
	4	0.6	1.0	0.54	0.27
	6	0.3	$8.8x10^{-4}$	0.22	$1.9x10^{-2}$
	8	0.13	$8.8x10^{-4}$	$8.8x10^{-2}$	$3.0x10^{-2}$
	10	$6.0x10^{-2}$	$5.6x10^{-5}$	$6.1x10^{-2}$	$1.8x10^{-3}$
1.5	12	$2.6x10^{-2}$	$3.2x10^{-5}$	$3.3x10^{-4}$	$2.8x10^{-3}$
	14	$1.1x10^{-2}$	$5.3x10^{-6}$	$1.8x10^{-3}$	$3.6x10^{-4}$
	16	$5.0x10^{-3}$		$7.9x10^{-4}$	$7.2x10^{-6}$
	18	$2.0x10^{-3}$		$5.2x10^{-4}$	$6.8x10^{-6}$
	20	$1.0x10^{-3}$		$2.7x10^{-5}$	$6.8x10^{-6}$
	4	$4.3x10^{-2}$	1.0	1.0	$9.4x10^{-2}$
	6	$2.3x10^{-2}$	$6.0x10^{-3}$	0.24	$1.2x10^{-2}$
	8	$5.9x10^{-3}$	$6.0x10^{-3}$	$6.6x10^{-3}$	$4.1x10^{-4}$
	10	$1.5x10^{-3}$	$1.2x10^{-4}$	$2.6x10^{-3}$	$1.6x10^{-6}$
2.0	12	$3.7x10^{-3}$	$1.0x10^{-5}$	$1.0x10^{-3}$	$6.1x10^{-6}$
	14	$9.2x10^{-5}$		$1.2x10^{-4}$	$1.8x10^{-6}$
	16	$2.3x10^{-5}$		$3.9x10^{-5}$	$3.6x10^{-7}$
	18	$5.7x10^{-6}$			$7.3x10^{-8}$
	20	$1.4x10^{-6}$			

Table 5: Truncation errors for the multipole expansion.

lattice sums with more rapidly converging series. One consequence of this is that the method can be applied only to sums over a complete lattice. In order to use the planewise method as part of a multipole method, the multipole sums are rewritten:

$$\sum_{\alpha\beta\gamma\neq nn} \frac{Y_{lm}(\hat{R}_{\alpha\beta\gamma})}{R_{\alpha\beta\gamma}^{l+1}} = \sum_{\alpha\beta\gamma}{}' \frac{Y_{lm}(\hat{R}_{\alpha\beta\gamma})}{R_{\alpha\beta\gamma}^{l+1}} - \sum_{nn}{}' \frac{Y_{lm}(\hat{R}_{\alpha\beta\gamma})}{R_{\alpha\beta\gamma}^{l+1}}$$

The prime denotes a sum over all lattice points except the origin. This sum can be calculated using the planewise summation method for each value of l and m. The terms in the sum over near neighbors are then calculated separately and subtracted from the planewise result.

The subtraction of two lattice sums which are nearly equal in value tends to exaggerate the numerical errors introduced with the planewise summation method. A truncation error in the planewise sums will produce errors relative to the lattice sum over all space, which is usually several orders of magnitude larger than a sum which is restricted to lattice points outside a cutoff

radius. The error in the total Coulomb energy is found to be

$$\epsilon \equiv | \frac{E_{coul} - E_{calc}}{E_{coul}} | \approx \frac{\epsilon^{\mu}_{PSM} \cdot E^{\mu}_{PSM}}{E_{coul}} + \frac{\epsilon_{\mu} \cdot E_{mp}}{E_{coul}} \approx \epsilon^{\mu}_{PSM} + \epsilon_{\mu} \frac{E_{mp}}{E_{coul}}$$

with ϵ^{μ}_{PSM} equal to the fractional truncation error for the planewise summation and

$$E^{\mu}_{PSM} \equiv \sum_{\nu=-\mu}^{\mu} \sum_{k=0}^{\mu} \sum_{n=-k}^{k} c_{kn;\mu-k,\nu-n} Q^{*}_{kn} Q^{*}_{\mu-k,\nu-n} {\sum_{\alpha\beta\gamma}}' \frac{Y_{\mu\nu}(\hat{R}_{\alpha\beta\gamma})}{R^{u+1}_{\alpha\beta\gamma}}$$

E^{μ}_{PSM} is generally of the same order of magnitude as the total Coulomb energy and can be several orders of magnitude larger than the multipole energy E_{mp}. Because of this, the planewise sum truncation error ϵ^{μ}_{PSM} must be much smaller than the multipole truncation error ϵ_{μ} in order to achieve similar error contributions in the total Coulomb energy sum.

The equations used to implement the planewise summation method are adapted from the formula of Massida for a general triclinic lattice, and are listed in Appendix D. When the reciprocal space summations are limited to indices with absolute values less than or equal to a positive integer M, the value of ϵ^{μ}_{PSM} is estimated as:

$$\epsilon^{\mu}_{PSM}(M) \equiv \epsilon_{\mu M} \approx 2(2\pi)^{\mu} \frac{(2\mu+1)^{\frac{1}{2}}}{\mu!} (M+1)^{\mu} e^{-2\pi(M+1)\frac{c_z}{a}}$$

c_z and a are the dimensions of the MD cell in the $\hat{z}$ and $\hat{x}$ directions respectively. Estimated values for ϵ^{μ}_{PSM} for various values of μ, c_z/a and M are given in Tables 6 and 7. The values listed under the crystals are the computed values for $\epsilon_{\mu M} \equiv \epsilon^{\mu}_{PSM}(M) \cdot E^{\mu}_{PSM}/E_{coul}$.

The estimates are seen to be fairly close to the calculated values for the monoclinic zirconia and sodium chloride crystals, where $c/a \approx 1$, and the tetragonal zirconia crystal, where $c/a \approx \sqrt{2}$. The convergence of the planewise summation method is strongly dependent on the c/a ratio, due to the analytic summation of terms along the $\hat{z}$ direction. Choosing a value of M to limit the truncation error in all cases, including $c/a << 1$, would necessitate a value of M which would in many cases be impractical. A value for M is chosen instead for crystals of approximately cubic symmetry, with the understanding that if the shape of the crystal becomes distorted in such a way that $c/a << 1$ then the entire MD cell must be rotated so that $c/a > 1$ and the required error tolerance is maintained.

Using the tables of estimated errors, sets of parameters may be specified to obtain a required error tolerance in the multipole and Ewald methods. A summary of these parameters is listed in Table 8.

In order to check the relative efficiency of the two methods, runs were made with each force routine for the same unit cell. Each run included 81 force and 3 energy calculations. The parameters used were M_{ew}=3, μ=14 and M_{PSM}=7 for an expected relative error of 10^{-6}. The results are plotted in Figure 5.

		$\epsilon_{\mu M} : c_z/a = 1$		
μ	M	*est.*	*NaCl*	$ZrO_2(mc)$
8	3	$4.0x10^{-4}$	$3.2x10^{-32}$	$1.1x10^{-6}$
	4	$4.4x10^{-6}$	$3.1x10^{-34}$	$5.0x10^{-8}$
	5	$3.5x10^{-8}$	$2.2x10^{-36}$	$4.6x10^{-10}$
10	3	$3.1x10^{-3}$	$1.8x10^{-4}$	$1.6x10^{-4}$
	4	$5.4x10^{-5}$	$2.6x10^{-6}$	$1.4x10^{-5}$
	5	$6.2x10^{-7}$	$2.7x10^{-8}$	$1.9x10^{-7}$
	6	$5.4x10^{-9}$	$2.1x10^{-10}$	$9.6x10^{-10}$
12	4	$4.3x10^{-4}$	$1.4x10^{-6}$	$3.7x10^{-5}$
	5	$7.3x10^{-6}$	$2.0x10^{-8}$	$7.1x10^{-7}$
	6	$8.7x10^{-8}$	$2.1x10^{-10}$	$4.8x10^{-9}$
14	5	$6.1x10^{-5}$	$1.1x10^{-6}$	$4.6x10^{-6}$
	6	$9.9x10^{-7}$	$1.6x10^{-8}$	$4.2x10^{-8}$
	7	$1.2x10^{-8}$	$1.7x10^{-10}$	$5.5x10^{-11}$
16	5	$3.9x10^{-4}$	$1.6x10^{-6}$	$1.6x10^{-4}$
	6	$8.5x10^{-6}$	$3.2x10^{-8}$	$1.9x10^{-6}$
	7	$1.3x10^{-7}$	$4.6x10^{-10}$	$2.4x10^{-9}$
18	6	$5.7x10^{-5}$	$1.5x10^{-7}$	$1.9x10^{-5}$
	7	$1.2x10^{-6}$	$2.8x10^{-9}$	$2.0x10^{-8}$
	8	$1.8x10^{-8}$	$4.0x10^{-11}$	$1.8x10^{-9}$
20	6	$3.1x10^{-4}$	$6.8x10^{-7}$	$8.1x10^{-5}$
	7	$8.2x10^{-6}$	$1.6x10^{-8}$	$4.1x10^{-8}$
	8	$1.6x10^{-7}$	$2.9x10^{-10}$	$1.5x10^{-8}$

Table 6: Truncation errors for the planewise summation: $\frac{c_z}{a} = 1$.

		$\epsilon_{\mu M}$		
μ	M	$est: c_z/a = \sqrt{2}$	$ZrO_2(ttr)$	$est.: c_z/a = 1/\sqrt{2}$
8	3	$1.2x10^{-8}$	$1.2x10^{-8}$	0.64
	4	$9.7x10^{-12}$	$8.5x10^{-12}$	$4.3x10^{-2}$
	5	$6.0x10^{-15}$	$4.4x10^{-15}$	$2.2x10^{-3}$
10	3	$9.3x10^{-8}$	$2.4x10^{-7}$	5.0
	4	$1.2x10^{-10}$	$2.8x10^{-10}$	0.53
	5	$1.1x10^{-13}$	$2.1x10^{-13}$	$3.8x10^{-2}$
	6	$6.5x10^{-17}$	$1.3x10^{-16}$	$2.1x10^{-3}$
12	4	$9.5x10^{-10}$	$3.4x10^{-9}$	4.3
	5	$1.2x10^{-12}$	$3.7x10^{-12}$	0.45
	6	$1.0x10^{-15}$	$2.9x10^{-15}$	$3.4x10^{-2}$
14	5	$1.0x10^{-11}$	$1.2x10^{-11}$	3.8
	6	$1.2x10^{-14}$	$1.3x10^{-14}$	0.39
	7		$1.0x10^{-17}$	
16	5	$6.6x10^{-11}$	$9.2x10^{-10}$	24.2
	6	$1.0x10^{-13}$	$1.4x10^{-12}$	3.3
	7	$1.1x10^{-17}$	$1.5x10^{-15}$	$3.0x10^{-2}$
18	6	$6.8x10^{-13}$	$3.9x10^{-12}$	22.2
	7	$1.1x10^{-15}$	$5.4x10^{-15}$	3.0
	8		$5.7x10^{-18}$	0.29
20	6	$3.7x10^{-12}$	$5.1x10^{-11}$	121
	7	$7.5x10^{-15}$	$9.1x10^{-14}$	20.5
	8	$1.1x10^{-17}$	$1.2x10^{-16}$	2.6

Table 7: Truncation errors for the planewise summation: $\frac{c_z}{a} \neq 1$.

ϵ_{coul}	*multipoles*				*Ewald*
	$n = 1.5$		$n = 2$		
	μ	M_{psm}	μ	M_{psm}	M_{ew}
10^{-4}	16	6	8	4	2
10^{-5}	20	8	12	6	3
10^{-6}	> 20	> 8	14	7	3
10^{-7}	> 20	> 8	16	8	4

Table 8: Parameters for error tolerances for multipole and Ewald methods.

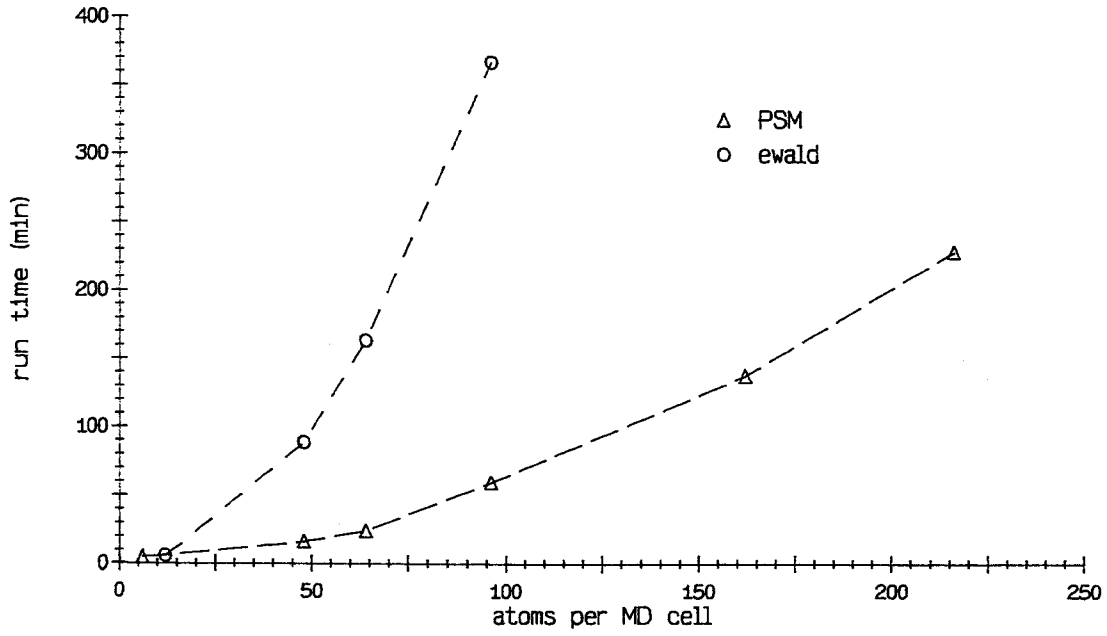

Figure 5: Computer run times for various numbers of atoms per unit cell. Forces are calculated by the Ewald method (circles) or by the planewise summation method (triangles).

Chapter 5

Program Description

5-1 General Description

The program **NPT** performs molecular dynamics simulations for a system of atoms by numerical integration of the classical equations of motion given in Section 3-6, which correspond to a constant pressure-constant temperature ensemble. The integrations are performed with either a fourth-order Runge-Kutta[69] or a fourth-order Gear[70] integration subroutine. The number and types of atoms are arbitrary. Forces between atoms are calculated from pairwise potentials of the form

$$U_{ij} = \frac{Z_i Z_j e^2}{r_{ij}} + \sum_{\gamma=1}^{\Gamma_{ij}} \frac{C_{ij\gamma}}{r_{ij}^{n_{ij\gamma}}}$$

In this expression i and j refer to atomic species, Z_i and Z_j are the atomic valence charges, $C_{ij\gamma}$ is a constant, r_{ij} is the separation between the atoms, and $n_{ij\gamma}$ is a positive integer. The number of terms in the short-range interaction is arbitrary. Periodic boundary conditions are imposed on the MD cell, and if the motion of an atom carries it outside the cell a lattice translation is performed which brings the atomic coordinates back into the cell. The energies and forces are calculated with algorithms utilizing either Ewald or planewise lattice summations for the long-range Coulomb interactions.

The virtual variables can optionally be held constant by setting the appropriate input parameters. If the virtual time variable is held constant the time averages of the particle coordinates and momenta correspond to those of an isoenthalpic-isobaric (NPH) ensemble. Holding the virtual cell variables constant yields canonical averages for a cell with constant shape and volume (NhT ensemble) and holding all virtual variables constant gives a constant energy-constant cell shape (EhN) ensemble.

Atomic parameters which must be specified are the mass, charge, and initial position for each atom and the force constant and exponent for each short-range interaction term. Initial parameters for atoms and unit cell vector components are listed in the file **crystals**.

Run parameters and output file toggles are taken from the auxiliary file **NPT.in.(fileno)**, with **(fileno)** an arbitrary character string which is used to label the run and which is automatically appended to the name of each output file. An **NPT.in.** file with typical input parameters

```
--------input parameters for NPT.c--------------------
--------                                        --------
external temperature (Kelvin):          300
external pressure (GPa):                  3.0
no. of samples:                         200
integrations per sample time:             5
time per integration (femtoseconds):      0.5
unit cell:                              zirc_mc
force routine:                           FMM
integration routine:                     Gr 4
no. of unit cells per MD cell edge:       2
seed:                                     1
Q(mass for 'virtual' time variable):      1.5e-21
W(mass for 'virtual' volume variables):   1.5e-21
constant time variable (s):               no
constant volume variables (a,b,c):        no
quench virtual variables:                 no
output files:
   NPT.x.[fileno] (atomic positions):     yes
   NPT.e.[fileno] (system energies):      yes
   NPT.sp.[fileno] (time variables):      yes
   NPT.abc.[fileno] (cell dimensions):    yes
   NPT.m.[fileno] (animation source):      no
   NPT.av.[fileno] (system averages):     yes
   NPT.nn.[fileno] (near neighbors):      yes
   NPT.pdist.[fileno] (momenta dist.):    yes
--------                                        --------
```

Figure 6: Typical input file for program **NPT**.

is given as Figure 6. Pressure may be any floating-point number, while temperature must be a positive integer. The available choices for the force routine are *ewald* and *FMM*(planewise method). Choices for the integration routine are *RK 4* and *Gr 4*. The *no. of cells per unit cell edges* is used to create MD cells by stacking unit cells along the lattice vectors; the number of atoms in the simulation is the number of atoms in the unit cell times the cube of this parameter. *Seed* is the input to a random number generator used in setting the initial atomic momenta. Output toggles are set by specifying *yes* or *no* for each file. If the file input is *yes* then the program will generate that output file. Files which normally take data from previous runs also recognize a *restart* input, which causes the earlier run data to be ignored.

To begin a simulation, the program run command is **NPT start (fileno)**. A subsequent command of **NPT cont (fileno)** causes the program to continue from the end of the previous run so that the output is that of a continuous, uninterrupted run. New parameters may be introduced

during the simulation by continuing with **NPT cont (fileno) (infile)**. In this case the program will resume with new parameters taken from the file **NPT.in.(infile)**. A flow diagram is given as Figure 7.

The output file **NPT.x.(fileno)** is the record file. Initial parameters and atomic and virtual coordinates and momenta are recorded at the start of a run, and final coordinates and momenta are recorded at the end of the first and each consecutive run. New parameters are listed whenever a change is made during a run. Since the parameters are read from the **.x** file instead of the initial input file, a continued run will retain the parameters of the previous run and parameter changes need not be reintroduced. The accumulated simulation time is also listed in this file.

Energy values for each sample are placed in **NPT.e.(fileno)**. Total energy, potential energy and kinetic temperature are tabulated. The total energy is conserved by the equations of motion, so that variations in this quantity are indicative of the accuracy of the integration routine. The kinetic temperature is defined as

$$T \equiv \frac{2KE}{3Nk_B}$$

In this expression, KE is the kinetic energy of the atoms, k_B is Boltzmann's constant, and N is the number of atoms.

Sampled values for the virtual time variable and its conjugate momentum are listed in **NPT.sp.(fileno)**. Values of the cell vector components at each sample time are listed in **NPT.abc.(fileno)**. **NPT.m.(fileno)** contains a list of particle positions and parameters for use in a graphic display of the particle motion.

Averages and standard deviations for various functions of the coordinates and momenta are tabulated in **NPT.av.(fileno)**. The magnitude of each virtual variable is included along with volume, energy and pressure terms. Kinetic, potential and total energy averages are separated into real and virtual components and kinetic energies are listed for each virtual variable. The corresponding kinetic temperature is given for each kinetic energy average. Averages of the total energy of the system and each independent component of the microscopic pressure tensor are also listed. Figure 16 in Chapter 6 is an example of this file.

Pair correlation data is placed in **NPT.nn.(fileno)**. Tabulated values for a given pair type and separation distance include all distinct pairs at each sample time. Totals are kept for separations up to a preset cutoff (usually 10 Angstroms). This data is primarily intended as an input file for a graphics program. In the output graph, the near neighbor numbers are divided by the square of the separation distance so that the values approach a constant asymptotic limit as the distance increases. Several examples of graphical output are given in Chapter 6.

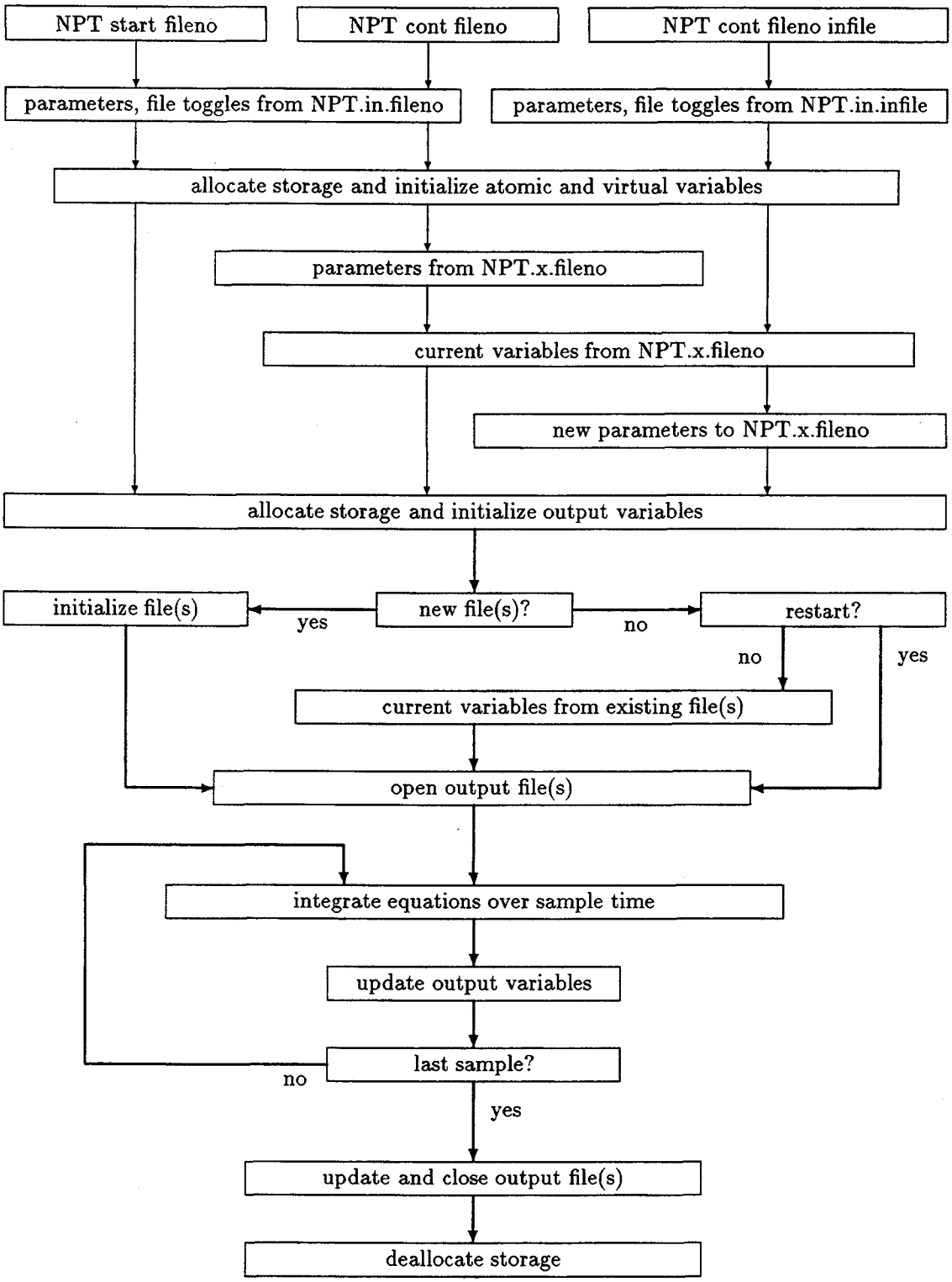

Figure 7: Main flow diagram for program **NPT**.

Momentum samples are tabulated in **NPT.pdist.(fileno)**. This data is also used primarily as input for a graphics program; examples of the output are given in Figure 2 in Chapter 3 and also in Chapter 6. The momentum data represents the number of atoms with a given total momentum at each sample time. The momenta are normalized by mass so that atoms with different masses contribute equally to the totals. The 'most probable momentum' used to scale the graphics output is calculated for the temperature set in the input file and does not necessarily correspond to that of the tabulated data. The ideal Maxwell-Boltzmann distribution plotted with the sampled values is constructed by requiring that the ideal curve have the same average kinetic energy as the sampled data and that the areas under the sampled and ideal curves are equal. The 'kinetic temperature' on the graph is calculated from the sampled data.

5-2 Program Structure

The programming language used is ANSI C[71]. Each atom and each virtual variable is assigned to a structure which holds all current data for that atom or variable. Information in each atomic structure includes the atomic type (given by the element symbol), mass, charge, position and momentum and their derivatives, and forces. Virtual structures are similar except that there is no associated charge and the information describes one dimension instead of three. The atomic structures are arranged in an array with length equal to the total number of atoms. Storage for the atomic array is allocated within the program, so that any number of atoms can be accommodated without resetting any internal program parameters.

Storage for other variable-length arrays and optional output variables are also allocated by the program as required. The memory required by the program is thus held to a minimum while input parameters remain flexible. Variables are initialized as part of the allocation routine.

The unit cell parameters used to initialize the atomic and virtual cell parameters are defined in the auxiliary file **crystals**. Each set of unit cell parameters is collected in a separate structure, and a particular unit cell can be selected by using the structure name as the *unit cell* parameter in the **NPT.in.(fileno)** file.

The structure definitions are rather lengthy, and have been placed into a file labelled **NPTdef**. This file also contains definitions of constants and abbreviations of commonly used expressions. **NPTdef** and **crystals** are referenced from the main part of the program with an **#include** statement.

Inappropriate input parameters in either start or continuation run commands or input files results in program termination accompanied by an explanatory error message. Faults in storage

allocation routines result in similar messages.

Due to the length of the program code, a number of subroutines are in files separate from the main program file, **NPT.c**. Subroutines used to control program flow or intitialize the principle data structures are contained in **NPTa.c**. Integration and storage allocation subroutines are in **NPTb.c**, and output file subroutines are in **NPTc.c**. There are 4451 lines in the complete program.

A graphics program for each output file, except record and average files, provides screen displays and plotter outputs of the sampled and tabulated data. Selection of data included in the output is generally made through arguments appended to the run command.

The program **xEgraph.c** displays data from **NPT.e.(fileno)** in a window environment. The run command **xEgraph (fileno) t** produces a plot of the kinetic temperature values at each sample time. The command **xEgraph (fileno) pe** produces a similar plot of the potential energy data from the same file.

Data from **NPT.sp.(fileno)** is plotted by the program **xSpgraph.c**. The command **xSpgraph (fileno)** produces a plot of the virtual time variable at each sample time. If **ps** is appended to the run command, the conjugate momentum is plotted instead.

Plots of the cell parameters and volume are produced by **xVgraph.c** with data taken from **NPT.abc.(fileno)**. The volume at each sample time is plotted with the run command **xVgraph (fileno)**. If one or more of the MD cell vector components **ax**, **bx**, **by**, **cx**, **cy**, or **cz** is appended to the run command, the sampled values of the appended components are plotted instead of the volume. For example, the run command **xVgraph (fileno) ax** produces a plot of the x component of the MD cell vector $\vec{a}$, and **xVgraph (fileno) ax by cz** plots on a single graph the x,y,and z components of $\vec{a}$,$\vec{b}$,and $\vec{c}$ respectively.

The file **NPT.m.(fileno)** is the input for the program **mds3d.c**. This program produces a three-dimensional display of the particles in motion. The display includes double-buffering and does not operate within a window environment. The run command is **mds3d (fileno)**.

The graphics programs associated with the **.nn** and **.pdist** output files are **Ngraph.c** and **Pgraph.c** respectively. **Ngraph (fileno) (pairtype)** and **Pgraph (fileno)** produce pair correlation and momentum distribution functions from **NPT.nn.(fileno)** and **NPT.pdist.(fileno)**. The **(pairtype)** appended to the **Ngraph** command is the name of a particular atomic pair, eg **Zr-Zr** or **Zr-O**.

Graphics programs utilize the Hewlett-Packard Starbase graphics language and will run only on machines which support this language. Programs also include commands which reference the X Window System version 11 although the number of references is relatively small and the

programs could be altered to run in a different windows environment with a minimal number of changes.

The total number of lines in the graphics programs is 1415.

5-3 Integration Subroutines

Subroutines for the numerical integration of the first-order differential equations were written with Runge-Kutta, Gear, and Adams[72] predictor-corrector algorithms. Of these, a sixth-order Gear routine used the least amount of computation time for given error tolerances but was numerically unstable for moderately large integration intervals. The fourth-order Gear routine does not show this instability while run time is about half that of the Runge-Kutta routine.

The Gear predictor-corrector algorithms achieve their accuracy by using values of variables and their derivatives from previous time steps to calculate the corrector. Because of this, these routines require only one force calculation for each integration. This is in contrast to the Runge-Kutta method, which requires four force calculations, and traditional predictor-corrector routines, which require two or more.

The fourth-order Gear routine **Gr4** uses values from the two previous integrations, so another routine must be used to obtain the first two sets of data. The Runge-Kutta subroutine **RK4** is used for this purpose. The extra storage needed to hold the two additional sets of coordinates, momenta and derivatives is provided by increasing the dimension of the atomic and virtual structure arrays from one to three. The same amount of storage is provided for the Runge-Kutta subroutine, which uses the additional storage to hold temporary values generated during integration.

While calculations made outside the integration routines generally change the values of current variables only, the subroutine **xcenter** also operates on the values from previous time steps. If the motion of an atom results in translation through a lattice vector, values from previous runs must also be translated in order to maintain continuity in the Gear routines.

Implementation of both Gear and Runge-Kutta algorithms is most convenient if the variables and their derivatives are arranged in linear arrays. The two subroutines **artos** and **stoar** transfer values between the linear arrays used in the algorithms and the atomic and virtual structure arrays.

5-4 Energy and Force Calculations

Long-range Coulomb interactions are calculated by the Ewald method or by planewise summation depending on the descriptor in the input file, *ewald* or *FMM*. The error tolerance of each of these routines is adjusted through internal parameters located at the beginning of each subroutine. Energy values are calculated if required by the **.av** or **.e** output files and do not affect the numerical integration of the equations of motion.

The Ewald method energy and force routines **ecoulomb** and **fcoulomb** use the equations of Appendix C to calculate the Coulomb terms over a truncated lattice sum. The lattice indices are set by the internal parameter M_{ew}. This is the same parameter used to estimate the numerical precision in the previous chapter; it is the maximum absolute value of any index.

A number of expressions in the lattice sums are independent of the atomic positions and are precalculated in a preliminary lattice summation. These values are stored in arrays with size proportional to $(2M_{ew}+1)^3$. Storage is allocated in the routine so that alteration of static array parameters is not necessary if M_{ew} is changed.

The free parameter in the Ewald equations is set equal to $\sqrt{\pi}/a_x$, with a_x the length of the lattice vector $\vec{a}$. The error functions are calculated by subroutines which use either a continued fraction or a series algorithm depending on the magnitude of the argument.

Short-range energy and forces are calculated by a direct sum over the same lattice indices used for the Coulomb sums. Expressions for the short-range energy and forces are given in Appendix G.

The multipole subroutines **eFMM** and **fFMM** calculate the long-range Coulomb energy and forces by the planewise summation method. An internal parameter in the subroutine **Rmax** sets the radius of a sphere about the origin as a multiple of the length of the maximum MD cell diagonal. All periodic translations of the MD cell which have their origin within this sphere are referred to as 'near neighbors'. Coulomb and short range energies and forces due to atoms in near neighbor cells are calculated directly. A direct calculation is also made for the compensating charges on the cell faces which form at the surface of the near neighbor volume. The equal and opposite charges which would cancel these charges within the near neighbor volume are contained in the multipole moments of the adjacent cells and so a net charge remains to be accounted for at these locations.

The index of the highest order terms included in the multipole sums is equal to the internal parameter μ_{max}. Multipole moments for the atomic and compensating charges and their derivatives are computed by the subroutines **mpole** and **dmpole**. Lattice sums are calculated

in the subroutine **PSM** according to the equations of Appendix D. Since the planewise sums include contributions corresponding to multipoles at the near neighbor sites, multipole sums for the near neighbors are calculated directly and subtracted from the planewise results. The planewise summation indices are set by the internal parameter M_{PSM}, again the same parameter used previously to characterize the numerical precision.

The planewise sums include a preliminary calculation of expressions which are independent of the multipole indices. Incomplete gamma functions are computed with a continued fraction algorithm.

The accuracy of the energy routines were ascertained by comparing the results of the two methods with each other and with published values of the Madelung constant for NaCl. The energies computed by different methods were found to have the same values to a precision of at least ten decimal places for NaCl and eight decimal places for monoclinic and tetragonal zirconia. Different unit cell definitions were tried in the tetragonal cell, and the differences in the total calculated values were used to help define the precision. The most accurate value found for the Madelung constant of NaCl, given by Slater[57], contains only six decimal places. Both methods give results that are consistent with this value.

Forces routines were tested by total energy calculations at each integration step. Both routines conserve the total energy of the system to a precision of at least ten decimal places. Drift due to the integration algorithms make it difficult to check the accuracy to any greater precision.

The short-range interactions tabulated in the **crystals** file are selected for each atom pair by comparing the atomic labels with the interaction labels. The interaction terms need have no particular order or number, although the total number of short-range interaction terms must be included with the values of the initial unit cell dimensions. The units of the force constants in the **crystals** file are those most conveniently used in the force routines. If an interaction potential is written with energy in Hartrees and distances in atomic units, the force constant for each interaction term in **crystals** is obtained by multiplying the constant in units of Hartree-(au)^n by a_0^{n-1}, a_0 being the Bohr radius in Angstroms.

5-5 Hardware

A Hewlett-Packard model 9000/835SRX workstation was used for writing and debugging simulation and graphics programs. This machine performs double precision operations at 2.0 Mflops. Standard RAM capacity is 8MB. Added accessories include an additional 8MB RAM

and an HP98721A graphics accelerator with a 16-plane frame buffer for graphics rendering. The video display is an HP model 98752A with 19" color screen and 1280x1024 pixel resolution.

Simulation runs were made on an HP Apollo series model 720 PA-RISC workstation rated at 17.0 Mflops. Memory includes 16MB RAM, 400MB on internal hard drives, and 1GB on external hard drives. The monitor is an HP model A1097 with 19" color display and 1280x1024 resolution.

Figures were plotted on an HP 7475A plotter.

Both computers are accessible through Ethernet. The address for the model 9000 is zircon.physics.orst.edu, and the Apollo series workstation is addressed as vangogh.physics.orst.edu.

Chapter 6

Results and Summary

6-1 Effective Potentials for Zirconia

The desired form for an effective interatomic potential in zirconia includes Coulomb interaction terms and short-range terms which are inversely proportional to higher powers of the separation distance between atoms. The determination of an appropriate potential involves the specification of an effective charge for each type of atom and short-range force constants for each combination of atomic species. The simplest potential of this form for zirconia has only three independent parameters: the effective valence charge on the zirconium atoms, an overall short-range force constant and a short-range inverse power exponent:

$$\begin{aligned} V_{Zr-Zr} &= \frac{z^2e^2}{r} + \frac{C}{r^n} \\ V_{Zr-O} &= -\frac{z(\frac{z}{2})e^2}{r} + \frac{C}{r^n} \\ V_{O-O} &= \frac{(\frac{z}{2})^2e^2}{r} + \frac{C}{r^n} \end{aligned}$$

The short-range constant C must be positive to provide a repulsive force between atoms. This is a soft-sphere potential corresponding to a system in which all atoms have the same size. As shown previously, a potential of this type with $n = 10$ produces a stable cubic crystal which does not undergo structural phase transitions with changes in the external temperature and pressure.

Introducing different crystal radii for the zirconium and oxygen atoms adds only one additional parameter to the potentials. The short-range constants are defined in terms of the zirconium radius σ_{Zr} and the oxygen radius σ_O as

$$\begin{aligned} C_{Zr-Zr} &= C(\sigma_{Zr} + \sigma_{Zr})^n = A(\frac{2\beta}{1+\beta})^n \\ C_{Zr-O} &= C(\sigma_{Zr} + \sigma_O)^n \equiv A \\ C_{O-O} &= C(\sigma_O + \sigma_O)^n = A(\frac{2}{1+\beta})^n \\ \beta &\equiv \frac{\sigma_{Zr}}{\sigma_O} \end{aligned}$$

According to Pauling[74], the effective ionic crystal radius for Zr^{4+} is 0.80Å and the crystal radius for O^{2-} is 1.40Å, so that $\beta = 0.57$. The assignment of the larger radius to the more mobile oxygen atoms is in contrast to the usual case for superionic conductors, in which a smaller mobile ion is considered to diffuse through a lattice of larger, less mobile ions.

The regularity of the charge density contours[38] in monoclinic zirconia suggests that steric effects play at least some role in the determination of the crystal structure. These contours are shown in Figure 8. Monoclinic zirconia is seen to be composed of layers of oxygen atoms separated by layers of zirconium atoms. The oxygen atoms are generally classified as O_I or O_{II} corresponding to the two inequivalent oxygen positions in the crystal. The layers of O_I atoms and the layers of Zr atoms form essentially square two-dimensional lattices. The O_{II} layers can be viewed as a set of squares which have been rotated to form a two-dimensional lattice of adjacent squares and triangles. The Zr atoms are coordinated to the O_{II} triangles on one side and the O_I squares on the other, resulting in the seven-fold coordination of Zr in the monoclinic crystal. A stable structure based on steric effects alone would be one in which a decreased energy due to a smaller separation between the Zr atoms and the O_{II} atoms outweighs the increased energy of a larger separation between the Zr atoms and a fourth O_{II} atom. The smaller coordination would be possible if the zirconium radius is smaller than the oxygen radius.

The determination of the equilibrium crystal structures which are possible with soft-sphere potentials is an interesting question in its own right, and one that can be answered in a straightforward manner through use of the program **NPT**. The results of an investigation into soft-sphere crystal structures are summarized in the next section. It is seen that the soft-sphere potentials do not produce any of the phases of zirconia except the cubic phase. In the following section, a potential which produces the monoclinic structure of zirconia is tested.

6-2 Soft-Sphere Ionic Crystals

The soft-sphere potential energy for a collection of ions is written as

$$U = \frac{1}{2}\sum_{ij}\sum_{\alpha\beta\gamma}{}' \left\{ \frac{z_i z_j e^2}{r_{ij\alpha\beta\gamma}} + C\left(\frac{\sigma_i + \sigma j}{r_{ij\alpha\beta\gamma}}\right)^n \right\}$$

In order to study the equilibrium crystal structures which result from this type of expression, the exponent n was set equal to 10 and the effective valences for the zirconium and oxygen atoms were set at +4 and -2 respectively. The atoms were placed in the equilibrium positions of the cubic zirconia crystal and the overall short-range force constant was adjusted to minimize the forces on the virtual lattice variables. The potential energy of the system was then minimized

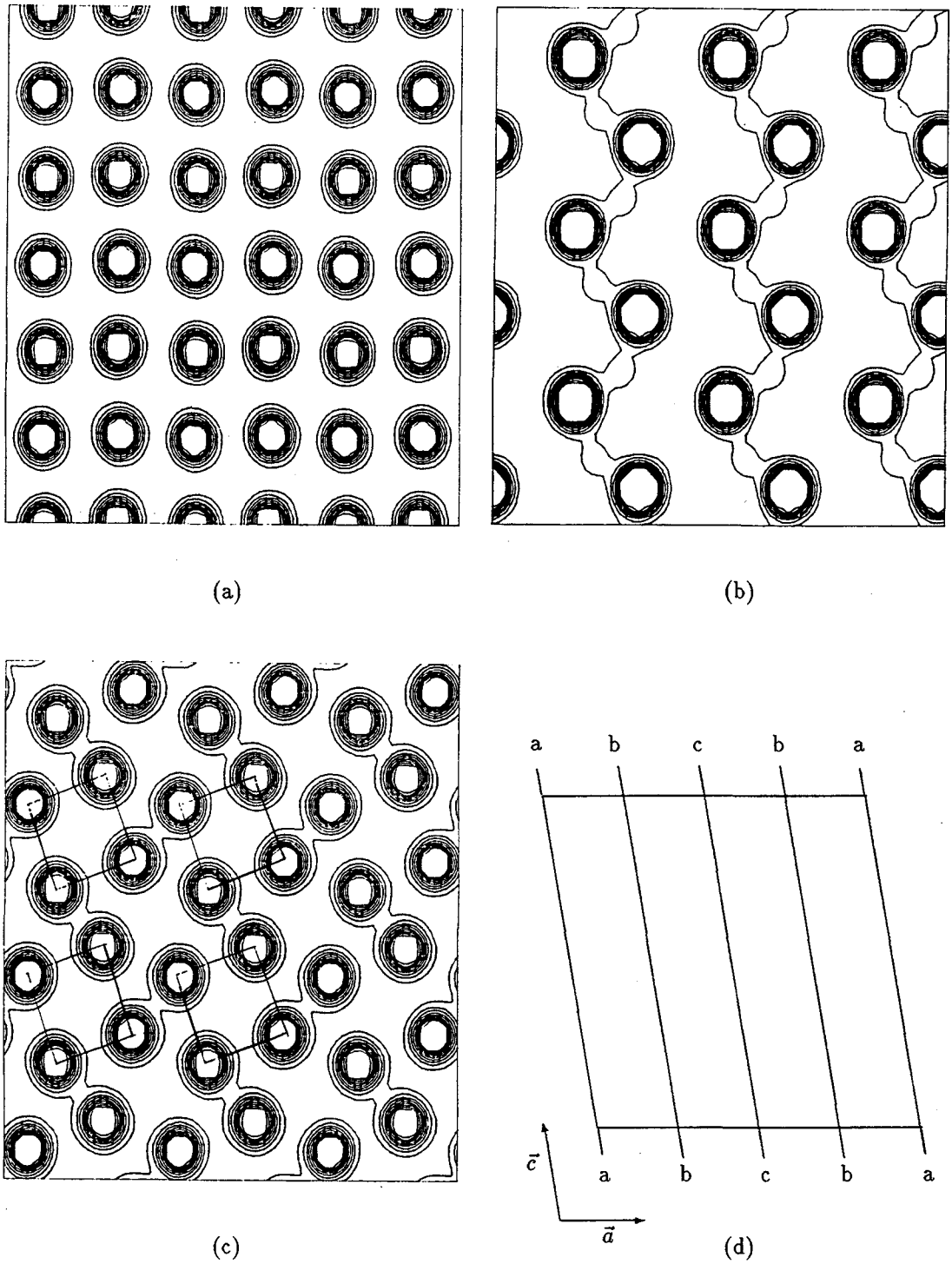

Figure 8: Charge density contours for monoclinic zirconia: (a)O_I atoms; (b)Zr atoms; (c)O_{II} atoms; (d) location of sections in crystal.

by running the program **NPT** with variable cell shape and a starting temperature of 2K. The kinetic energy was removed after each twenty time steps by resetting all real and virtual momenta to zero. This procedure was repeated for values of the zirconium-oxygen radius ratio β between 0.41 and 3.5, yielding several different minimum energy structures.

For $\beta \geq 0.8$, the structures remained in the original fluorite configuration, hereafter designated 'cubic I'. In this structure the coordination number for the zirconium atoms is 8. The zirconium atoms form an FCC lattice while the oxygen atoms are in a simple cubic configuration. A structural diagram and an oxygen-oxygen pair correlation plot for this crystal are given in Figure 9. In the structural diagram, the smaller circles represent zirconium atoms and the larger circles are oxygen atoms. The numbers within the circles are the fractional unit cell coordinates perpendicular to the plane of the paper. This notation is common to all of the structural diagrams in this section.

With $\beta = 0.78$ or 0.79, the unit cell remained cubic but the positions of the oxygen atoms shifted so that the Zr-O coordination changed from 8 to 6. This 'cubic II' structure is shown in Figure 10, along with the associated O-O pair correlation diagram.

All crystals with $0.52 \leq \beta \leq 0.77$ were minimized to an orthorhombic unit cell, with the zirconium lattice distorted from that of the fluorite structure and the oxygen atoms rearranged to give a Zr-O coordination of 6. The oxygen atoms form approximate hexagonal close-packed lattices with c/a ratios from a maximum of 1.69 for β=.75 to a minumum of 1.65 for β=0.52, slightly larger than the 'ideal' HCP c/a ratio of 1.63. The crystal structure is similar for all radius ratios in this range. The structure and O-O pair correlations are shown in Figure 11.

With $\beta = 0.45$ and $\beta = 0.48$, the system minimized to the tetragonal structure shown in Figure 12. In this configuration the Zr-O coordination is 4.

Finally, for $\beta = 0.414$, a cubic phase with a Zr-O coordination of 4 was obtained. This phase is designated here as 'cubic III'. The structure and O-O pair correlations are displayed in Figure 13. In this phase the oxygen atoms have achieved a close-packed FCC configuration. The zirconium atoms form a BCC lattice with a lattice constant that is equal to the oxygen lattice constant.

These results are expected to be generally representative of the minimum energy structures for compounds with the formula AB_2, since the atomic masses do not affect the equilibrium positions. A change in the effective valences or overall short-range force constant is equivalent to a change in scale, so that variation of either of these parameters will change the equilibrium volume but not the crystal structure.

The effect of varying the exponent n can be assessed to at least some degree by comparing

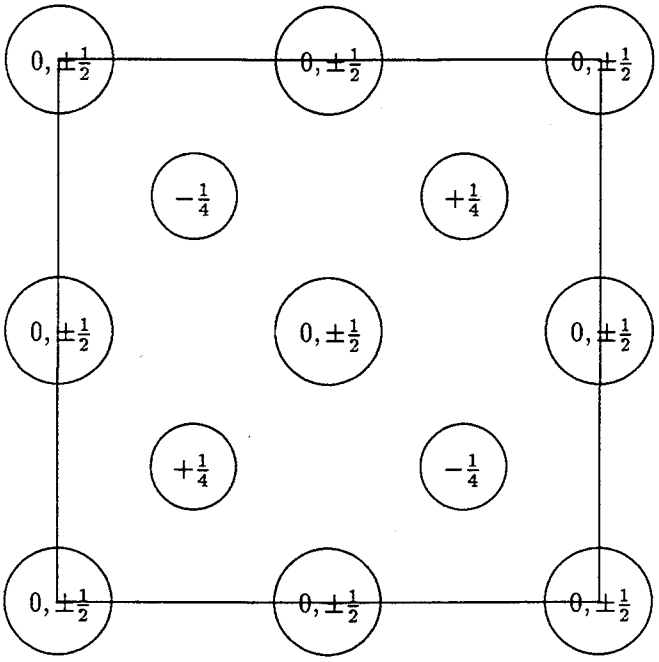

(a)

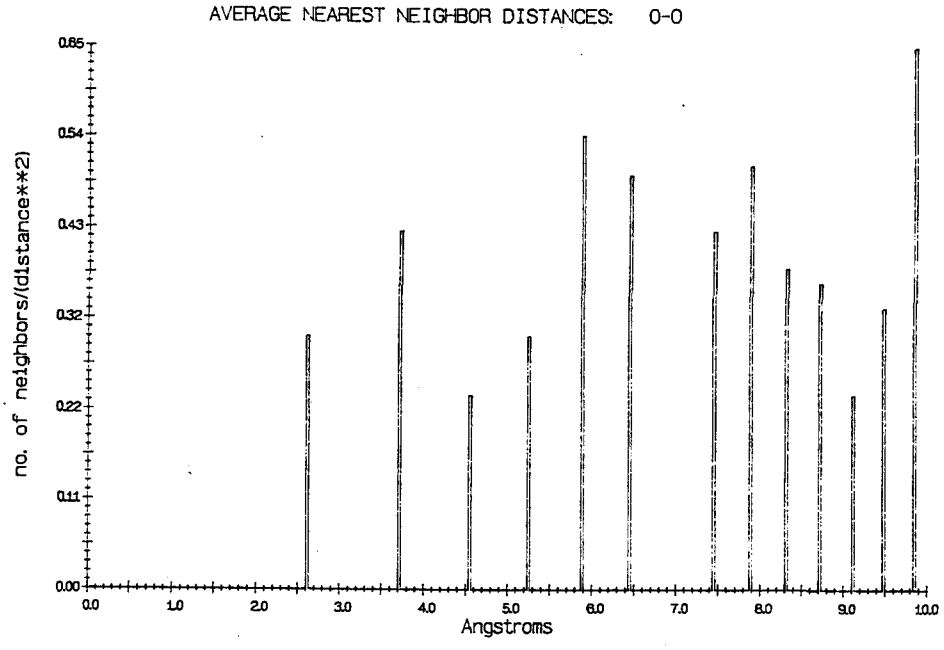

(b)

Figure 9: Crystal structure and pair correlations for $\beta \geq 0.8$.

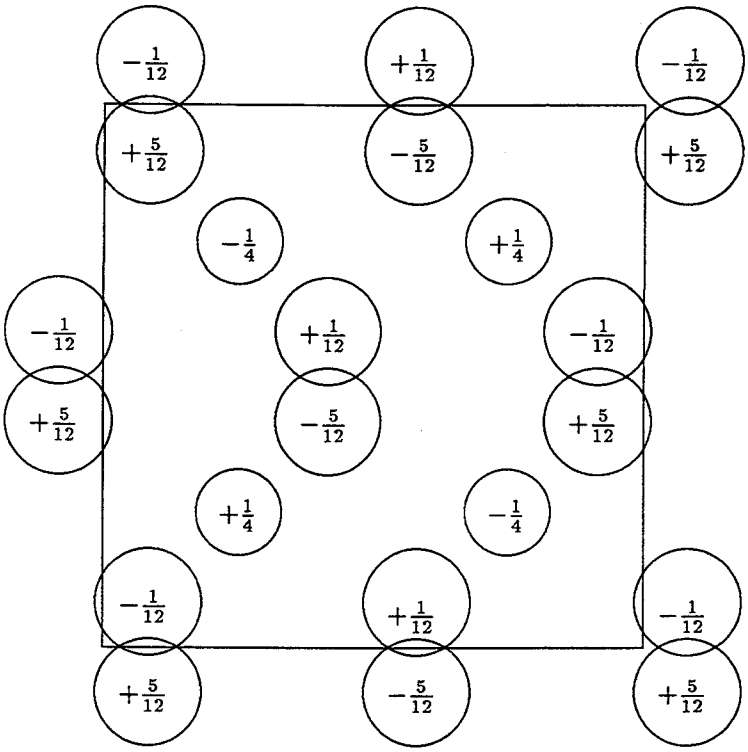

(a)

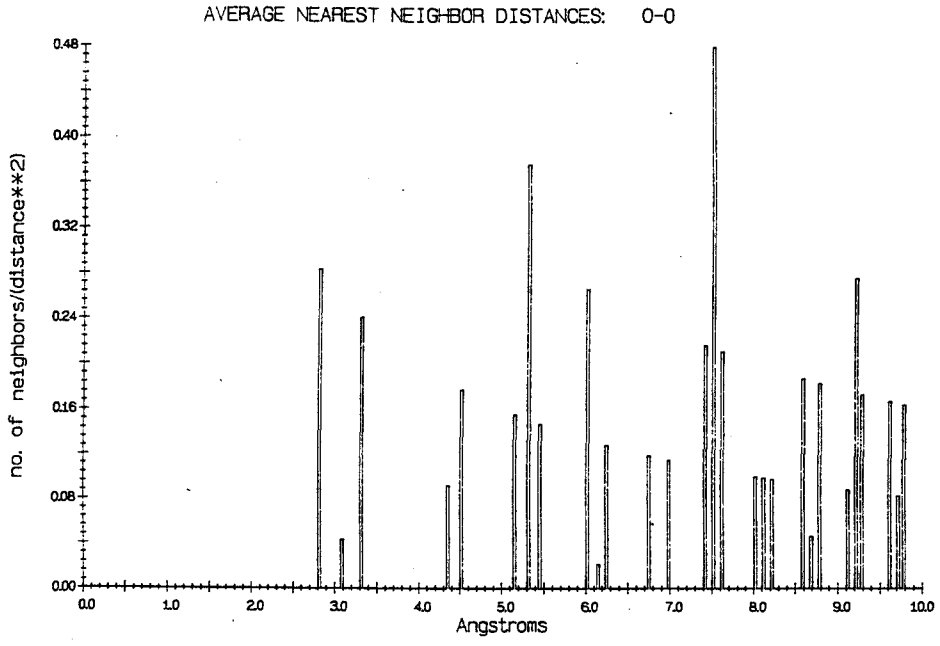

(b)

Figure 10: Crystal structure and pair correlations for $\beta = 0.78$.

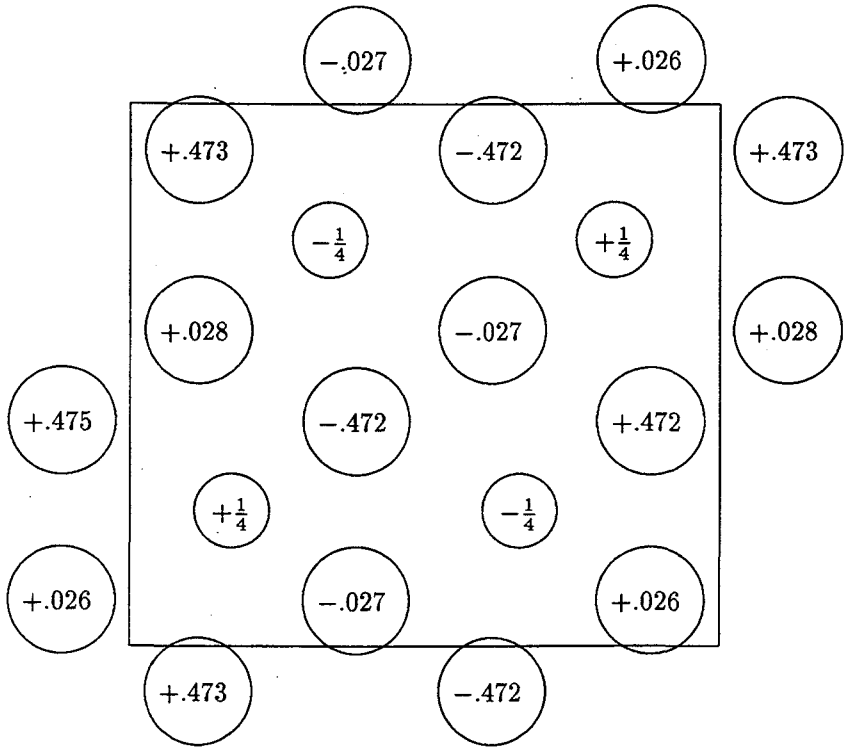

(a)

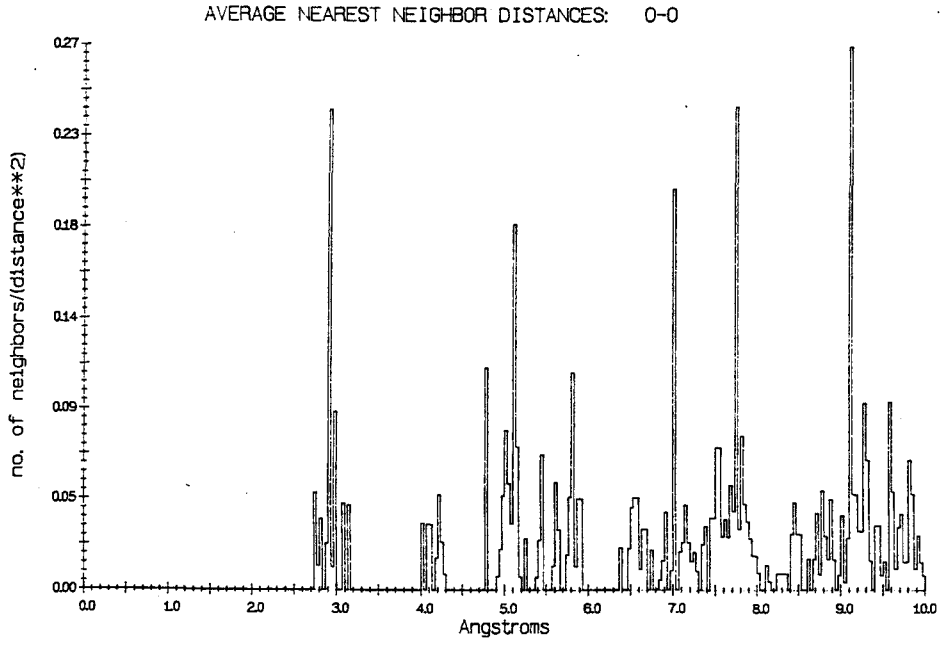

(b)

Figure 11: Crystal structure and pair correlations for $\beta = 0.73$.

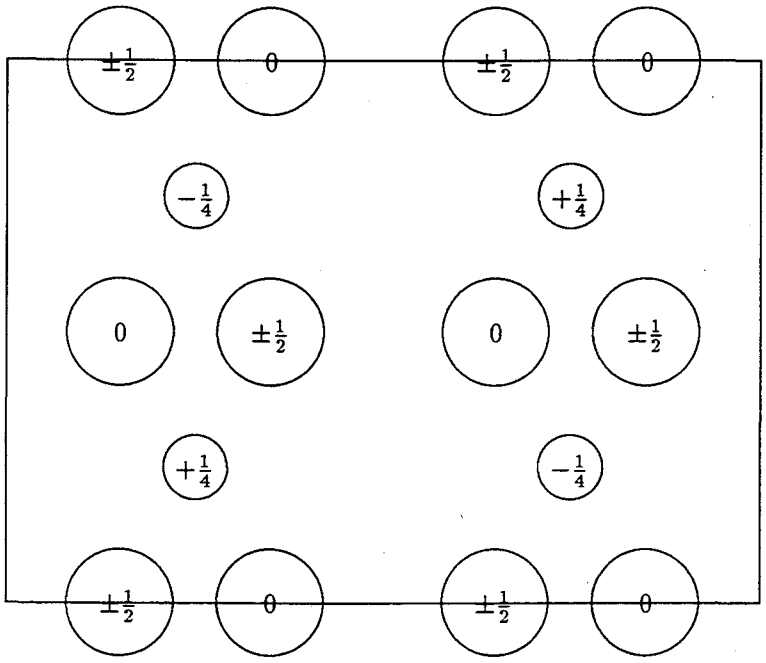

(a)

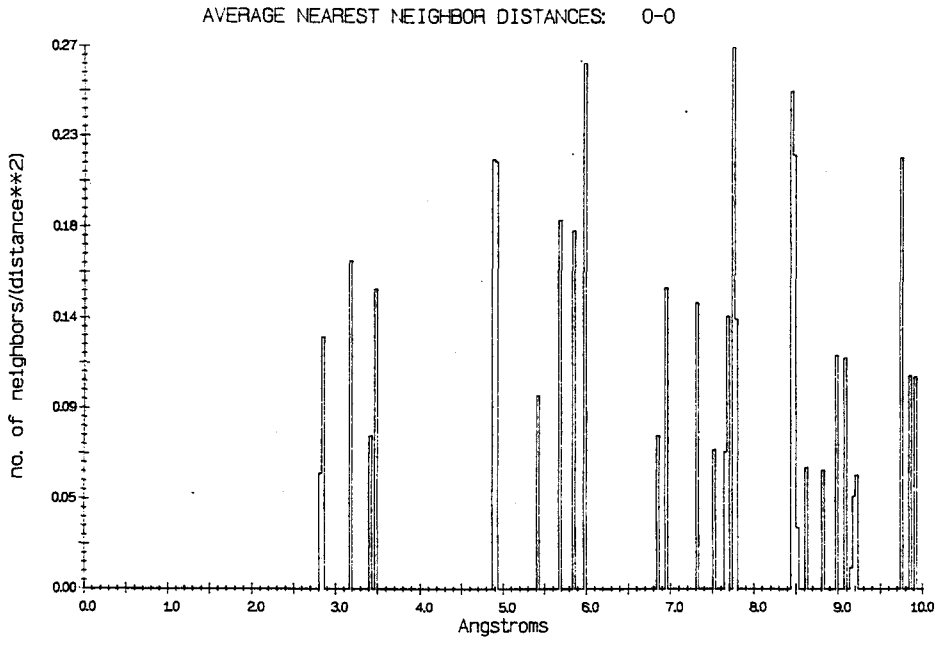

(b)

Figure 12: Crystal structure and pair correlations for $\beta = 0.48$.

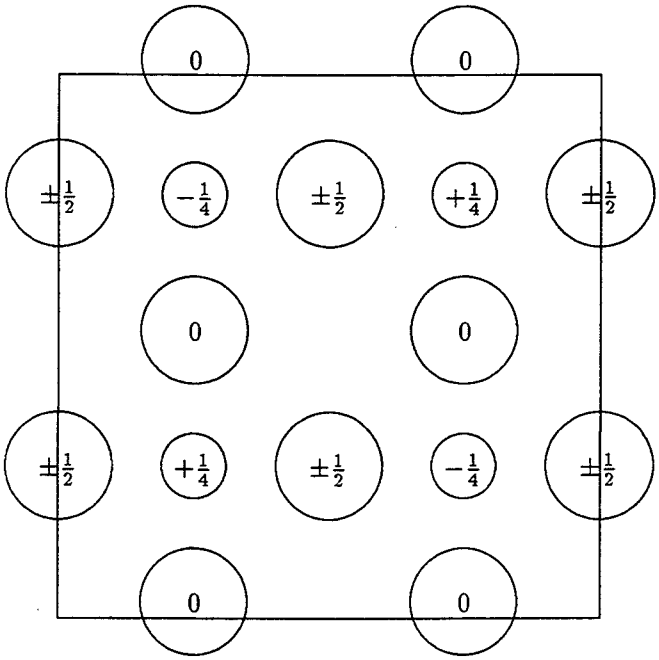

(a)

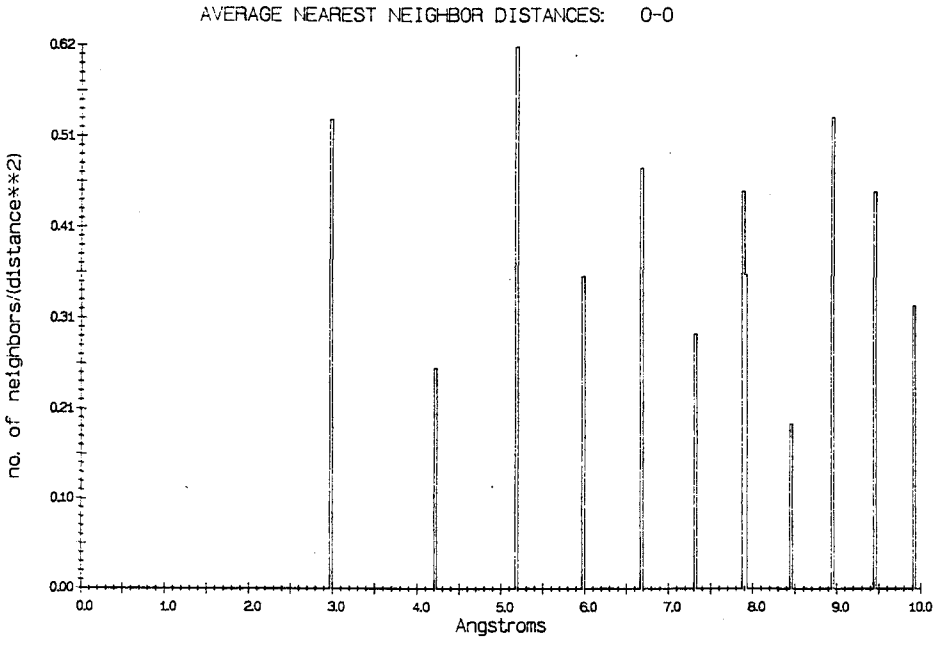

(b)

Figure 13: Crystal structure and pair correlations for $\beta = 0.414$.

the soft-sphere results to the limiting case of a hard-sphere potential ($n \rightarrow \infty$). The coordination numbers for hard-sphere systems can be found analytically by assuming that the smaller ions will be surrounded by the largest possible number of larger ions[75], resulting in coordination numbers of 4 for $0.225 < \beta < 0.414$, 6 for $0.414 < \beta < 0.732$, 8 for $0.732 < \beta < 1.0$, and 12 for $\beta = 1.0$. The last case is that for close-packed spheres and is not directly applicable to AB_2 compounds. In general, the soft sphere structures change coordination at values of β which are slightly higher than those predicted for hard spheres. Also, the simple analysis of the hard-sphere situation predicts only one crystal structure for a given coordination number.

Results for soft-sphere crystal structures are summarized in Table 9. Lengths are given in Angstroms. This tabulation may not be complete, since other structures are possible with $\beta < 0.414$ and intermediate structures such as the 'cubic II' crystal found for $\beta = 0.78$ and 0.79 may exist for $0.48 < \beta < 0.52$. It is also possible that the final structure depends on the initial conditions and that some or all of the structures found may represent local rather than global energy minima. The consistency of the results within the various ranges of β even when the final cell orientations differ suggests that this is not the case.

Dynamic stability and temperature and pressure dependence of the soft-sphere structures were investigated by performing NPH simulations at temperatures of approximately 100K, 1000K, and 2000K at zero external pressure and at 100K with an external pressure of 30GPa. The simulations were started in the minimum-energy structures found for β equal to 0.414, 0.48, 0.52, and 0.75. The unit cell contained the minimal number of 12 atoms, which was judged sufficient for determination of the general properties of the potentials. Equilibrium was achieved relatively quickly in most cases. In all cases but two, simulations were continued until the momenta distribution gave a good approximation of the Maxwell-Boltzmann curve and all cyclical variables were observed to have constant averages. The exceptions were the simulations at zero pressure and at 30GPa with kinetic temperatures of 100K for β equal to 0.48. In all other respects these two simulations appeared to produce stable averages, but the momenta did not appear to be approaching thermal equilibrium even after repeated quenching of the virtual momenta before continuations of the simulation. This cannot be due to any effects of a virtual time variable, since this variable was held constant throughout all of the simulations.

Results of the dynamic simulations are shown in Table 10. Lengths are again in Angstroms. The values listed under each cell vector component on lines labelled 'α' are the linear thermal expansion coefficients calculated from the values of the preceding line. The expansion coefficients are found to be somewhat anisotropic while the magnitudes are of the same general order as that of most real crystals. For simulations with the external pressure set to zero the average internal

β	a_x	b_y	cz	*volume*	*structure*
0.414	5.97	4.22	5.97	150.4	*cubicIII*
0.45	7.08	4.84	4.84	165.8	*tetragonal*
0.48	6.86	4.92	4.92	166.1	"
0.52	5.81	4.79	5.13	142.8	*orthorhombic*
0.60	5.82	4.85	5.27	148.8	"
0.70	5.88	4.93	5.39	156.2	"
0.73	5.90	5.42	4.96	158.6	"
0.75	5.90	4.98	5.44	159.8	"
0.76	5.91	5.44	4.99	160.4	"
0.77	5.91	5.00	5.45	161.0	"
0.78	5.31	5.31	5.31	149.7	*cubicII*
0.79	5.32	5.32	5.32	150.6	"
0.80	5.26	5.26	5.26	145.5	*cubicI*
0.85	5.26	5.26	5.26	145.5	"
0.95	5.26	5.26	5.26	145.5	"
1.00	5.26	5.26	5.26	145.5	"
1.20	5.26	5.26	5.26	145.5	"
3.50	5.26	5.26	5.26	145.5	"

Table 9: Crystal structures for soft-sphere potentials.

pressures are not exactly zero in all cases, indicating that there is some internal stress in the crystal. This may explain in part the resistance of the low-temperature simulations for $\beta = 0.414$ to achieve thermal equilibrium, but it should be noted that in all cases with zero external pressure the fluctations in the internal pressure are greater in magnitude than the average pressures listed here. In the high-pressure simulations, the pressure fluctuations were much less than the pressure averages.

With two exceptions, the structures retained the original crystal symmetry under all of the imposed conditions. A typical example of a stable structure is given by the simulation results for β equal to 0.52 at 1000K and zero pressure. The momentum distribution and oxygen-oxygen pair correlations are shown in Figure 14. The time evolution of the volume and the MD cell lattice vectors are shown in Figure 15, and the output file containing the average values of the dynamic variables is given in Figure 16. It can be seen from the volume and lattice vector component plots that the structure reached equilibrium rather quickly. A comparison of the pair correlation plot with that of Figure 11(b) shows a structure differing from the minimum-energy configuration only by the broadening and overlap of the peaks. Zirconium-zirconium and zirconium-oxygen pair correlations show the same correspondence.

In the case of β equal to 0.48 at 100K and 30GPa, a phase transformation was observed from the tetragonal phase to the orthorhombic soft-sphere structure. The O-O pair distribution function for this case as well as that for β equal to 0.48 at 100K and zero pressure are shown for comparison in Figure 17. The similarity of the high-pressure structure to the orthorhombic structures is even more evident if Figure 17(b) is compared to Figure 14(b), the corresponding plot for β=0.52 at 1000K. The averages of the lattice vector components also show the change from the tetragonal to the orthorhombic structure. The structural changes in these simulations represents a clear departure from that possible with hard-sphere potentials, since hard spheres are by definition incompressible.

A phase transition was also observed for β equal to 0.52 at 2000K and zero pressure. During the course of the simulation the volume expanded to approximately three times that of the original unit cell and the unit cell became monoclinic. The structure was relatively slow to stabilize, and the simulation time required for completion of the structural change was much longer than the time required by the other cases. The evolution of the volume and the lattice parameters are shown in Figure 18.

These simulation results demonstrate that soft-sphere potentials are capable of generating pressure- and temperature-dependent phase transitions, and it would be interesting to generate a full set of phase diagrams with β, T and P as parameters. There are clearly transitions beyond

β	$T(K)$	$P(GPa)$	a_x	b_y	cz	*volume*	*structure*
0.414	0		5.97	4.22	5.97	150.4	*cubicIII*
	165	1.6	5.97	4.22	5.97	150.7	"
	976	0.7	5.98	4.25	5.98	151.9	"
α			$1.4x10^{-6}$	$6.1x10^{-6}$	$1.9x10^{-6}$		
	1906	0.4	6.01	4.26	6.01	153.5	"
α			$4.7x10^{-6}$	$2.3x10^{-6}$	$4.5x10^{-6}$		
	195	32.0	5.89	4.16	5.89	144.3	"
0.48	0		6.86	4.92	4.92	166.1	*tetragonal*
	573	1.4	7.41	4.88	4.88	176.5	"
	1053	1.1	7.44	4.90	4.90	178.3	"
α			$9.3x10^{-6}$	$5.1x10^{-6}$	$6.0x10^{-6}$		
	1907	0.1	7.48	4.91	4.92	180.4	"
α			$6.1x10^{-6}$	$3.8x10^{-6}$	$4.3x10^{-6}$		
	242	29.8	5.72	4.70	5.00	134.3	*orthorhombic*
0.52	0		5.81	4.79	5.13	142.8	*orthorhombic*
	74	0.0	5.81	4.79	5.13	142.8	"
	944	0.0	5.86	4.83	5.14	145.5	"
α			$9.9x10^{-6}$	$8.6x10^{-6}$	$2.5x10^{-6}$		
	1990	0.0	14.16	6.28	5.41	481.0	*monoclinic*
	81	30.1	5.70	4.70	5.08	136.2	*orthorhombic*
0.75	0		5.90	4.98	5.44	159.8	*orthorhombic*
	53	0.0	5.91	4.98	5.44	160.0	"
	965	0.0	5.92	5.00	5.46	161.5	"
α			$1.8x10^{-6}$	$5.0x10^{-6}$	$3.3x10^{-6}$		
	1923	−0.1	5.93	5.03	5.48	163.2	"
α			$2.3x10^{-6}$	$5.2x10^{-6}$	$3.4x10^{-6}$		
	57	30.4	5.80	4.90	5.35	151.8	"

Table 10: Dynamic simulation results for soft-sphere potentials

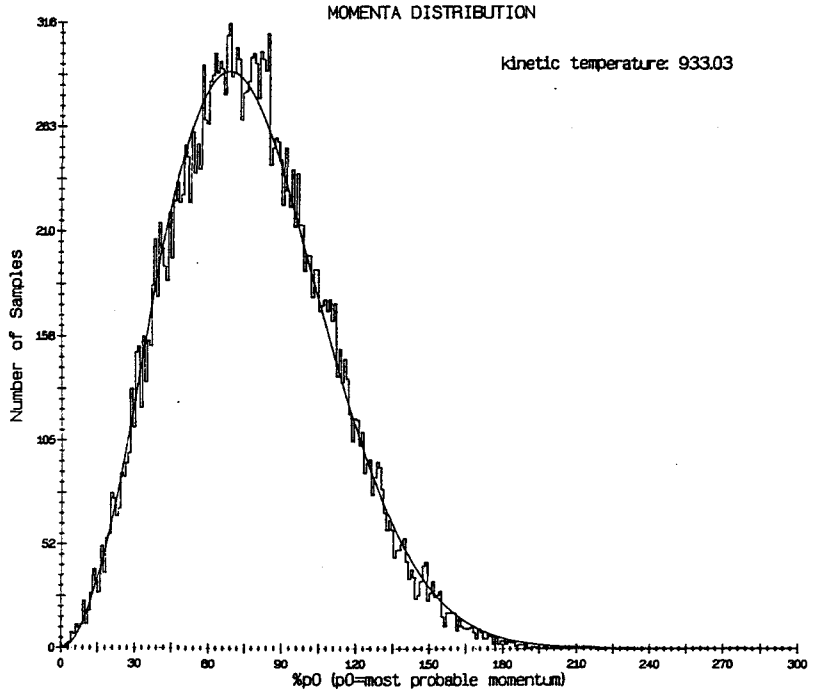

(a)

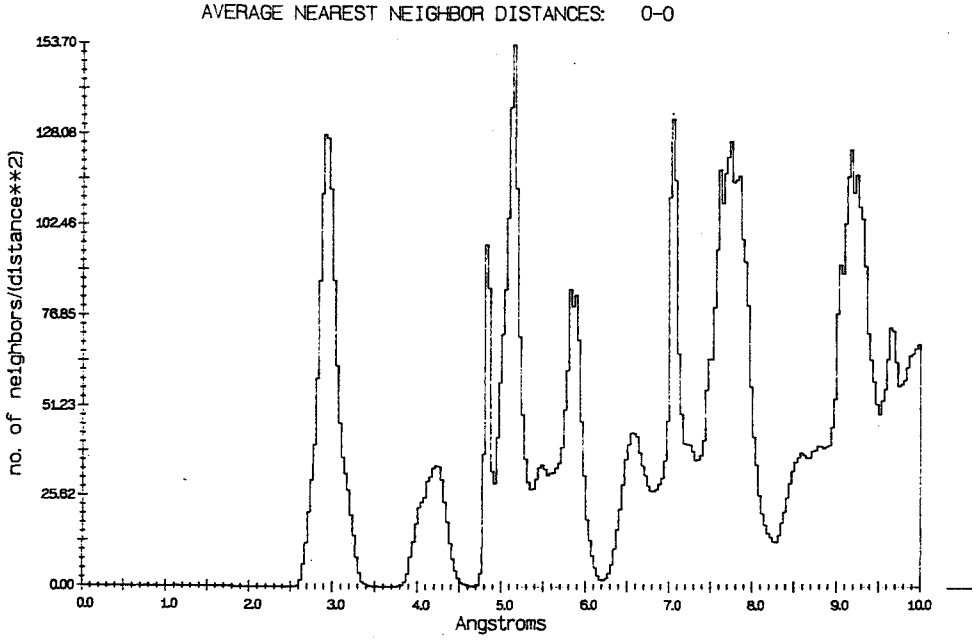

(b)

Figure 14: $\beta = 0.52$,T=1000K,P=0:(a) momentum distribution; (b) oxygen-oxygen pair correlations.

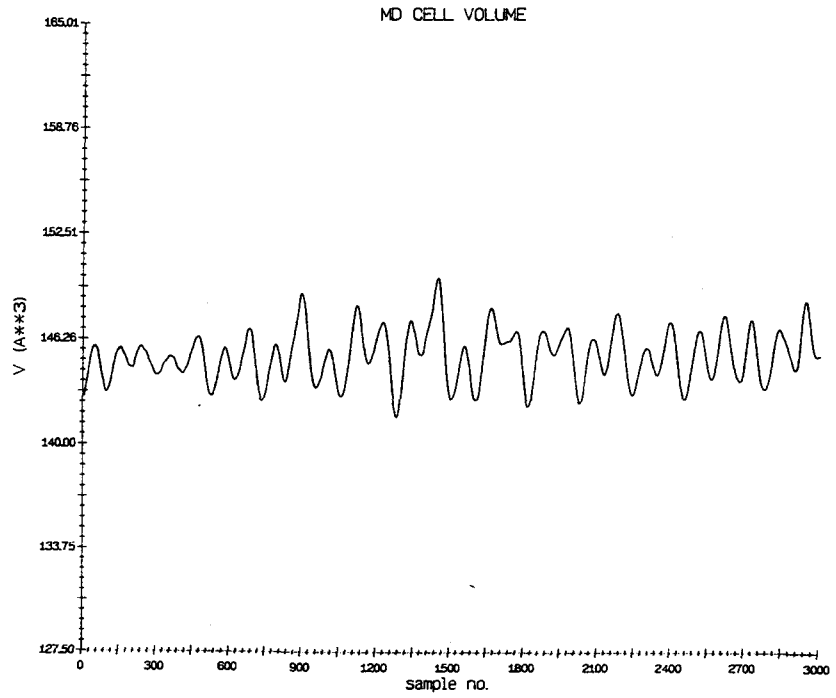

(a)

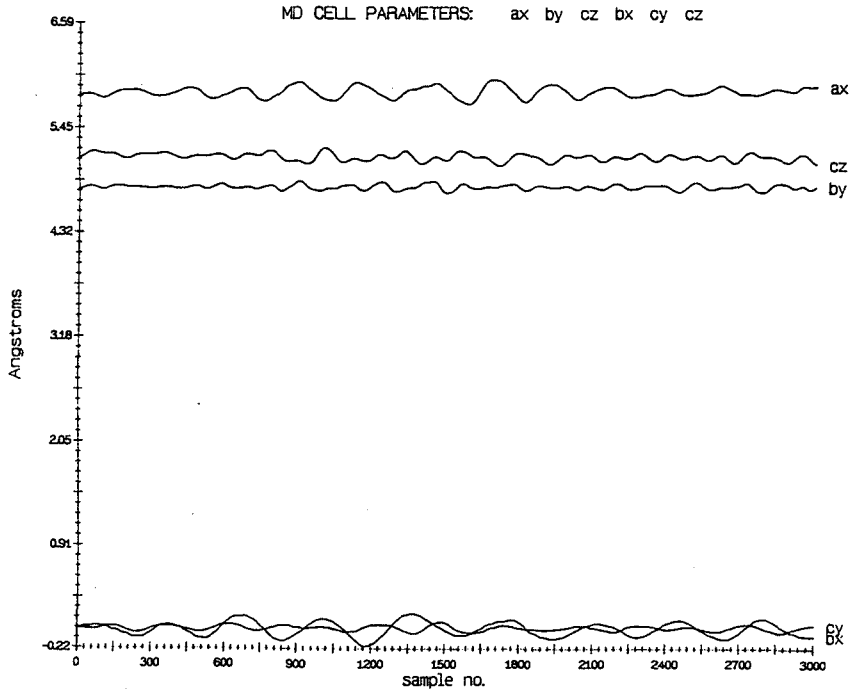

(b)

Figure 15: $\beta = 0.52$,T=1000K,P=0:(a) volume; (b) unit cell lattice vector components.

NPT.av.32

samples	variable	<A>	sqrt(<A*A>-<A>*<A>)	kinetic temp (deg K)
1001				
	s	1.00000000e+00	0.00000000e+00	
	ax	5.83915396e+00	4.92148201e-02	
	bx	-1.17834457e-02	7.59906650e-02	
	by	4.81535545e+00	2.06904739e-02	
	cx	-4.94574494e-03	3.53029530e-02	
	cy	2.09263976e-03	2.50957033e-02	
	cz	5.15447211e+00	3.17965960e-02	
	vol	1.44927258e+02	1.21716025e+00	
	ke re	1.53417205e-02	2.71382662e-03	988.713
	pe re	-4.81542882e+00	2.70902615e-03	
	etot re	-4.80008710e+00	4.32073256e-04	
	ke vi	5.57955735e-04	4.03562031e-04	184.927
	pe vi	0.00000000e+00	0.00000000e+00	
	etot vi	5.57955735e-04	4.03562031e-04	
	etot (ev)	-4.79952914e+00	3.79581453e-05	
	ke ps	0.00000000e+00	0.00000000e+00	0.000
	ke pax	1.31929027e-04	1.57215959e-04	306.083
	ke pbx	1.76970776e-04	1.82662425e-04	410.582
	ke pby	7.14661191e-05	1.05948380e-04	165.806
	ke pcx	3.21410822e-05	4.43349739e-05	74.569
	ke pcy	3.65784925e-05	3.53760854e-05	84.864
	ke pcz	1.08870239e-04	2.02302870e-04	252.585
	pxx (GPa)	-1.15210670e-01	6.26934557e+00	
	pyy (GPa)	3.64361029e-01	7.60397421e+00	
	pzz (GPa)	7.60256806e-02	5.86020892e+00	
	pxy (GPa)	-4.91260187e-03	6.68659506e+00	
	pxz (GPa)	4.66008641e-02	3.58348479e+00	
	pyz (GPa)	-4.19885848e-02	3.51744461e+00	
2001				
	s	1.00000000e+00	0.00000000e+00	
	ax	5.86143538e+00	5.88562852e-02	
	bx	-6.52586512e-03	8.39319726e-02	
	by	4.82593598e+00	2.76831913e-02	
	cx	1.83981408e-02	1.49267762e-01	
	cy	2.37976955e-03	2.96732328e-02	
	cz	5.14418609e+00	3.60155094e-02	
	vol	1.45508626e+02	1.59889654e+00	
	ke re	1.46383886e-02	2.40389579e-03	943.386
	pe re	-4.81545368e+00	2.43426849e-03	
	etot re	-4.80081529e+00	5.52762418e-04	
	ke vi	1.12692211e-03	5.57677323e-04	373.504
	pe vi	0.00000000e+00	0.00000000e+00	
	etot vi	1.12692211e-03	5.57677323e-04	
	etot (ev)	-4.79968837e+00	5.62657744e-05	
	ke ps	0.00000000e+00	0.00000000e+00	0.000
	ke pax	1.84668731e-04	2.46303568e-04	428.442
	ke pbx	1.60483818e-04	1.66260534e-04	372.332
	ke pby	1.25902880e-04	1.79325820e-04	292.102
	ke pcx	4.40987019e-04	4.17742803e-04	1023.115
	ke pcy	4.56699576e-05	6.08313383e-05	105.957
	ke pcz	1.69166061e-04	1.80598815e-04	392.475
	pxx (GPa)	-1.17188506e-01	6.66078259e+00	
	pyy (GPa)	2.26116067e-01	8.07547280e+00	
	pzz (GPa)	-8.66624858e-02	7.20035034e+00	
	pxy (GPa)	-1.81949507e-02	5.05364710e+00	
	pxz (GPa)	-1.37752185e-01	6.49406156e+00	
	pyz (GPa)	2.57200023e-02	3.59360603e+00	

Figure 16: $\beta = 0.52$,T=1000K,P=0: averages of dynamic variables.

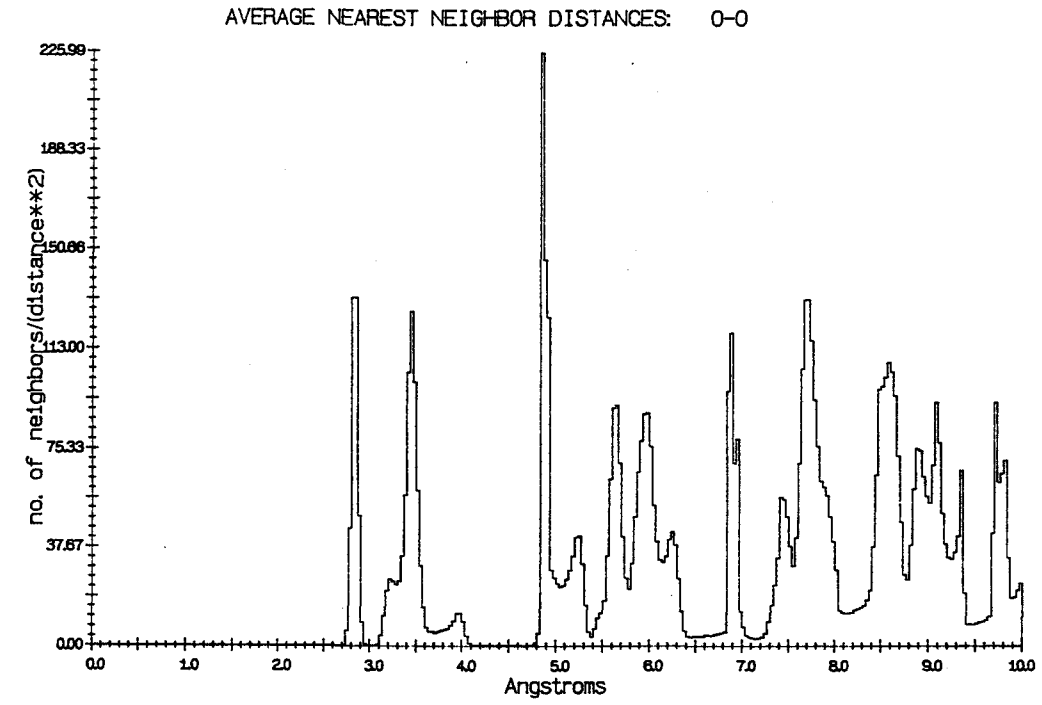

(a)

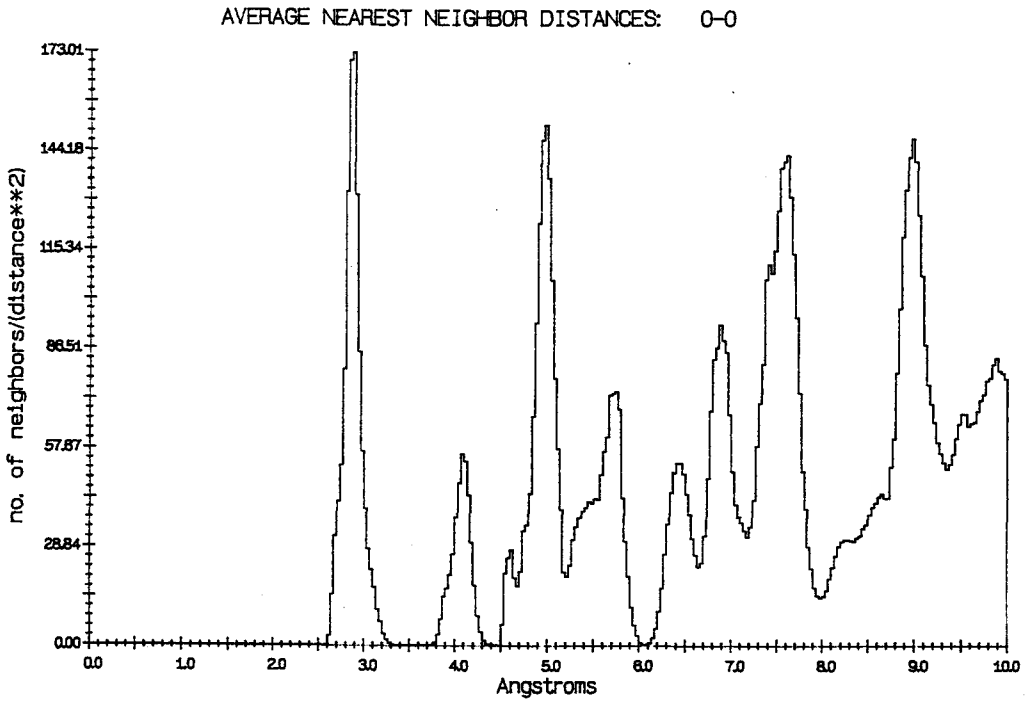

(b)

Figure 17: Low-temperature pair correlations for β=0.48 at (a) zero external pressure and (b) 30GPa external pressure.

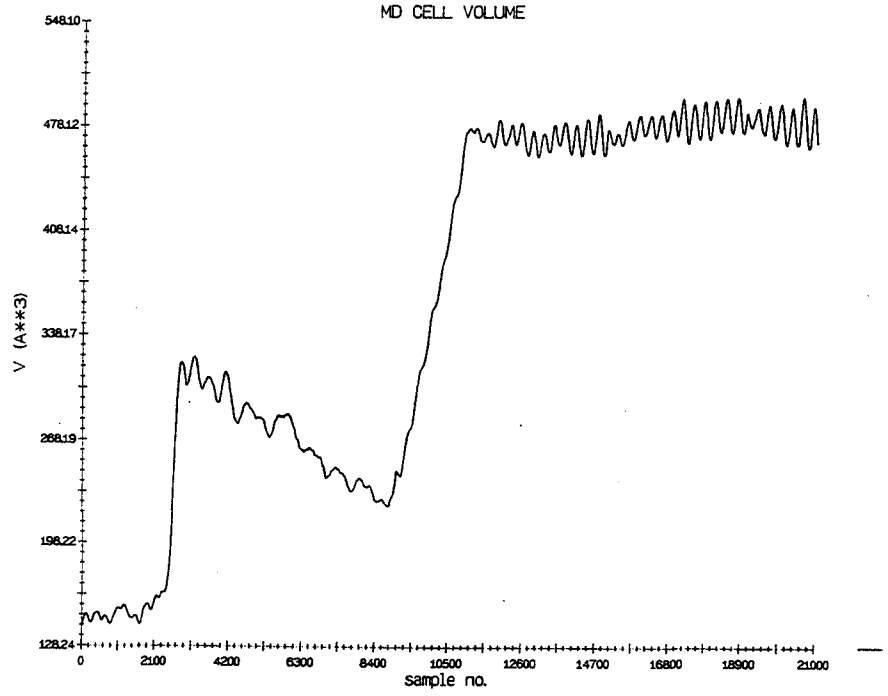

(a)

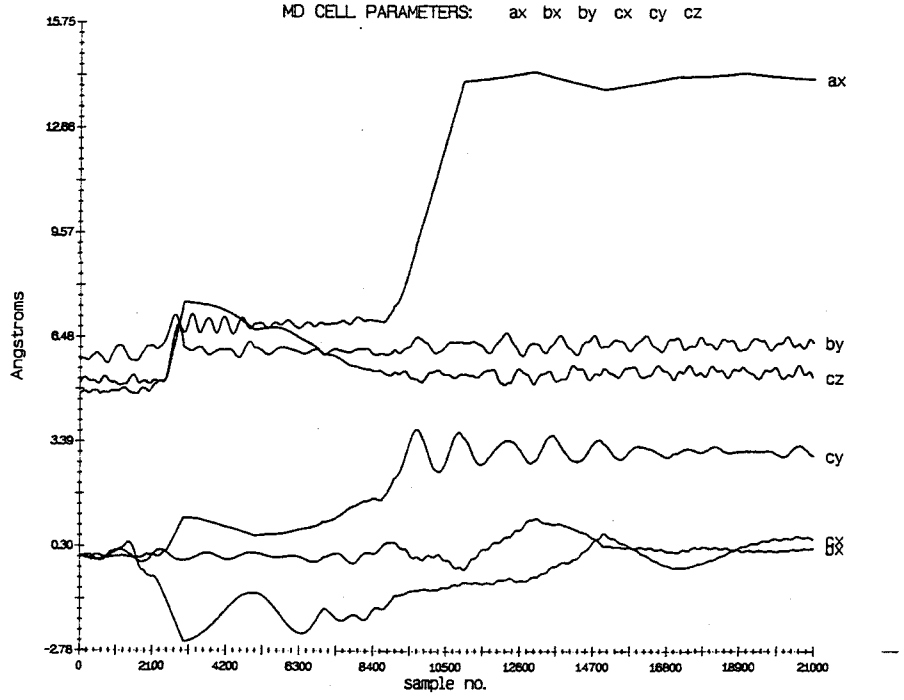

(b)

Figure 18: β=0.52 at 2000K and zero pressure: (a)volume; (b) unit cell lattice vector components.

those obtained for relatively small number of examples here. For example, at sufficiently high temperatures all of the crystals should display pair correlations indicative of melting, which was not observed in any of the simulations described here. Unfortunately, none of the structures obtained for the soft-sphere potentials seem capable of reproducing any of the low temperature or high pressure phases of zirconia.

6-3 Simulation of a Monoclinic Crystal

At the present time, the best potential available for modelling the monoclinic zirconia crystal is[76]:

$$
\begin{aligned}
V_{Zr-Zr} &= \frac{0.5266}{r} - \frac{28.24}{r^4} + \frac{3.233x10^5}{r^{10}} \\
V_{Zr-O} &= -\frac{0.2633}{r} - \frac{8.63}{r^4} + \frac{1.511x10^4}{r^{10}} \\
V_{O-O} &= \frac{0.13164}{r} + \frac{10.96}{r^4} + \frac{1.903x10^5}{r^{11}}
\end{aligned}
$$

In these expressions, distance is in atomic units and energy is in Hartrees. The constants were obtained by a numerical fit to density-functional total energy calculations for monoclinic zirconia. The Coulomb terms imply effective charges of +0.7256 for the zirconia ions and -0.3628 for the oxygen ions.

In addition to the Coulomb and short-range potentials, this potential contains terms proportional to r^{-4}. These terms represent charge-dipole interactions and are found in potentials for other ionic superconductors, such as those used in simulations of Ag_2S[43] and AgI[44]. The inclusion of these terms in the force and energy routines of the program **NPT** is accomplished by considering these to be short-range terms. This is expected to have an adverse effect on the overall precision of the force and energy calculations because of the relatively long-range nature of the r^{-4} potential. For the preliminary structural studies done here, this loss of precision is not expected be important and a cutoff radius is imposed to truncate the r^{-4} terms along with the r^{-10} and r^{-11} terms. The use of a cutoff radius for r^{-4} interactions in molecular dynamics studies is common in the literature, including the simulations of the two superionic conductors just cited.

The minimum-energy structure for the zirconia potential was obtained through the same procedure used to determine soft-sphere structures. The unit cell remained monoclinic but in

a simulation at zero pressure the components of the cell vectors did not attain stable values. When an external pressure of 310 GPa was imposed during a second minimization from the experimental structure, the structure again remained monoclinic. The stability of the high-pressure structure was investigated with an NPT simulation at 310 GPa with 12 atoms in the MD cell with temperatures of 300K, 1000K, and 2000K. Throughout these simulations the structure remained essentially unchanged. An additional simulation was performed at 3 GPa and 150K, and the high-pressure structure was again found to retain the original monoclinic symmetry. In a subsequent simulation starting from the high-pressure structure at zero pressure the components of the cell vectors again did not attain stable values. Apparently, this potential will produce a stable monoclinic crystal structure only with the application of external pressure. Zirconium-zirconium and zirconium-oxygen pair correlation plots for the static monoclinic structure are shown in Figure 19.

A larger system with 96 atoms in the MD cell was used to obtain more detailed results for the zirconia potential. The external pressure was held constant at 3 GPa and simulations were performed with NPT dynamics. The system was first brought to equilibrium at 300K, then the external temperature was reset to 2000K and the system was again brought to equilibrium. The virtual momenta were reset to zero after every few hundred samples. Momentum distributions for the system at 300K and 2000K are shown in Figure 20. Kinetic energy and potential energy plots are given in Figure 21. The evolution of the MD cell volume and lattice vector components are shown in Figure 22, and the virtual time variable and associated momentum are give in Figure 23. The effects of quenching the virtual momenta are seen as discontinuities in the slopes of the plots of the virtual variables, and in the discontinuity of the momentum associated with the virtual time variable. The pair correlation plots in Figures 24 and 25 may be compared to those of the static monoclinic crystal. It is seen that the structure is unchanged, and at 300K the effect of raising the temperture is mainly to broaden the widths of the peaks. At 2000K the structure is no longer visible. At this temperature the structure is evident only in the averages of the lattice vector components. Simulation results are summarized in Table 11. Lengths in this table are in Angstroms. The cell dimensions for the 96 atom system have been divided by two for comparison with the values obtained for 12 atoms.

The results for 96 atoms at 300K are quite similar to those for 12 atoms, which provides at least some justification for the use of the smaller MD cells to obtain preliminary results. The simulation times were 6.245 ps for 12 atoms and 11.225 ps for 96 atoms, representing about one day and two weeks, respectively, of computer run time.

The simulation of 96 atoms at 2000K was very slow to reach an internal pressure in ap-

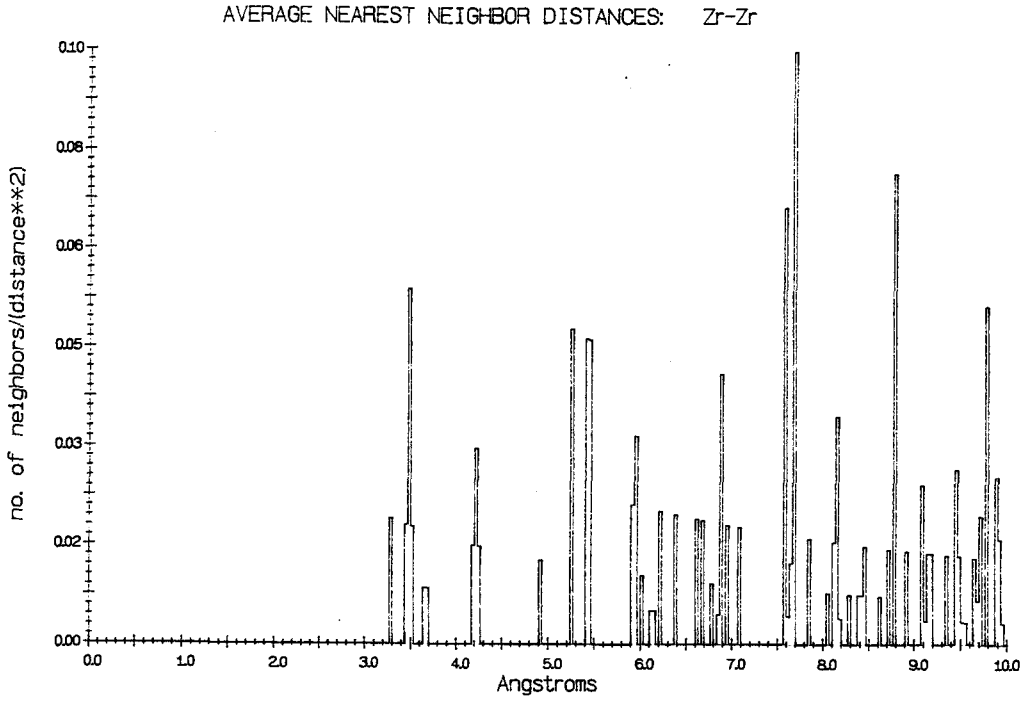

(a)

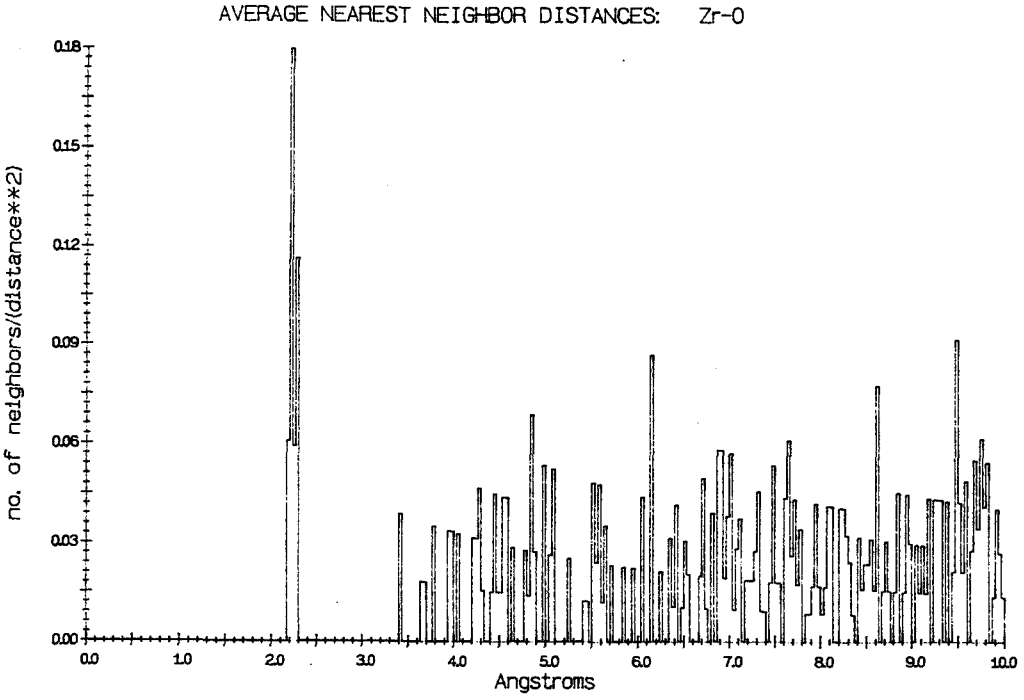

(b)

Figure 19: Pair correlations for the static monoclinic crystal: (a) Zr-Zr; (b) Zr-O.

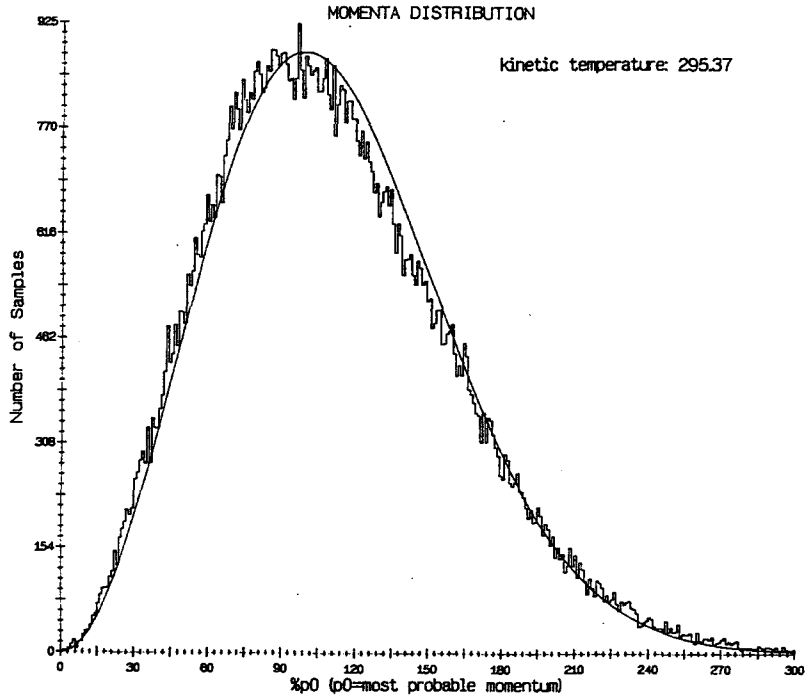

(a)

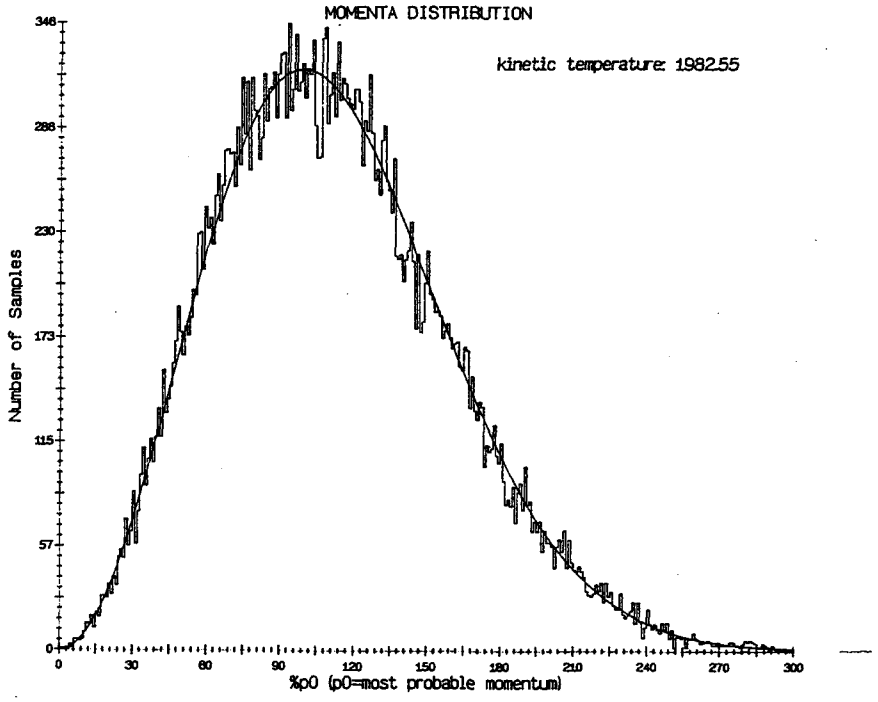

(b)

Figure 20: Momentum distributions for the monoclinic crystal: (a) 300K; (b) 2000K.

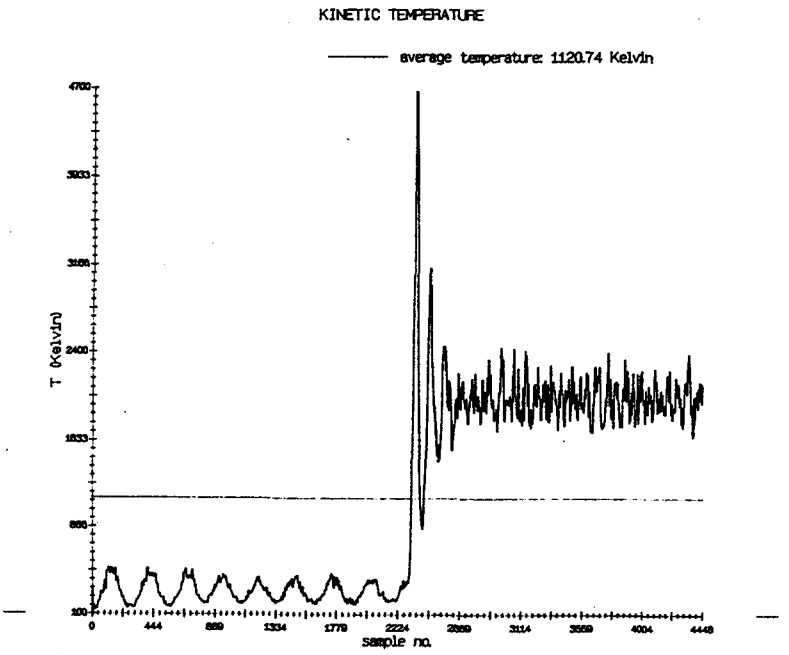

(a)

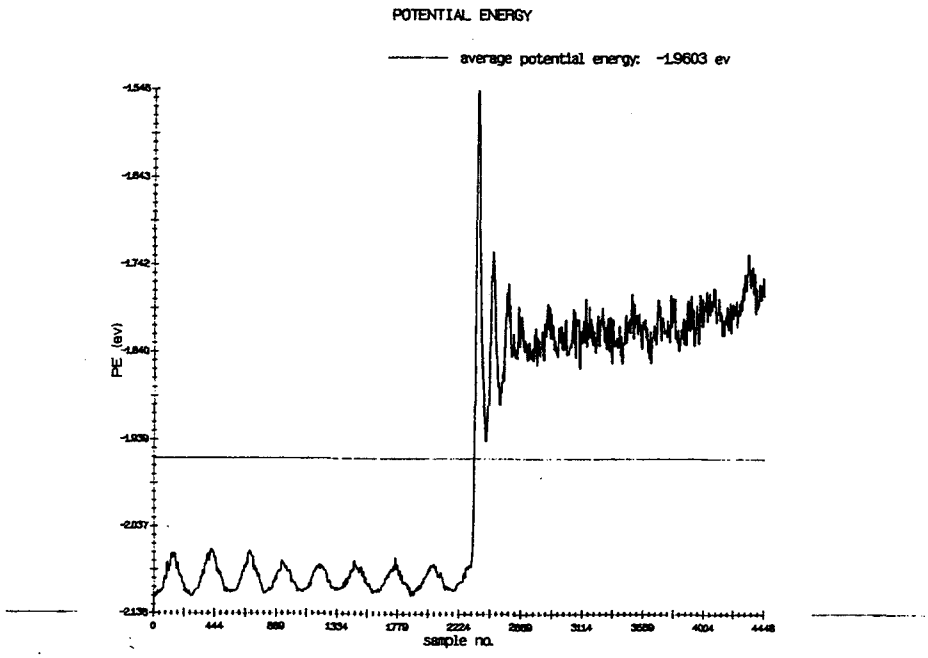

(b)

Figure 21: Total energies for the monoclinic crystal: (a) kinetic energy; (b) potential energy.

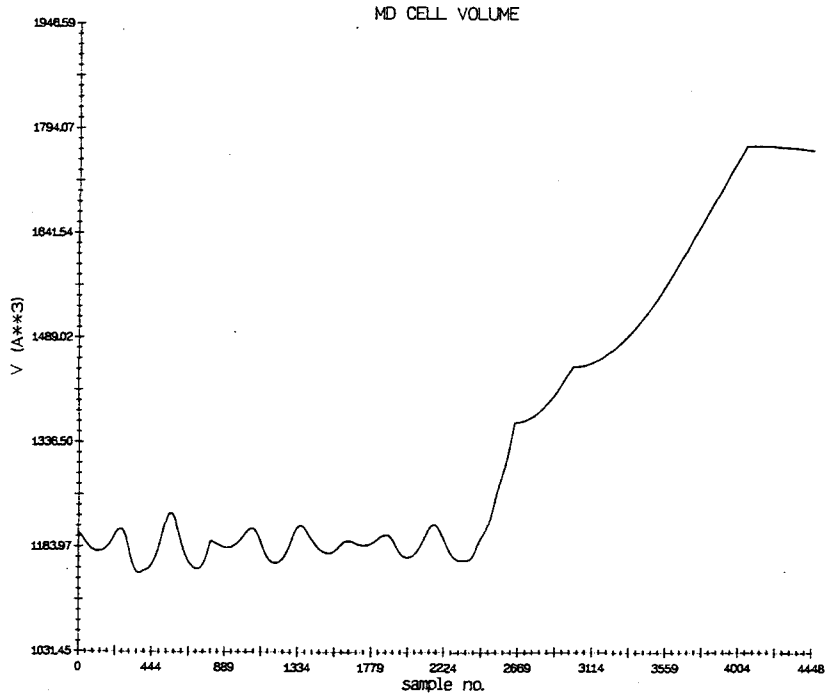

(a)

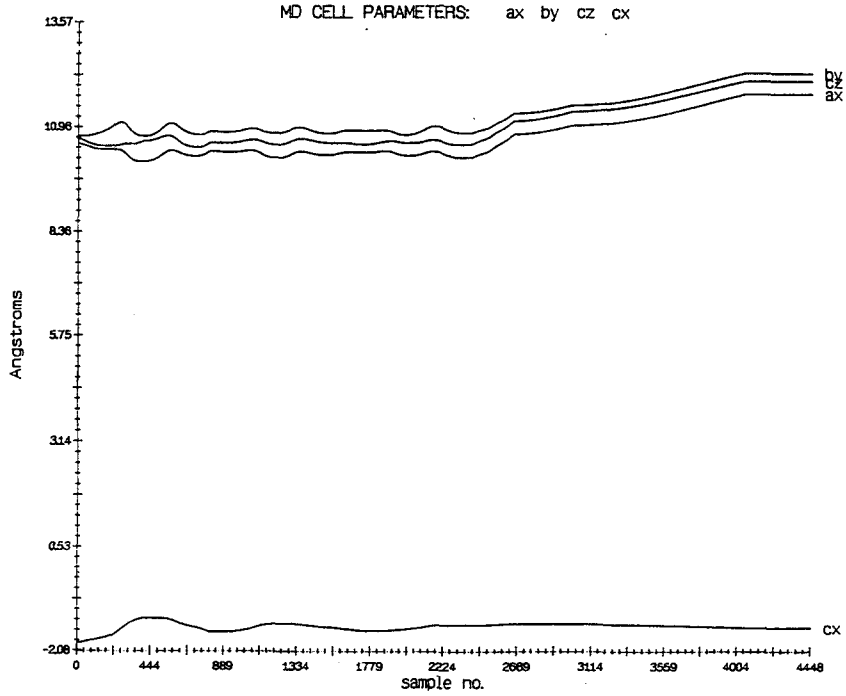

(b)

Figure 22: Lattice parameters for the monoclinic crystal: (a) volume; (b) unit cell lattice vector components.

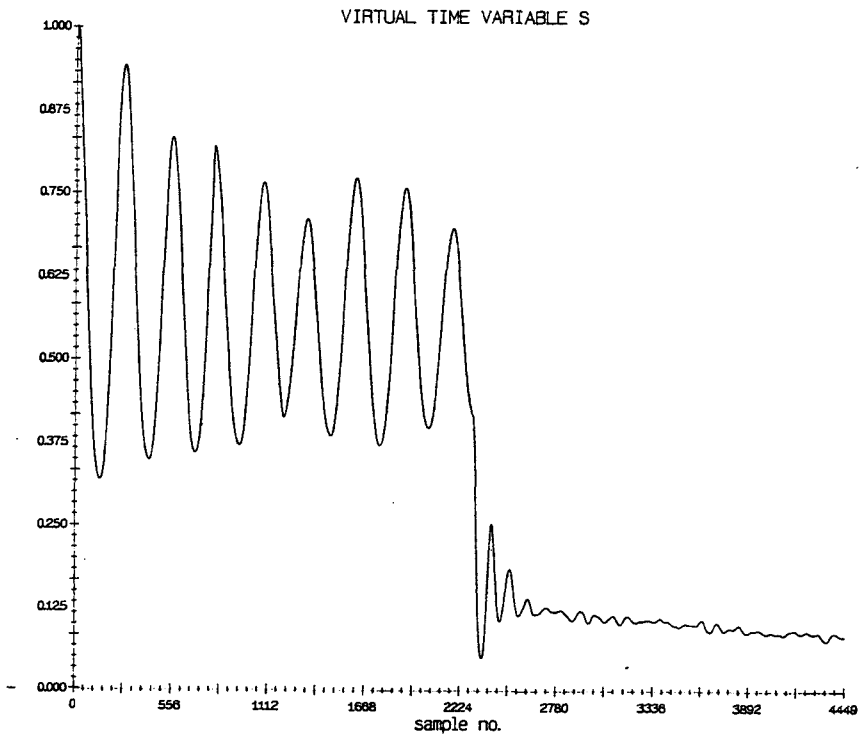

(a)

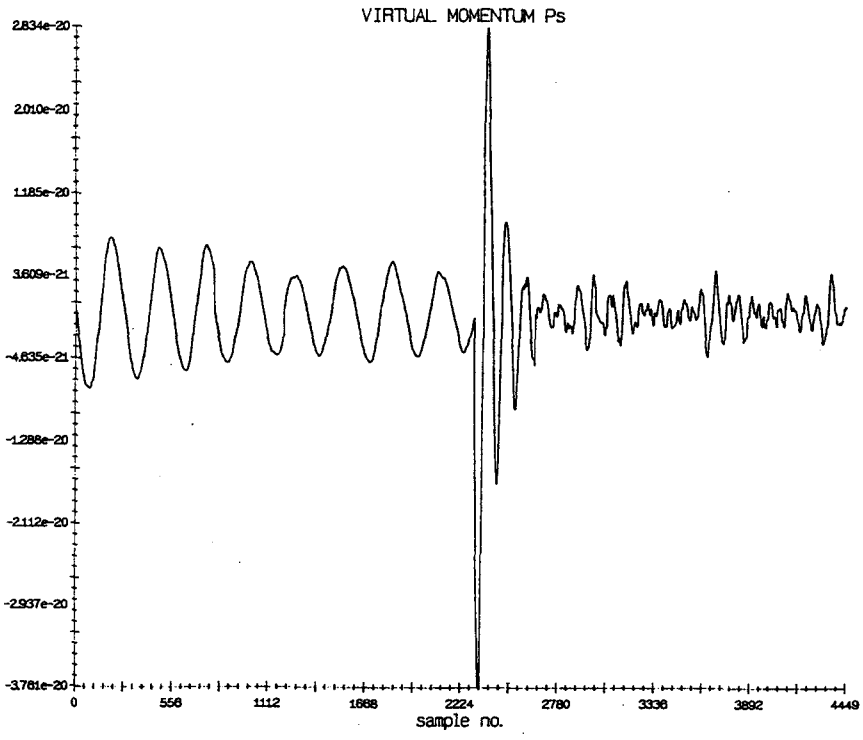

(b)

Figure 23: Virtual variables for the monoclinic crystal: (a)virtual time variable s; (b) associated momentum p_s.

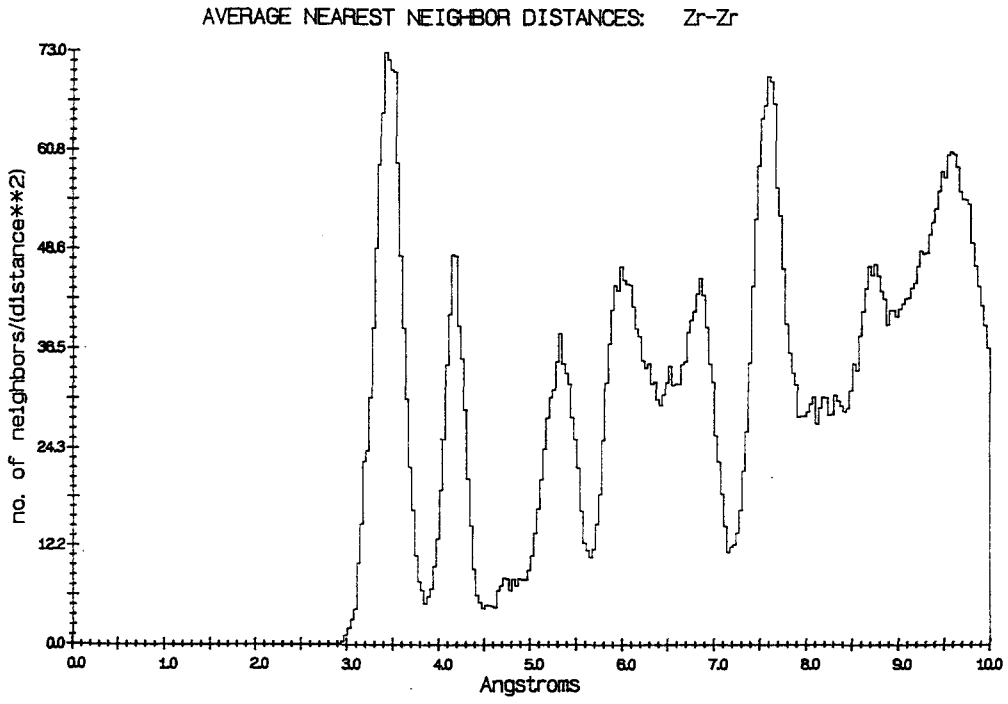

(a)

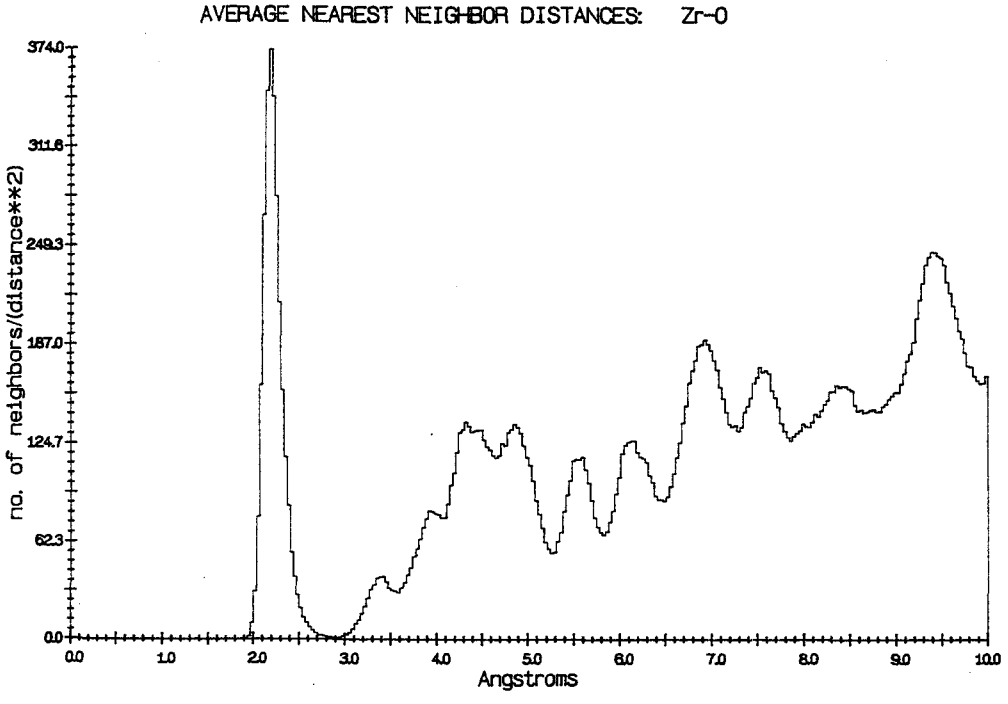

(b)

Figure 24: Pair correlations for the monoclinic crystal at 300K: (a) Zr-Zr; (b) Zr-O.

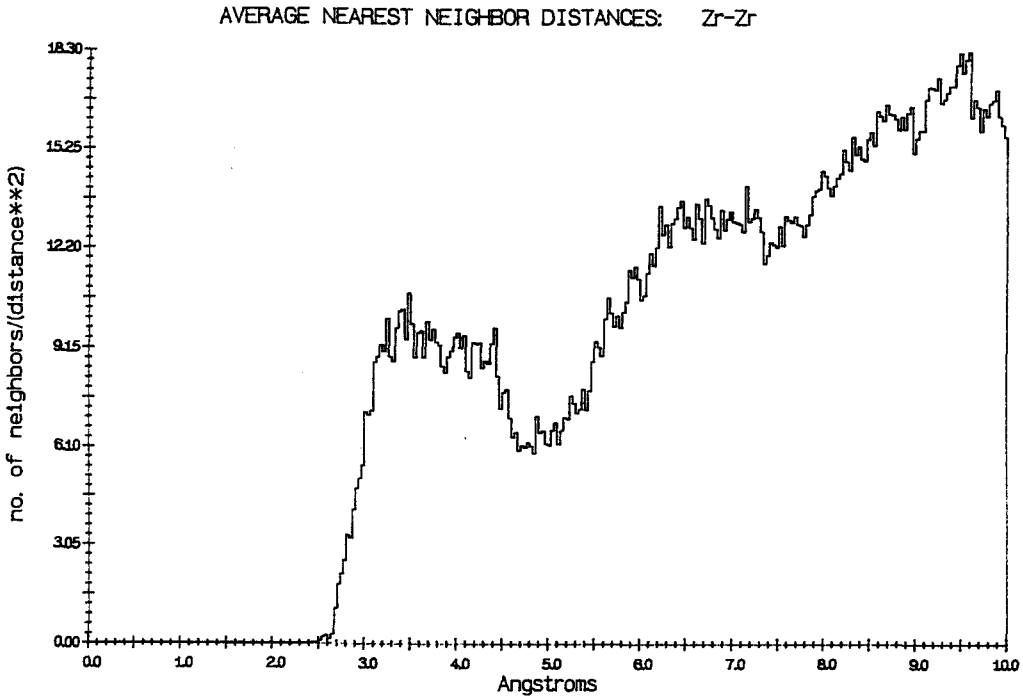

(a)

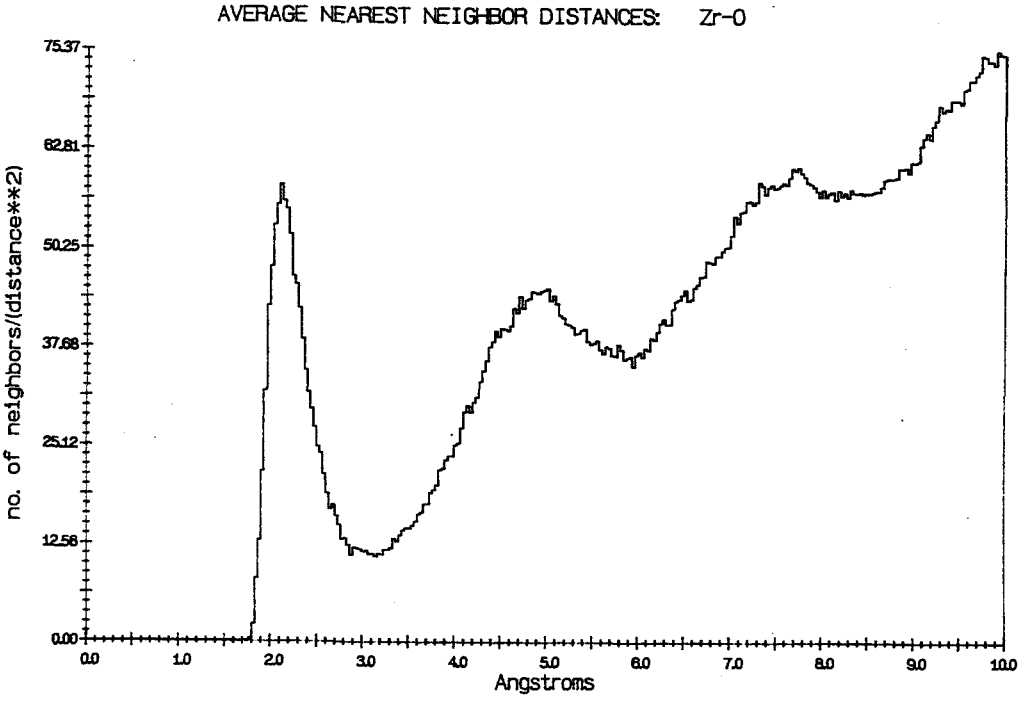

(b)

Figure 25: Pair correlations for the monoclinic crystal at 2000K: (a) Zr-Zr; (b) Zr-O.

	$T(K)$	a_x	b_y	c_x	cz	*volume*	$P(GPa)$	*samples*
$N = 12$	155	5.17	5.42	−.77	5.29	148.3	2.9	1000
	153	5.16	5.43	−.76	5.29	148.2	3.0	2500
$N = 96$	301	5.16	5.43	−.76	5.29	148.0	3.7	1200
	300	5.16	5.44	−.75	5.30	148.6	3.2	1100
	1984	5.21	5.50	−.71	5.37	153.9	13.9	350
	2007	5.45	5.70	−.70	6.14	174.4	7.6	350
	2000	5.54	5.79	−.71	5.71	183.1	6.2	350
	1993	5.58	5.84	−.72	5.76	187.8	5.6	650
	2008	5.81	6.07	−.74	5.98	210.7	3.3	400
	2002	5.91	6.16	−.75	6.07	220.9	2.5	400

Table 11: NPT simulation results for zirconia potential

proximate agreement with the external pressure. Better agreement between these two quantities would be desirable if very well-defined cell dimensions are required. In this study, the simulation was terminated after it became clear that no phase transformations were forthcoming.

The lack of phase transitions is an obvious shortcoming of the potential used. Another deficiency is found when the lattice constants in Table 11 are used to calculate the linear thermal expansion coefficients for the simulated crystal. The measured value of this parameter for monoclinic zirconia is 8.12×10^{-6}/degree K, while the calculated figure for the sides of the simulated crystals are 71.3-79.2x10^{-6}/degree K. This is difference of a full order of magnitude.

6-4 Discussion

The studies of soft-sphere and monoclinic potentials described in the previous sections demonstrate the general usefulness of NPT molecular dynamics. The program **NPT**, originally designed for investigation into the dynamic properties of classical systems, has been shown to useful as well in the determination of static properties such as the minimum-energy structures associated with a given potential.

While the systematic study of soft-sphere potentials has produced some interesting results, the small number of atoms used in the simulations leaves some doubt as to the general validity of these results. This true for the dynamic studies in particular, as the static minimum-energy

structures can realistically be expected to have the periodic symmetry imposed on the system by the small unit cell size. It is encouraging that the small cells reach dynamic equilibrium in most cases, but in some cases all of the tests of equilibrium are not met. While there are many possible reasons for this, without complementary studies of larger systems conclusions reached for the limited number of atoms must remain suspect.

Most of the molecular dynamics studies found in the literature involve several hundred atoms and several thousand time steps. The techniques for the calculation of forces in these studies are similar to those used in the program **NPT**. Considering the computer time consumed in studies of 12 or 96 atoms, this implies that molecular dynamics must be done with supercomputers in order to produce meaningful results. Even so, the intense computational requirements have had a pronounced effect on the types of potentials which have been investigated through molecular dynamics.

The complexity of the force calculations has paralleled the development of faster, more powerful computers, with comparatively little improvement in computational techniques. Molecular dynamics was originally applied to hard-sphere systems, progressing through Lennard-Jones and other short-range potentials to current types of potentials such as classical three-body potentials, short-range potentials calculated from simplified versions of density-functional theory, or long-range potentials calculated using Ewald-type methods. The emphasis in most molecular dynamics research has been on increasing the size of the systems, while the precision of the calculations is rarely addressed. The 'minimum image' convention commonly used with periodic boundary conditions illustrates this point. With this convention, of all of the 'image' atoms generated by periodic boundary conditions, only the one nearest in position to a given atom is included in the force calculations for that atom. The number of calculations for a single term in the potential is then exactly N^2, with N the number of atoms in the system. The error analysis performed earlier for short-range force cutoffs gives a quantitative measure of the low precision of this approach. Long-range forces are usually calculated with a version of the Ewald method which restricts the number of terms containing the error function to cells immediately adjacent to the original MD cell, another practice which sacrifices precision for speed.

While development of techniques which allow the simulation of systems at constant pressure and temperature have increased the range of problems which may be investigated with molecular dynamics, these techniques also increase the computational burden.

With all of the limitations imposed by the need to minimize computational time, the applications of molecular dynamics are, at present, limited to the study of systems for which an accurate potential is already available. The systematic study of a general type of potential,

even one so simple as soft-spheres, is practically impossible to perform for the large variety of system sizes and initial conditions required to produce unambiguous results. Potentials must be obtained either by fitting to empirical data or by the analysis of large numbers of ab initio atomic calculations. In either case, the potentials produced apply only to a single element or compound. As demonstrated in the study of monoclinic zirconia, there is no guarantee that a potential so derived will give realistic results in a dynamic simulation. If the potential is unsuccessful, variation of the parameters for further simulation testing is too time consuming for serious consideration.

While the problems associated with the computational demands of molecular dynamics are imposing, there is still considerable room for improvement through the development of more efficient numerical techniques. The problems of calculating realistic forces can be divided into two general categories: those associated with the short-range forces due to the overlap of the quantum-mechanical wave functions of adjacent atoms, and those of the calculation of the lattice sums required by the long-range electrostatic forces.

The most promising approaches for dealing with the short-range forces involve the application of density-functional methods. At present, most of these methods calculate energy differences for the overlap of static, precalculated wave functions. Ideally, the wave functions should be allowed to vary with time. This is the approach taken in 'quantum molecular dynamics'. Hopefully, the development of similar techniques using charge density instead of wave amplitudes as the fundamental variable will eventually result in methods amenable to general application.

Long-range electrostatic forces for molecular dynamics programs are almost universally calculated by some variation of the Ewald method. There has been no substantial improvement in the application of this method in the last twenty-five years. The use of multipole methods offers a viable alternative to the present state of long-range force calculations. As outlined in earlier chapters, multipole methods offer several advantages over the presently used techniques. First, a full implementation of a fast multipole method requires a number of calculations proportional to N, rather than N^2, and the short-range interactions are limited to adjacent atoms. This eliminates the need for minimum-image conventions, near neighbor lists, and short-range cutoffs. Second, the separation of the potential into charge, dipole and higher order multipoles gives a more intuitive picture of the physical interactions. This is clearly illustrated by the problems associated with periodic boundary conditions. In the multipole formulation, the dipole terms are clearly distinguished as the source of inconsistencies with boundary conditions, while the Ewald formulation tends to obscure the situation to the point where the implicit cancellation of

dipole moments is generally unrecognized. The calculation of higher-order terms such as charge-dipole or dipole-dipole interactions are also made transparent by the multipole methods, while Ewald-type lattice sums can at best model these terms with potentials which vary as r^{-4} or r^{-6}.

The implementation of the multipole method used in the simulations described in the previous section for a system of 96 atoms is a first step in the use of these methods. While the formulation presented here is more or less competitive with the Ewald lattice sums in computational run time, the additional complexity of the program code makes it unlikely to appeal to many researchers in its present form. Before this type of method is generally accepted, either the code must be drastically simplified or the efficiency must be increased to a point that the additional complexity is justified.

6-5 Summary

Experimental data on the structural phases changes in zirconia has been gathered from the literature and summarized. The computational techniques of molecular dynamics were reviewed and equations of motion were formulated which allow, in principle, the study of phase changes as a function of temperature and pressure.

The molecular dynamics program **NPT** was written and tested. This program performs numerical integration of the classical equations of motions in simulations which allow a varying cell size and shape. The simulations produce time averages which are related to the thermodynamic ensemble averages of any of several different types of ensembles.

Routines used to calculated the interatomic forces are provided for potentials which vary as the inverse power of the separation distance between atoms. Calculation of Coulomb forces is done either with the Ewald method or by a multipole method, with selection of method as an input option. The multipole routine was adapted from equations of the planewise summation method for triclinic lattices. The two methods are shown to be analytically equivalent and the precision and speed of the two routines are compared.

Initial conditions and parameters are varied through changes in a separate input file. Output selections include momentum distributions, pair correlations, averages of dynamic variables, and sampled values of virtual variables and system energies. Graphics programs are provided for all appropriate output files.

Results generated by the program **NPT** were presented for energy minimization of crystal structures and for dynamic simulations.

A number of different minimum-energy structures for soft-sphere potentials were found.

Simulations were performed for several soft-sphere structures and dynamic properties were established. Structural phase changes were observed in two cases.

A potential derived from ab initio calculations for monoclinic zirconia was tested. No phase transitions were observed for this potential.

Bibliography

[1]A.J.Hathaway and J.B.Munro, Ceram Bull **63**, 690 (1984)

[2]K.Nassau, Gems and Gemology **17**, 9 (1981)

[3]K.Negita and H.Takao, J Phys Chem Solids **50**, 1686 (1989)

[4]R.T.Sproule, Matls Eng **79**, 48 (1974)

[5]H.S.Spacil and C.S.Tedman Jr., J Electrochem Soc **116**, 1618 (1969)

[6]G.Fisher, Ceram Bull **65**, 1355 (1986)

[7]A.H.Heuer, J Am Ceram Soc **70**, 689 (1987)

[8]H.J.F.Jansen, Phys Rev B **43**, 7267 (1991)

[9]H.J.F.Jansen and J.A.Gardner, Physica B **150**, 10 (1988)

[10]F.Zandiehnadem, R.A.Murray and W.Y.Ching, Physica B **150**, 19 (1988)

[11]R.C.Garvie and M.C.Swain, J Mat Sci **20**, 1193 (1985)

[12]P.M.Kelly and C.J.Ball, J Am Ceram Soc **69**, 259 (1986)

[13]M.Shibata-Yanagisawa, Masaharu Kato, H.Seto, N.Ishizawa, N.Mizutani, and Masanori Kato, J Am Ceram Soc **70**, 503 (1987)

[14]J.D.McCullough and K.N.Trueblood, Acta Cryst **12**, 507 (1959)

[15]D.K.Smith and H.W.Newkirk, Acta Cryst **18**, 983 (1965)

[16]R.E.Hann, P.R.Suitch and J.L.Pentecost, J Am Ceram Soc **68**, C-285 (1985)

[17]C.J.Howard, R.J.Hill and B.E.Reichert, Acta Cryst **B44**, 116 (1988)

[18]W.L.Baun, Science **140**, 1330 (1963)

[19]H.S.Maiti, K.V.G.K.Gakhale and E.C.Subbarao, J Am Ceram Soc **55**, 317 (1972)

[20]R.C.Garvie, J Phys Chem **69**, 1238 (1965)

[21]G.Teufer, Acta Cryst **15**, 1187 (1962)

[22]D.K.Smith and C.F.Cline, J Am Ceram Soc **45**, 249 (1962)

[23]P.Aldebert and J.P.Traverse, J Am Ceram Soc **68**, 34 (1985)

[24]R.Ruh and H.J.Garrett, J Am Ceram Soc **50**, 257 (1967)

[25]R.J.Ackermann, S.P.Garg, and E.G.Rauh, J Am Ceram Soc **60**, 341 (1977)

[26]S.Block, J.A.H.Jornada and G.J.Piermarini, J Am Ceram Soc **68**, 497 (1985)

[27]J.A.H.Jornada, G.J.Piermarini and S.Block, J Am Ceram Soc **70**, 628 (1987)

[28]Y.Kudoh, H.Takeda and H.Arashi, Phys Chem Miner **13**, 233 (1986)

[29]R.Suyama, T.Ashida and S.Kume, J Am Ceram Soc **68**, C-314 (1985)

[30]B.Alzyab, C.H.Perry and R.P.Ingel, J Am Ceram Soc **70**, 760 (1987)

[31]O.Ohtaka and S.Kume, J Am Ceram Soc **71**, C-448 (1988)

[32]H.Arashi, T.Yage, S.Akimoto and Y.Kudoh, Phys Rev B **41**, 4309 (1990)

[33]G.Fisher, Cer Bull **65**, 1355 (1986)

[34]R.Car and M.Parrinello, Phys Rev Lett **55**, 2471 (1985)

[35]M.S.Daw and M.I.Baskes, Phys Rev B **29**, 6443 (1984)

[36]R.G.Gordon and Y.S.Kim, J Chem Phys **56**, 3122 (1972)

[37]M.W.Finnis and J.E.Sinclair, Phil Mag A **50**, 45 (1984)

[38]H.J.F.Jansen, unpublished

[39]N.Metropolis, A.W.Metropolis, M.N.Rosenbluth, A.H.Teller and E.Teller, J Chem Phys **21**, 1087 (1953)

[40]H.C.Anderson, J Chem Phys **72**, 2384 (1980)

[41]M.Parrinello and A.Rahman, Phys Rev Lett **45**, 1196 (1980)

[42]S.Nosé, Mol Phys **52**, 255 (1984)

[43]J.R.Ray and P.Vashishta, J Chem Phys **90**, 6580 (1989)

[44]M.Parrinello, A.Rahman and P.Vashishta, Phys Rev Lett **50**, 1073 (1983)

[45]W.G.Hoover, Phys Rev A **31**, 1695 (1985)

[46]H.J.F.Jansen and M.J.Love, to be published

[47]H.A.Posch, W.G.Hoover and F.J.Vesely, Phys Rev A **33**, 4235 (1986)

[48]I.Hamilton, Phys Rev A **38**, 3120 (1988)

[49]J.Jellinek, J Phys Chem **92**, 3163 (1988)

[50]A.Bulgac and D.Kusnezov, Phys Rev A **42**, 5045 (1990)

[51]W.G.Hoover, D.J.Evans, R.B.Hickman, A.J.C.Ladd,W.T.Ashurst and B.Moran, Phys Rev A **22**, 1690 (1980)

[52]J.R.Ray and A.Rahman, J Chem Phys **80**, 4423 (1984)

[53]J.R.Ray, J Chem Phys **79**, 5128 (1983)

[54]C.L.Cleveland, J Chem Phys **89**, 4987 (1988)

[55]S.Nosé, J Chem Phys **81**, 511 (1984)

[56]M.Ferrario and J.P.Ryckaert, Mol Phys **54**, 587 (1985)

[57]see, for example, J.C.Slater, "Insulators, Semiconductors and Metals" (McGraw Hill, New York, 1967) Ch 9

[58]E.Evjen, Phys Rev **39**, 675 (1932)

[59]B.R.A.Nijboer and F.W.deWette, Physica **24**, 422 (1958)

[60]B.R.A.Nijboer and F.W.deWette, Physica **23**, 309 (1957)

[61]M.J.L.Sangster and M.Dixon, Adv Phys **25**, 247 (1976)

[62]N.Karasawa and W.A.Goddard, J Phys Chem **93**, 7320 (1989)

[63]D.E.Williams, Acta Cryst A **27**, 452 (1971)

[64]B.R.A.Nijboer and F.W.deWette, Physica **24**, 1105 (1958)

[65]V.Massidda and J.A.Hernando, Physica **101B**, 159 (1980)

[66]V.Massidda, Physica **95B**, 317 (1978)

[67]L.Greengard and V.Rokhlin, J Comp Phys **73**, 325 (1987)

[68]C.A.Scholl, Proc Phys Soc **87**, 897 (1966)

[69]W.H.Press, B.P.Flannery, S.A.Teukolsky, W.T.Vetterling, "Numerical Recipes in C" (Cambridge, New York, 1988) pp569-573

[70]C.W.Gear, "Numerical Initial Value Problems in Ordinary Differential Equations" (Englewood Cliffs, New Jersey, 1971)

[71]B.W.Kernighan and D.M.Ritchie, "The C Programming Language, Second Edition" (Prentice Hall, Englewood Cliffs, New Jersey, 1988)

[72]J.R.Rice, "Numerical Methods, Software and Analysis" (McGraw Hill, New York, 1983) p.278

[73]I.S.Gradshteyn and J.M.Ryzhik, "Tables of Integrals, Series, and Products" (Academic Press, Orlando, Florida, 1980) p.686

[74]L.Pauling, "The Nature of the Chemical Bond" (Cornell University Press, Ithaca, New York, 1948) p.346

[75]W.G.Moffatt, G.W.Pearsal, and J.Wulff, "The Structure and Properties of Materials, Volume I: Structure "(John Wiley and Sons, New York, 1964) p.36

[76]Yiquing Zhou, unpublished

Appendices

Appendix A

NPT Dynamics

A-1 Derivation of the Equations of Motion

The following classical Lagrangian is proposed for simulations of systems of atoms at constant external temperature T_{ex} and constant external pressure P_{ex}:

$$\begin{aligned} L &= \frac{s^2}{2}\sum_{i=1}^{N} m_i \dot{\vec{q}}_i^{\,T} h^T h \dot{\vec{q}}_i - \Phi(h\vec{q}, h) \\ &+ \frac{Q}{2}\dot{s}^2 - 3Nk_B T_{ex} ln(s) + \frac{W}{2}\sum_{\alpha\beta=1}^{6} \dot{h}_{\alpha\beta}^2 - P_{ex}V(h) \end{aligned}$$

In this expression h is the 3x3 matrix composed of the MD cell vectors $\vec{a}$, $\vec{b}$,and $\vec{c}$, and $\vec{q}_i$ is the position of the i^{th} atom projected along the cell vectors, and V(h) is the volume of the cell. projected along the cell vectors. Each component of $\vec{q}_i$ has a range of $-\frac{1}{2}$ to $+\frac{1}{2}$.

$$h \equiv \begin{pmatrix} a_x & b_x & c_x \\ 0 & b_y & c_y \\ 0 & 0 & c_z \end{pmatrix}$$

$$\vec{r}_i = \begin{pmatrix} x_i \\ y_i \\ z_i \end{pmatrix} = h\vec{q}_i = h \begin{pmatrix} \xi_i \\ \eta_i \\ \zeta_i \end{pmatrix}$$

The momenta are defined as

$$\vec{p}_i^{(v)} \equiv \frac{\partial L}{\partial \dot{\vec{q}}_i} = \begin{pmatrix} p_{\xi_i} \\ p_{\eta_i} \\ p_{\zeta_i} \end{pmatrix} = m_i s^2 h^T h \dot{\vec{q}}_i$$

$$p_s \equiv \frac{\partial L}{\partial \dot{s}} = Q\dot{s}$$

$$p_{h_{\alpha\beta}} \equiv \frac{\partial L}{\partial \dot{h}_{\alpha\beta}} = W\dot{h}_{\alpha\beta}$$

The Hamiltonian is then

$$\begin{aligned} H &\equiv \sum_{i=1}^{N}(p_{\xi_i}\dot{\xi}_i + p_{\eta_i}\dot{\eta}_i + p\zeta_i\dot{\zeta}_i) + p_s\dot{s} + \sum_{\alpha\beta} p_{h_{\alpha\beta}}\dot{h}_{\alpha\beta} - L \\ &= \frac{1}{s^2}\sum_i \frac{1}{2m_i}\vec{p}_i^{(v)T}h^{-1}h^{T-1}\vec{p}_i^{(v)} + \Phi(h\vec{q},h) + \frac{p_s^2}{2Q} \\ &\quad +3Nk_BT_{ex}ln(s) + \sum_{\alpha\beta}\frac{p_{\alpha\beta}^2}{2W} + P_{ex}V(h) \end{aligned}$$

Hamilton's equations of motion are taken from this expression:

$$\begin{aligned} \dot{\vec{q}}_i &= \frac{\partial H}{\partial \vec{p}_i^{(v)}} = \frac{1}{m_i s^2}h^{-1}h^{T-1}p_i^{(v)} \\ \dot{\vec{p}}_i^{(v)} &= -\frac{\partial H}{\partial \vec{q}_i^{(v)}} = -\frac{\partial\Phi(h\vec{q}_i)}{\partial\vec{q}_i} \\ &= -h^T\vec{\nabla}_i\Phi(\vec{r},h) \equiv h^T\vec{f}_i \\ \dot{s} &= \frac{\partial H}{\partial p_s} = \frac{p_s}{Q} \\ \dot{p}_s &= -\frac{\partial H}{\partial s} = \frac{2}{s^3}\sum_i \frac{1}{2mi}\vec{p}_i^{(v)T}h^{-1}h^{T-1}\vec{p}_i^{(v)} - \frac{3Nk_BT_{ex}}{s} \\ \dot{h}_{\alpha\beta} &= \frac{\partial H}{\partial p_{h_{\alpha\beta}}} = \frac{p_{h_{\alpha\beta}}}{W} \\ \dot{p}_{h_{\alpha\beta}} &= -\frac{\partial H}{h_{\alpha\beta}} \\ &= \frac{1}{s^2}\sum_i \frac{1}{m_i}(h^{T-1}p_i^{(v)})(h^{-1}h^{T-1}p_i^{(v)})^T + \sum_i \vec{f}_i\vec{q}_i^T \\ &\quad -\frac{\partial\Phi(\vec{r},h)}{\partial h_{\alpha\beta}} - P_{ex}\frac{\partial V}{\partial h_{\alpha\beta}} \end{aligned}$$

On changing to the 'real' variables

$$\vec{r}_i = h\vec{q}_i$$

$$\vec{p}_i = \frac{1}{s}h^{T-1}\vec{p}_i^{(v)} = sm_i\dot{h}\dot{\vec{q}}_i$$

the equations of motion become:

$$\begin{aligned} \dot{\vec{r}}_i &= \dot{h}q_i + h\dot{\vec{q}}_i = \frac{p_h}{W}h^{-1}\vec{r}_i + \frac{\vec{p}_i}{sm_i} \\ \dot{\vec{p}}_i &= -\frac{\dot{s}}{s^2}h^{T-1}p_i^{(v)} + \frac{1}{s}\dot{h}^{T-1}p_i^{(v)} + \frac{1}{s}h^{T-1}\dot{\vec{p}}_i^{(v)} \\ &= \frac{1}{s}\vec{f}_i - \frac{p_s\vec{p}_i}{sQ} - \frac{1}{W}h^{T-1}p_h^T\vec{p}_i \end{aligned}$$

$$
\begin{aligned}
\dot{s} &= \frac{p_s}{Q} \\
\dot{p_s} &= \frac{1}{s}\sum_i \frac{1}{mi}\vec{p}_i^T\vec{p}_i - \frac{3Nk_BT_{ex}}{s} \\
\dot{h} &= \frac{p_{h_{\alpha\beta}}}{W} \\
\dot{p_h} &= (\sum_i \frac{1}{m_i}p_i p_i^T + \sum_i \vec{f}_i\vec{r}_i^T - \frac{\partial\Phi(\vec{r},h)}{\partial h}h^T - P_{ex}\frac{\partial V}{\partial h}h^T)h^{T-1}
\end{aligned}
$$

With the time differential dt replaced with a new 'scaled' time variable $d\tau = \frac{1}{s}dt$, the equations of motion are

$$
\begin{aligned}
\dot{\vec{r}}_i &= \frac{d\vec{r}}{d\tau} = \frac{\vec{p}_i}{m_i} + \frac{sp_h}{W}h^{-1}\vec{r}_i \\
\dot{\vec{p}}_i &= \frac{d\vec{p}_i}{d\tau} = \vec{f}_i - \frac{p_s}{Q}\vec{p}_i - \frac{s}{W}h^{T_1}p_h^T\vec{p}_i \\
\dot{s} &= \frac{ds}{d\tau} = \frac{sp_s}{Q} \\
\dot{p}_s &= \frac{p_s}{d\tau} = \sum_i \frac{1}{m_i}\vec{p}_i^T\vec{p}_i - 3Nk_BT_{ex} \\
\dot{h} &= \frac{dh}{d\tau} = s\frac{p_h}{W} \\
\dot{p}_h &= \frac{dp_h}{d\tau} = s(\sum_i \frac{1}{m_i}\vec{p}_i\vec{p}_i^T + \sum_i \vec{f}_i\vec{r}_i^T + f_h h^T - P_{ex}V)h^{T-1} \\
(f_h)_{\alpha\beta} &\equiv -\frac{\partial\Phi(\vec{r},h)}{\partial h_{\alpha\beta}} \\
(\dot{h})_{\alpha\beta} &\equiv \dot{h}_{\alpha\beta} \\
(\dot{p}_h)_{\alpha\beta} &\equiv \dot{p}_{h_{\alpha\beta}}
\end{aligned}
$$

A-2 Equivalence to NPT Ensemble

The classical isothermal-isobaric (NPT) ensemble average for any function A of the particle coordinates and momenta and the system volume is usually given as

$$
\langle A\rangle_{NPT} = \frac{\int_0^\infty dV \int_V d^{3N}r \int d^{3N}p \; e^{-(\frac{H_0(p,r,V)+P_{ex}V}{k_BT_{ex}})}A(p,r,V)}{\int_0^\infty dV \int_V d^{3N}r \int d^{3N}p \; e^{-(\frac{H_0(p,r,V)+P_{ex}V}{k_BT_{ex}})}}
$$

In this equation

$$
H_0(p,r,V) \equiv \sum_i^N \frac{p_i^2}{2m_i} + \Phi(r,V)
$$

The 6N variables $\vec{r}_1, \ldots, \vec{r}_N$ and $\vec{p}_1, \ldots, \vec{p}_N$ are represented by r and p,and V is the volume of the system.

In order to obtain averages which include variable cell shape, the volume integral is replaced by integrations over each component of the cell vectors $\vec{a}$,$\vec{b}$,and$\vec{c}$. The appropriate ensemble average is then

$$\langle A \rangle_{NPT} = \frac{\int d^6h \int_h d^{3N}r \int d^{3N}p \; e^{-(\frac{H_0(p,r,h)+P_{ex}V(h)}{k_B T_{ex}})} A(p,r,V)}{\int d^6h \int_h d^{3N}r \int d^{3N}p \; e^{-(\frac{H_0(p,r,h)+P_{ex}V(h)}{k_B T_{ex}})}}$$

The Lagrangian proposed for simulation of NPT ensembles given in the preceding section results in equations of motion which conserve the total energy E of the system. The ensemble average appropriate to this Lagrangian and the associated Hamiltonian is the microcanonical average

$$\langle A \rangle_{MD} = \frac{\int d^6h \int d^6p_h \int ds \int dp_s \int d^{3N}q \int d^{3N}p^{(v)} \delta(H_{(MD)} - E) A(r,p,h,p_h,s,p_s)}{\int d^6h \int d^6p_h \int ds \int dp_s \int d^{3N}q \int d^{3N}p^{(v)} \delta(H_{(MD)} - E)}$$

With a change to the 'real' variables $\vec{p}_i$ and $\vec{r}_i$, the Hamiltonian becomes

$$H_{(MD)} = H_0(r,p,h) + \frac{p_s^2}{2Q} + f k_B T_{ex} ln(s) + \sum_{\alpha\beta} \frac{p_{\alpha\beta}^2}{2W} + P_{ex} V(h)$$

In this equation f is a constant which will eventually be set equal to 3N. The Jacobians for the transformations are

$$\frac{\partial(\xi_i, \eta_i, \zeta_i)}{\partial(x_i, y_i, z_i)} = \mid h^{-1} \mid = \frac{1}{V}$$

$$\frac{\partial(p_{\xi_i}, p_{\eta_i}, p_{\zeta_i})}{\partial(p_{x_i}, p_{y_i}, p_{z_i})} = s^3 \mid h^T \mid = s^3 V$$

The ensemble average for a function A of p,r,and h is now

$$\langle A \rangle_{MD} = \frac{\int d^6h \int d^{3N}p \int d^{3N}r A(r,p,h) \int dp_s \int d^6p_h \int ds s^{3N} \delta(H_{(MD)} - E)}{\int d^6h \int d^{3N}p \int d^{3N}r \int dp_s \int d^6p_h \int ds s^{3N} \delta(H_{(MD)} - E)}$$

The integral over s can be performed analytically by taking $H_{MD} - E = g(s)$ and using

$$\delta[g(s)] = \frac{\delta(s - s_o)}{g'(s_o)}$$

s_0 is the value of s for which $g(s) = 0$ and $g'(s_0)$ is the derivative of $g(s)$ at $s = s_0$:

$$s_0 = e^{-\frac{1}{f k_B T_{ex}}[H_0(r,p,h) + P_{ex}V(h) + \frac{p_s^2}{2Q} + \sum_{\alpha\beta} \frac{p_{\alpha\beta}^2}{2W} - E]}$$

$$g'(s_0) = \frac{f k_B T_{ex}}{s_0}$$

$$\langle A\rangle_{MD} = \frac{\int d^6h \int d^{3N}p \int d^{3N}r A(r,p,h) \int dp_s \int d^6p_h s_0^{3N+1}}{\int d^6h \int d^{3N}p \int d^{3N}r \int dp_s \int d^6p_h s_0^{3N+1}}$$

The common factors of $\frac{1}{fk_BT_{ex}}$ have been cancelled from this expression. The integrations over the virtual momenta can now be performed analytically, resulting in factors of of $\frac{7}{2}\frac{fk_BT_{ex}}{3N+1}$ in both numerator and denominator. When these factors as well as the constant $e^{\frac{(3N+1)E}{fk_BT_{ex}}}$ are cancelled, the following result is obtained:

$$\langle A\rangle_{MD} = \frac{\int d^6h \int d^{3N}p \int d^{3N}r A(r,p,h) e^{-\frac{(3N+1)}{fk_BT_{ex}}[H_0(r,p,h)+P_{ex}V(h)]}}{\int d^6h \int d^{3N}p \int d^{3N}r e^{-\frac{(3N+1)}{fk_BT_{ex}}[H_0(r,p,h)+P_{ex}V(h)]}}$$

If $f = 3N+1$, this is identical to $\langle A\rangle_{NPT}$.

According to the ergodic theorem, for sufficiently long time intervals the time average of A is equal to the ensemble average:

$$\begin{aligned} \overline{A}_{MD} &\equiv \lim_{T\to\infty}\frac{1}{T}\int_0^T d\tau A(p(\tau),r(\tau),h(\tau)) \\ &\equiv \langle A\rangle_{MD} \end{aligned}$$

If the time averages are evaluated with equations of motion which include a scaled time variable $dt = \frac{1}{s}d\tau$, the time average is

$$\begin{aligned} \overline{A}'_{MD} &= \lim_{T\to\infty}\frac{1}{T}\int_0^T dt A(p(t),r(t),h(t)) \\ &= \frac{\lim_{T\to\infty}\int_0^T d\tau\frac{1}{s}A(p(\tau),r(\tau),h(\tau))}{\lim_{T\to\infty}\int_0^T d\tau\frac{1}{s}} \\ &= \frac{\langle\frac{A}{s}\rangle_{MD}}{\langle\frac{1}{s}\rangle_{MD}} \end{aligned}$$

The additional factor of s in each of these averages reduces the factor in the numerator of $\langle A\rangle_{MD}$ to $3N$. The partition function is unchanged by the time scaling, but in the ratio of the averages the partition functions cancel and

$$\langle A\rangle'_{MD} = \frac{\int d^6h \int d^{3N}p \int d^{3N}r A(r,p,h) e^{-\frac{(3N)}{fk_BT_{ex}}[H_0(r,p,h)+P_{ex}V(h)]}}{\int d^6h \int d^{3N}p \int d^{3N}r e^{-\frac{(3N)}{fk_BT_{ex}}[H_0(r,p,h)+P_{ex}V(h)]}}$$

If $f \equiv 3N$, then $\overline{A}'_{MD} = \langle A\rangle_{NPT}$.

Appendix B

Stress Tensor Calculations

The microscopic stress tensor is defined for systems with periodic boundary conditions as

$$\mathcal{P} = \sum_i \frac{1}{m_i} \vec{p}_i \vec{p}_i^T + \sum_i \vec{f}_i \vec{r}_i^T - \frac{\partial \Phi(\vec{r}, h)}{\partial h} h^T$$

If the potential for an MD simulation is formulated with only six components in the cell matrix h, with a_y,a_z, and b_z set to zero, the potential becomes

$$\Phi(\vec{r}, h') = \Phi(\vec{r}, h) \mid_{a_y = a_z = b_z = 0}$$

To obtain expressions for the elements of the pressure tensor from $\Phi(\vec{r}, h')$ it necessary to eliminate from the definition of $\mathcal{P}$ any partial derivatives with respect to a_y,a_z, and b_z.

Explicit expressions for the diagonal elements are:

$$\begin{aligned}
\mathcal{P}_{xx} &= \sum_i \frac{1}{m_i} p_{x_i}^2 + \sum_i f_{x_i} x_i - a_x \frac{\partial \Phi}{\partial a_x} - b_x \frac{\partial \Phi}{\partial b_x} - c_x \frac{\partial \Phi}{\partial c_x} \\
\mathcal{P}_{yy} &= \sum_i \frac{1}{m_i} p_{y_i}^2 + \sum_i f_{y_i} y_i - a_y \frac{\partial \Phi}{\partial a_y} - b_y \frac{\partial \Phi}{\partial b_y} - c_y \frac{\partial \Phi}{\partial c_y} \\
\mathcal{P}_{zz} &= \sum_i \frac{1}{m_i} p_{z_i}^2 + \sum_i f_{z_i} z_i - a_z \frac{\partial \Phi}{\partial a_z} - b_z \frac{\partial \Phi}{\partial b_z} - c_z \frac{\partial \Phi}{\partial c_z}
\end{aligned}$$

In these expressions, it is not necessary to evaluate any of the derivatives with respect to a_y,a_z, or b_z since the terms containing these derivatives are all equal to zero. Removing similar terms from the off-diagonal elements leaves:

$$\begin{aligned}
\mathcal{P}_{xy} &= \sum_i \frac{1}{m_i} p_{x_i} p_{y_i} + \sum_i f_{x_i} y_i - b_y \frac{\partial \Phi}{\partial b_x} - c_y \frac{\partial \Phi}{\partial c_x} \\
\mathcal{P}_{xz} &= \sum_i \frac{1}{m_i} p_{x_i} p_{z_i} + \sum_i f_{x_i} z_i - c_z \frac{\partial \Phi}{\partial c_x} \\
\mathcal{P}_{yz} &= \sum_i \frac{1}{m_i} p_{y_i} p_{z_i} + \sum_i f_{y_i} z_i - c_z \frac{\partial \Phi}{\partial c_y} \\
\mathcal{P}_{yx} &= \sum_i \frac{1}{m_i} p_{y_i} p_{x_i} + \sum_i f_{y_i} x_i - a_x \frac{\partial \Phi}{\partial a_y} - b_x \frac{\partial \Phi}{\partial b_y} - c_x \frac{\partial \Phi}{\partial c_y} \\
\mathcal{P}_{zx} &= \sum_i \frac{1}{m_i} p_{z_i} p_{x_i} + \sum_i f_{z_i} x_i - a_x \frac{\partial \Phi}{\partial a_z} - b_x \frac{\partial \Phi}{\partial b_z} - c_x \frac{\partial \Phi}{\partial c_z} \\
\mathcal{P}_{zy} &= \sum_i \frac{1}{m_i} p_{z_i} p_{y_i} + \sum_i f_{z_i} y_i - b_y \frac{\partial \Phi}{\partial b_z} - c_y \frac{\partial \Phi}{\partial c_z}
\end{aligned}$$

The expressions for the last three elements contain the deriatives of a_y, a_z, and b_z in terms which do not necessarily vanish. By appealing to the invariance of the total potential energy under coordinate rotations, an additional relationship between these terms is found. The total potential energy of any system interacting through pairwise forces and periodic boundary conditions can be written:

$$\Phi(\vec{r},h)=\sum_i\sum_j\sum_{\alpha\beta\gamma}\Phi(\vec{r}_i-\vec{r}_j+\vec{R}_{\alpha\beta\gamma})$$

In this equation α,β, and γ are the indices for the summations along the lattice vectors $\vec{a}$,$\vec{b}$, and $\vec{c}$, and $\vec{R}_{\alpha\beta\gamma}\equiv\alpha\vec{a}+\beta\vec{b}+\gamma\vec{c}$.

A coordinate rotation around the z-axis is obtained by changing the x- and y-coordinates into cylindrical form and introducing a rotation angle θ:

$$\begin{aligned}
x_i &= \rho_i\cos(\theta_i+\theta)\\
y_i &= \rho_i\sin(\theta_i+\theta)\\
X_{\alpha\beta\gamma} &= \rho_{\alpha\beta\gamma}\cos(\theta_{\alpha\beta\gamma}+\theta)\\
Y_{\alpha\beta\gamma} &= \rho_{\alpha\beta\gamma}\sin(\theta_{\alpha\beta\gamma}+\theta)
\end{aligned}$$

Since the total potential energy is the same for any value of θ,

$$\begin{aligned}
\frac{\partial\Phi(\vec{r},h)}{\partial\theta} &= 0\\
&= \sum_i\left(\frac{\partial\Phi}{\partial x_i}\frac{\partial x_i}{\partial\theta}\right)+\frac{\partial\Phi}{\partial y_i}\frac{\partial y_i}{\partial\theta}\Big)+\sum_{\alpha\beta\gamma}\left(\frac{\partial\Phi}{\partial X_{\alpha\beta\gamma}}\frac{\partial X_{\alpha\beta\gamma}}{\partial\theta}\right)+\frac{\partial\Phi}{\partial Y_{\alpha\beta\gamma}}\frac{\partial Y_{\alpha\beta\gamma}}{\partial\theta}\Big)\\
&= \sum_i(f_{x_i}y_i-f_{y_i}x_i)-\sum_{\alpha\beta\gamma}\left(\frac{\partial\Phi}{\partial X_{\alpha\beta\gamma}}Y_{\alpha\beta\gamma}-\frac{\partial\Phi}{\partial Y_{\alpha\beta\gamma}}X_{\alpha\beta\gamma}\right)\\
&= \sum_i(f_{x_i}y_i-f_{y_i}x_i)-a_y\sum_{\alpha\beta\gamma}\frac{\partial\Phi}{\partial X_{\alpha\beta\gamma}}\alpha-b_y\sum_{\alpha\beta\gamma}\frac{\partial\Phi}{\partial X_{\alpha\beta\gamma}}\beta\\
&\quad -c_y\sum_{\alpha\beta\gamma}\frac{\partial\Phi}{\partial X_{\alpha\beta\gamma}}\gamma+a_x\sum_{\alpha\beta\gamma}\frac{\partial\Phi}{\partial Y_{\alpha\beta\gamma}}\alpha+b_x\sum_{\alpha\beta\gamma}\frac{\partial\Phi}{\partial Y_{\alpha\beta\gamma}}\beta+c_x\sum_{\alpha\beta\gamma}\frac{\partial\Phi}{\partial Y_{\alpha\beta\gamma}}\gamma\\
&= \sum_i(f_{x_i}y_i-f_{y_i}x_i)-b_y\frac{\partial\Phi}{\partial b_x}-c_y\frac{\partial\Phi}{\partial c_x}+a_x\frac{\partial\Phi}{\partial a_y}+b_x\frac{\partial\Phi}{\partial b_y}+c_x\frac{\partial\Phi}{\partial c_y}
\end{aligned}$$

Solving this equation for $a_x \frac{\partial \Phi}{\partial a_y}$ and substituting the result in $\mathcal{P}_{yx}$ leads to

$$\begin{aligned}
\mathcal{P}_{yx} &= \sum_i \frac{1}{m_i} p_{y_i} p_{x_i} + \sum_i f_{y_i} x_i - b_x \frac{\partial \Phi}{\partial b_y} - c_x \frac{\partial \Phi}{\partial c_y} \\
&\quad + \sum_i (f_{x_i} y_i - f_{y_i} x_i) - b_y \frac{\partial \Phi}{\partial b_x} - c_y \frac{\partial \Phi}{\partial c_x} + b_x \frac{\partial \Phi}{\partial b_y} + c_x \frac{\partial \Phi}{\partial c_y} \\
&= \sum_i \frac{1}{m_i} p_{y_i} p_{x_i} + \sum_i f_{x_i} y_i - b_y \frac{\partial \Phi}{\partial b_x} - c_y \frac{\partial \Phi}{\partial c_x} \\
&= \mathcal{P}_{xy}
\end{aligned}$$

The same method applied to rotations around the y- and x-axes leads to the equalities for the other off-diagonal elements:

$$\begin{aligned}
\mathcal{P}_{xz} &= \mathcal{P}_{zx} \\
\mathcal{P}_{yz} &= \mathcal{P}_{zy}
\end{aligned}$$

The microscopic stress tensor is symmetric, with six independent components instead of nine. The expressions used for the off-diagonal elements are those which do not contain partial derivatives with respect to a_y, a_z or b_z.

By subtracting equal off-diagonal elements from each other, expressions are found for the components of the total torque exerted on the particles:

$$\begin{aligned}
\mathcal{P}_{xy} - \mathcal{P}_{yx} &= 0 \\
&= \sum_i (f_{x_i} y_i - f_{y_i} x_i) - b_y \frac{\partial \Phi}{\partial b_x} - c_y \frac{\partial \Phi}{\partial c_x} + a_x \frac{\partial \Phi}{\partial a_y} + b_x \frac{\partial \Phi}{\partial b_y} + c_x \frac{\partial \Phi}{\partial c_y}
\end{aligned}$$

$$\begin{aligned}
N_z &\equiv \sum_i (\vec{r}_i \times \vec{f}_i)_z \\
&= \sum_i (x_i f_{y_i} - y_i f_{x_i}) \\
&\quad (a_x \frac{\partial \Phi}{\partial a_y} - a_y \frac{\partial \Phi}{\partial a_x}) + (b_x \frac{\partial \Phi}{\partial b_y} - b_y \frac{\partial \Phi}{\partial b_x}) + (c_x \frac{\partial \Phi}{\partial c_y} - c_y \frac{\partial \Phi}{\partial c_x}) \\
&= (\vec{a} \times \frac{\partial \Phi}{\partial \vec{a}})_z + (\vec{b} \times \frac{\partial \Phi}{\partial \vec{b}})_z + (\vec{c} \times \frac{\partial \Phi}{\partial \vec{c}})_z
\end{aligned}$$

The expressions for the x and y components of the torque are found in similar fashion from the relationships between the two other pairs of off-diagonal elements. In matrix notation, the complete expression for the torque is

$$\begin{aligned}\vec{N} &\equiv \sum_i (\vec{r}_i \times \vec{f}_i) \\ &= \vec{a} \times \frac{\partial \Phi}{\partial \vec{a}} + \vec{b} \times \frac{\partial \Phi}{\partial \vec{b}} + \vec{c} \times \frac{\partial \Phi}{\partial \vec{c}}\end{aligned}$$

Appendix C

The Ewald Method of Lattice Summations

C-1 Derivation of the Total Energy Sum

The electrostatic potential at a point $\vec{r}$ in an infinite Bravais lattice of unit point charges plus a neutralizing background charge is

$$\Phi^{(V)}(\vec{r},h) \equiv \lim_{A,B,C\to\infty} \sum_{\alpha=-A}^{A} \sum_{\beta=-B}^{B} \sum_{\gamma=-C}^{C} \left\{ \frac{1}{\mid \vec{R}_{\alpha\beta\gamma} - \vec{r} \mid} - \frac{1}{V} \int_{V_{\alpha\beta\gamma}} d^3r' \frac{1}{\mid \vec{R}_{\alpha\beta\gamma} + \vec{r}' - \vec{r} \mid} \right\}$$

This lattice sum converges, although the value of the sum may depend on the manner in which the limits are approached. V is the volume of the unit cell and $V_{\alpha\beta\gamma}$ is the volume around the lattice point $\vec{R}_{\alpha\beta\gamma}$.

In the Ewald method, the potential is evaluated by adding and subtracting a Gaussian charge distribution at each lattice point. The potential at a point $\vec{r}$ due to the Gaussian centered at $\vec{R}_{\alpha\beta\gamma}$ is defined as

$$\Phi^{(g)}_{\alpha\beta\gamma}(\vec{r}) = (\frac{\epsilon}{\sqrt{\pi}})^3 \int d^3r' \frac{e^{-\epsilon^2 r'^2}}{\mid \vec{R}_{\alpha\beta\gamma} + \vec{r}' - \vec{r} \mid}$$

This integral can be evaluated directly, giving

$$\begin{aligned} \Phi^{(g)}_{\alpha\beta\gamma}(\vec{r}) &= \frac{1}{\mid \vec{R}_{\alpha\beta\gamma} - \vec{r} \mid} \frac{2}{\sqrt{\pi}} \int_0^{\epsilon \mid \vec{R}_{\alpha\beta\gamma} - \vec{r} \mid} e^{-t^2} dt \\ &= \frac{erf(\epsilon \mid \vec{R}_{\alpha\beta\gamma} - \vec{r} \mid)}{\mid \vec{R}_{\alpha\beta\gamma} - \vec{r} \mid} \end{aligned}$$

When this expression is subtracted from the first term in $\Phi^{(V)}$, the result is

$$\begin{aligned} \Phi^{(d)}_{ew}(\vec{r}) &= \lim_{A,B,C\to\infty} \sum_{\alpha=-A}^{A} \sum_{\beta=-B}^{B} \sum_{\gamma=-C}^{C} \left\{ \frac{1}{\mid \vec{R}_{\alpha\beta\gamma} - \vec{r} \mid} - \frac{erf(\epsilon \mid \vec{R}_{\alpha\beta\gamma} - \vec{r} \mid)}{\mid \vec{R}_{\alpha\beta\gamma} - \vec{r} \mid} \right\} \\ &= \sum_{\alpha\beta\gamma=-\infty}^{\infty} \frac{erfc(\epsilon \mid \vec{R}_{\alpha\beta\gamma} - \vec{r} \mid)}{\mid \vec{R}_{\alpha\beta\gamma} - \vec{r} \mid} \end{aligned}$$

The limit has been taken to infinity. Since this expression is absolutely convergent, the limit of this term is independent of the details of the summation.

The potentials from the volume charge and the Gaussian distribution are combined in a second term:

$$\Phi_{ew}^{(h)} = \lim_{A,B,C\to\infty} \sum_{\alpha=-A}^{A} \sum_{\beta=-B}^{B} \sum_{\gamma=-C}^{C} \left\{ \int d^3r' \frac{\rho_g(\vec{r}') - \rho_V(\vec{r}')}{\mid \vec{r}' + \vec{R}_{\alpha\beta\gamma} - \vec{r} \mid} \right\}$$

The integral is related to an integral in reciprocal space through Parseval's theorem:

$$\int d^3r f(\vec{r}) g^*(\vec{r}) = \int d^3h F(\vec{h}) G^*(\vec{h})$$

The usual factors of 2π are absent from this expression due to the definition used for the Fourier transforms. With

$$\begin{aligned}
F_g(\vec{h}) &= \int d^3r' \rho_g(r') e^{-i2\pi\vec{h}\cdot\vec{r}'} \\
&= (\frac{\epsilon}{\sqrt{\pi}})^3 \int d^3r' e^{-\epsilon^2 r'^2} e^{-i2\pi\vec{h}\cdot\vec{r}'} \\
&= e^{-\frac{(2\pi h)^2}{4\epsilon^2}} \\
F_V(\vec{h}) &= \int d^3r' \rho_V(r') e^{-i2\pi\vec{h}\cdot\vec{r}'} \\
&= \frac{1}{V} \int_{-\frac{1}{2}}^{\frac{1}{2}} d\xi \int_{-\frac{1}{2}}^{\frac{1}{2}} d\eta \int_{-\frac{1}{2}}^{\frac{1}{2}} d\zeta e^{-i2\pi\vec{h}\cdot(\xi\vec{a}+\eta\vec{b}+\zeta\vec{c})} \frac{\partial(x,y,z)}{\partial(\xi,\eta,\zeta)} \\
&= \frac{\sin(\pi\vec{h}\cdot\vec{a})\sin(\pi\vec{h}\cdot\vec{b})\sin(\pi\vec{h}\cdot\vec{c})}{\pi^3(\vec{h}\cdot\vec{a})(\vec{h}\cdot\vec{b})(\vec{h}\cdot\vec{c})} \\
G(\vec{h}) &= \int d^3r' \frac{e^{-i2\pi\vec{h}\cdot\vec{r}'}}{\mid \vec{R}_{\alpha\beta\gamma} + \vec{r}' - \vec{r} \mid} \\
&= e^{2\pi\vec{h}\cdot(\vec{R}_{\alpha\beta\gamma}-\vec{r})} \int d^3r'' \frac{e^{i2\pi\vec{h}\cdot\vec{r}''}}{r''} \\
&= \frac{1}{\pi h^2} e^{-i2\pi\vec{h}\cdot\vec{r}} e^{i2\pi\vec{h}\cdot\vec{R}_{\alpha\beta\gamma}}
\end{aligned}$$

the reciprocal space integral is written

$$\Phi_{ew}^{(h)} = \int d^3h \frac{1}{\pi h^2} e^{-i2\pi\vec{h}\cdot\vec{r}} \left\{ e^{-\frac{(2\pi h)^2}{4\epsilon^2}} - F_V(\vec{h}) \right\} \lim_{A,B,C\to\infty} \sum_{\alpha=-A}^{A} \sum_{\beta=-B}^{B} \sum_{\gamma=-C}^{C} e^{i2\pi\vec{h}\cdot\vec{R}_{\alpha\beta\gamma}}$$

When the lattice limits are taken to infinity the lattice sum is equal to[60]:

$$\lim_{A,B,C\to\infty} \sum_{\alpha=-A}^{A} \sum_{\beta=-B}^{B} \sum_{\gamma=-C}^{C} e^{i2\pi\vec{h}\cdot\vec{R}_{\alpha\beta\gamma}} = \frac{1}{V} \sum_{\alpha=-\infty}^{\infty} \sum_{\beta=-\infty}^{\infty} \sum_{\gamma=-\infty}^{\infty} \delta(\vec{h} - \vec{h}_{\alpha\beta\gamma})$$

$$\vec{h}_{\alpha\beta\gamma} \equiv \alpha\vec{h}_a + \beta\vec{h}_b + \gamma\vec{h}_c$$

$$\vec{h}_i \cdot \vec{j} = \delta_{ij} \quad i,j = a,b,c$$

Using this expression, integration is straightforward for all terms except the one for which $\vec{h}_{\alpha\beta\gamma}$ is equal to zero. For this case the integrand must be replaced with the limit as $\vec{h} \rightarrow 0$:

$$\begin{aligned}\lim_{\vec{h}\rightarrow 0}\left\{\frac{e^{-i2\pi\vec{h}\cdot\vec{r}}}{\pi h^2}\left[e^{-(\frac{\pi h}{\epsilon})^2} - F_V(\vec{h})\right]\right\} &= -\frac{\pi}{\epsilon^2} + \lim_{\vec{h}\rightarrow 0}\frac{\pi}{3}((\hat{h}\cdot\vec{a})^2 + (\hat{h}\cdot\vec{b})^2 + (\hat{h}\cdot\vec{c})^2)) \\ &\equiv -\frac{\pi}{\epsilon^2} + c^{(V)}\end{aligned}$$

The limit is retained in the second term because the value of this term depends on the direction of $\vec{h}$ as the limit is approached. If the lattice has cubic symmetry, a unique limit is obtained. For lattices with less than cubic symmetry, the limit is not unique and the lattice sum is said to be conditionally convergent.

A general expression for the potential due to the unit point charge lattice with neutralizing background is

$$\Phi(\vec{r}) = \sum_{\alpha\beta\gamma=-\infty}^{\infty} \frac{erfc(\epsilon \mid \vec{R}_{\alpha\beta\gamma} - \vec{r} \mid)}{\mid \vec{R}_{\alpha\beta\gamma} - \vec{r} \mid} + \frac{4\pi}{V} \sum_{\alpha\beta\gamma=-\infty}^{\infty}{}' \frac{1}{K^2_{\alpha\beta\gamma}} e^{-\frac{K^2_{\alpha\beta\gamma}}{4\epsilon^2}} e^{-i\vec{K}_{\alpha\beta\gamma}\cdot\vec{r}} - \frac{\pi}{\epsilon^2} + c^{(V)}$$

$$\vec{K}_{\alpha\beta\gamma} \equiv 2\pi\vec{h}_{\alpha\beta\gamma}$$

This is the general form of the Ewald potential. The last term, $c^{(V)}$, is a constant with a known value if the direction in which the limit is approached is known.

Another way to obtain expressions for $c^{(V)}$ is to change variables in the reciprocal space integral so that the directions of the integrations coincide with the directions of the lattice vectors $\vec{a}$,$\vec{b}$, and $\vec{c}$. As each lattice sum is extended to infinity, it is replaced by a delta function in a single dimension and the integration is performed. The limit $\vec{h} \rightarrow 0$ need be taken only in the last of the three integrations, so the order of the summation determines a particular value for $c^{(V)}$. For example, if the last summation is taken in the $\vec{h}_b$ direction, then

$$c_b^{(V)} \equiv \frac{\pi}{3h_b^2}$$

The potential at $\vec{r} = 0$ is undefined for the term in the direct lattice sum if $\alpha = \beta = \gamma = 0$. This term is evaluated by subtracting the self-energy term and taking the limit as $\vec{r} \rightarrow 0$:

$$\begin{aligned}\Phi_{000}(\vec{r}=0) &= \lim_{\vec{r}\rightarrow 0}(\Phi_{000}^{(ew)} - \frac{1}{r}) \\ &= \lim_{\vec{r}\rightarrow 0}(-\frac{erf(\epsilon r)}{r}) \\ &= -\frac{2\epsilon}{\sqrt{\pi}}\end{aligned}$$

The total electrostatic energy of a collection of N particles in a unit cell described by lattice vectors $\vec{a}$,$\vec{b}$, and $\vec{c}$ is then

$$
\begin{aligned}
U^{(ew)} &= \frac{1}{2}\sum_i\sum_j z_i z_j e^2 \Phi(\vec{r}_j - \vec{r}_i) \\
&= \frac{1}{2}\sum_i\sum_{j\neq i} z_i z_j e^2 \left\{ \sum_{\alpha\beta\gamma} \frac{erfc(\epsilon \mid \vec{R}_{\alpha\beta\gamma} - \vec{r}_j + \vec{r}_i \mid)}{\mid \vec{R} - \vec{r}_j + \vec{r}_i \mid} + \frac{4\pi}{V} {\sum_{\alpha\beta\gamma}}' \frac{e^{-\frac{K^2_{\alpha\beta\gamma}}{4\epsilon^2}}}{K^2_{\alpha\beta\gamma}} e^{-i\vec{K}_{\alpha\beta\gamma}\cdot(\vec{r}_j - \vec{r}_i)} \right\} \\
&+ \frac{1}{2}\sum_i z_i^2 e^2 \left\{ {\sum_{\alpha\beta\gamma}}' \left[\frac{erfc(\epsilon R_{\alpha\beta\gamma})}{R_{\alpha\beta\gamma}} + \frac{4\pi}{V}\frac{1}{K^2_{\alpha\beta\gamma}} e^{-\frac{K^2_{\alpha\beta\gamma}}{4\epsilon^2}} \right] - \frac{2\epsilon}{\sqrt{\pi}} \right\} \\
&+ \frac{1}{2}\sum_i\sum_j z_i z_j e^2 (-\frac{\pi}{\epsilon^2} + c_j^{(V)})
\end{aligned}
$$

The subscript on $c^{(V)}$ allows for the possibility that the sums were not performed in the same manner for each term in the potential. If the summations are taken in an identical manner for each term then $c^{(V)}$ is a single constant and the last term will vanish as long as the total charge in the unit cell is zero. If the last term is set to zero, then this expression is the Ewald energy per unit cell.

From the original definition of the Ewald potential as a sum of potentials from point charges and volume charges, it is also possible to write the electrostatic energy in the Ewald formulation as

$$
\begin{aligned}
U^{(ew)} &= U^{(coul)} + U^{(S)} \\
U^{(coul)} &= \lim_{A,B,C\to\infty} \sum_{\alpha=-A}^{A}\sum_{\beta=-B}^{B}\sum_{\gamma=-C}^{C}\sum_{i=1}^{N}\sum_{j=1}^{N} z_i z_j e^2 \frac{1}{\mid \vec{R}_{\alpha\beta\gamma} - \vec{r}_j + \vec{r}_i \mid} \\
U^{(S)} &= -\lim_{A,B,C\to\infty} \sum_{\alpha=-A}^{A}\sum_{\beta=-B}^{B}\sum_{\gamma=-C}^{C}\sum_{i=1}^{N}\sum_{j=1}^{N} z_i z_j e^2 \frac{1}{V}\int_{V_{\alpha\beta\gamma}} d^3r' \frac{1}{\mid \vec{R}_{\alpha\beta\gamma} + \vec{r}' - \vec{r}_j + \vec{r}_i \mid}
\end{aligned}
$$

The sum over particles has been taken inside the lattice summation. This insures that the summations are identical for each term in the potential and that the energy is equal to the usual Ewald value.

The potential due to the volume charges can be replaced with a sum of surface integrals by first making a change of variables:

$$
\begin{aligned}
\vec{r}'' &= \vec{r}' + \vec{r}_i + \vec{R}_{\alpha\beta\gamma} \\
&= \xi''\vec{a} + \eta''\vec{b} + \zeta''\vec{c} \\
\vec{r}_i &= \xi_i\vec{a} + \eta_i\vec{b} + \zeta_i\vec{c}
\end{aligned}
$$

$$\vec{r}_j = \xi_j \vec{a} + \eta_j \vec{b} + \zeta_j \vec{c}$$

Then

$$U^S = \lim_{A,B,C\to\infty} -e^2 \left\{ \sum_j z_j \sum_i z_i \int_{-A-\frac{1}{2}+\xi_i}^{A+\frac{1}{2}+\xi i} d\xi'' \int_{-B-\frac{1}{2}+\eta_i}^{B+\frac{1}{2}+\eta i} d\eta'' \int_{-B-\frac{1}{2}+\zeta_i}^{B+\frac{1}{2}+\zeta i} d\zeta'' \frac{1}{|\vec{r}'' - \vec{r}_j|} \right\}$$

With a neutral unit cell, the volume charge is zero within the limits $-A+\frac{1}{2}$ to $A-\frac{1}{2}$, $-B+\frac{1}{2}$ to $B-\frac{1}{2}$, and $-C+\frac{1}{2}$ to $C-\frac{1}{2}$. If this volume is excluded from the sum, the contributions from the volume charges are limited to integrations over cells which are at the limits of the lattice sums. If the limits are sufficiently large, the volume charge may be approximated by a surface charge concentrated at the limit. For example,

$$\begin{aligned} -\sum_i \int_{A-\frac{1}{2}}^{A+\frac{1}{2}+\xi_i} \frac{d\xi''}{|\vec{r}'' - \vec{r}_j|} &\approx -\sum_i z_i \frac{A+\frac{1}{2}+\xi_i - A+\frac{1}{2}}{|\vec{r}''_{\eta\zeta} + A\vec{a} - \vec{r}_j|} \\ &= \frac{-1}{|\vec{r}''_{\eta\zeta} + A\vec{a} - \vec{r}_j|} \sum_i z_i \xi_i \end{aligned}$$

$$\vec{r}''_{\eta\zeta} = \eta''\vec{b} + \zeta''\vec{c}$$

The potential due to the surface charge is found by performing the surface integration over η'' and ζ''. Neglecting edge and corner effects, the total energy due to the surface charges is

$$\begin{aligned} U_a^S = \lim_{A,B,C\to\infty} \sum_j z_j \Bigg\{ & \int_{-B}^{B} d\eta \int_{-C}^{C} d\zeta \left[\frac{\rho_a}{|\vec{r}_{\eta\zeta} + A\vec{a} - \vec{r}_j|} - \frac{\rho_a}{|\vec{r}_{\eta\zeta} - A\vec{a} - \vec{r}_j|} \right] \\ & + \int_{-A}^{A} d\xi \int_{-C}^{C} d\zeta \left[\frac{\rho_b}{|\vec{r}_{\xi\zeta} + B\vec{b} - \vec{r}_j|} - \frac{\rho_b}{|\vec{r}_{\xi\zeta} - B\vec{b} - \vec{r}_j|} \right] \\ & + \int_{-A}^{A} d\xi \int_{-B}^{B} d\eta \left[\frac{\rho_c}{|\vec{r}_{\xi\eta} + C\vec{c} - \vec{r}_j|} - \frac{\rho_c}{|\vec{r}_{\xi\eta} - C\vec{c} - \vec{r}_j|} \right] \Bigg\} \end{aligned}$$

$$\rho_a = -\sum_i z_i \xi_i$$

$$\rho_b = -\sum_i z_i \eta_i$$

$$\rho_c = -\sum_i z_i \zeta_i$$

If the surface charge is approximated by a point charge of the appropriate value at each surface lattice point, the integrals can be replaced with two-dimensional lattice sums. The value

of the point charge is found to be numerically equal to that of the surface charge. As the limits are taken to infinity, the volume, surface and point charge representations become equivalent.

C-2 Ewald Force Summations

In order to simplify the expressions for the forces, the Ewald energy is written

$$\begin{aligned} U^{(ew)} &= \frac{1}{2}\sum_i z_i^2 e^2 \sum_{\alpha\beta\gamma}{}' \left[c_{\alpha\beta\gamma} + \frac{erfc(\epsilon R_{\alpha\beta\gamma})}{R_{\alpha\beta\gamma}}\right] - \frac{\epsilon}{\sqrt{\pi}}\sum_i z_i^2 e^2 \\ &+ \sum_i \sum_{j<i} z_i z_j e^2 \sum_{\alpha\beta\gamma}{}' \left[c_{\alpha\beta\gamma} cos(\vec{K}_{\alpha\beta\gamma}\cdot\vec{r}_{ij}) + \frac{erfc(\epsilon \mid \vec{R}_{\alpha\beta\gamma} - \vec{r}_{ij} \mid)}{\mid \vec{R} - \vec{r}_{ij} \mid}\right] \\ &+ \sum_i \sum_{j<i} z_i z_j e^2 \frac{erfc(\epsilon r_{ij})}{r_{ij}} \end{aligned}$$

With

$$\begin{aligned} c_{\alpha\beta\gamma} &= \frac{4\pi}{a_x b_y c_z}\frac{1}{K^2_{\alpha\beta\gamma}} e^{-\frac{K^2_{\alpha\beta\gamma}}{4\epsilon^2}} \\ \vec{K}_{\alpha\beta\gamma} &= \frac{2\pi}{a_x}\alpha\hat{x} + \frac{2\pi}{b_y}(\beta - \frac{b_x}{a_x}\alpha)\hat{y} + \frac{2\pi}{c_z}(\gamma - \frac{c_y}{b_y}\beta + \frac{b_x c_y - c_x b_y}{a_x b_y}\alpha)\hat{z} \\ \vec{R}_{\alpha\beta\gamma} &= \alpha\vec{a} + \beta\vec{b} + \gamma\vec{c} \\ &= (\alpha a_x + \beta b_x + \gamma c_x)\hat{x} + (\beta b_y + \gamma c_y)\hat{y} + (\gamma c_z)\hat{z} \\ \vec{r}_{ij} &= \vec{r}_j - \vec{r}_i \end{aligned}$$

The force on the k^{th} particle is then

$$\begin{aligned} \vec{f}_k &= -\frac{\partial U^{(ew)}}{\partial \vec{r}_k} \\ &= -\sum_i \sum_{j<i} z_i z_j e^2 \sum_{\alpha\beta\gamma}{}' (\delta_{ik}\vec{\nabla}_i + \delta_{jk}\vec{\nabla}_j) c_{\alpha\beta\gamma} cos(\vec{K}_{\alpha\beta\gamma}\cdot\vec{r}_{ij}) \\ &\quad -\sum_i \sum_{j<i} z_i z_j e^2 \sum_{\alpha\beta\gamma}{}' (\delta_{ik}\vec{\nabla}_i + \delta_{jk}\vec{\nabla}_j) \frac{erfc(\epsilon \mid \vec{R}_{\alpha\beta\gamma} - \vec{r}_{ij} \mid)}{\mid \vec{R}_{\alpha\beta\gamma} - \vec{r}_{ij} \mid} \\ &\quad -\sum_i \sum_{j<i} z_i z_j e^2 (\delta_{ik}\vec{\nabla}_i + \delta_{jk}\vec{\nabla}_j) \frac{erfc(\epsilon r_{ij})}{r_{ij}} \\ &= -\sum_{j\neq k} z_k z_j e^2 \sum_{\alpha\beta\gamma}{}' c_{\alpha\beta\gamma} sin(\vec{K}_{\alpha\beta\gamma}\cdot\vec{r}_{kj})\vec{K}_{\alpha\beta\gamma} \\ &\quad -\sum_{j\neq k} z_k z_j e^2 \sum_{\alpha\beta\gamma} \left[\frac{2\epsilon}{\sqrt{\pi}} e^{-\epsilon^2 |\vec{R}_{\alpha\beta\gamma} - \vec{r}_{kj}|^2} + \frac{erfc(\epsilon \mid \vec{R}_{\alpha\beta\gamma} - \vec{r}_{kj} \mid)}{\mid \vec{R}_{\alpha\beta\gamma} - \vec{r}_{kj} \mid}\right] \frac{(\vec{R}_{\alpha\beta\gamma} - \vec{r}_{kj})}{\mid \vec{R}_{\alpha\beta\gamma} - \vec{r}_{kj} \mid^2} \end{aligned}$$

The forces associated with the components of the cell vectors $\vec{a}$, $\vec{b}$, and $\vec{c}$ are defined as

$$(f_h)_{st} = -\frac{\partial U^{(ew)}(\vec{r},h)}{\partial h_{st}}$$

$$\begin{aligned}
f_h &= -\frac{1}{2}\sum_i z_i^2 e^2 {\sum_{\alpha\beta\gamma}}' \left[\frac{\partial c_{\alpha\beta\gamma}}{h} + \frac{\partial}{\partial R_{\alpha\beta\gamma}}\left(\frac{erfc(\epsilon R_{\alpha\beta\gamma})}{R_{\alpha\beta\gamma}}\right)\frac{\partial R_{\alpha\beta\gamma}}{\partial h}\right] \\
&\quad -\sum_i\sum_{j<i} z_i z_j e^2 {\sum_{\alpha\beta\gamma}}' \frac{\partial c_{\alpha\beta\gamma}}{\partial h} cos(\vec{K}_{\alpha\beta\gamma}\cdot\vec{r}_{ij}) \\
&\quad +\sum_i\sum_{j<i} z_i z_j e^2 {\sum_{\alpha\beta\gamma}}' c_{\alpha\beta\gamma} sin(\vec{K}_{\alpha\beta\gamma}\cdot\vec{r}_{ij})\frac{\partial(\vec{K}_{\alpha\beta\gamma}\cdot\vec{r}_{ij})}{\partial h} \\
&\quad -\sum_i\sum_{j<i} z_i z_j e^2 {\sum_{\alpha\beta\gamma}}' \frac{\partial}{\partial \mid R_{\alpha\beta\gamma}-\vec{r}_{ij}\mid}\left(\frac{erfc(\epsilon \mid \vec{R}_{\alpha\beta\gamma}-\vec{r}_{ij}\mid)}{\mid \vec{R}_{\alpha\beta\gamma}-\vec{r}_{ij}\mid}\right)\frac{\partial \mid \vec{R}_{\alpha\beta\gamma}-\vec{r}_{ij}\mid}{\partial h}
\end{aligned}$$

The partial differentials are:

$$\begin{aligned}
\frac{\partial c_{\alpha\beta\gamma}}{\partial h} &= c_{\alpha\beta\gamma}\left[8\pi^2\left(\frac{1}{4\epsilon^2}+\frac{1}{K_{\alpha\beta\gamma}^2}\right)h^{T-1}MM^T h^{-1}h^{T-1} - h^{T-1}\right] \\
&= c_{\alpha\beta\gamma}\left[2\left(\frac{1}{4\epsilon^2}+\frac{1}{K_{\alpha\beta\gamma}^2}\right)\vec{K}_{\alpha\beta\gamma}\vec{K}_{\alpha\beta\gamma}^T - \bar{1}\right]h^{T-1} \\
&\equiv c_{\alpha\beta\gamma}^{(h)} \\
M &\equiv \begin{pmatrix}\alpha\\ \beta\\ \gamma\end{pmatrix} \\
\frac{\partial}{\partial R}\left(\frac{erfc(\epsilon R)}{R}\right) &= -\frac{1}{R}\left(\frac{erfc(\epsilon R)}{R}+\frac{2\epsilon}{\sqrt{\pi}}e^{-\epsilon^2R^2}\right) \equiv -Rg(R) \\
\frac{\partial R_{\alpha\beta\gamma}}{\partial h} &= \frac{1}{R_{\alpha\beta\gamma}}\vec{R}_{\alpha\beta\gamma}M^T \\
\frac{\partial \mid R_{\alpha\beta\gamma}-\vec{r}_{ij}\mid}{\partial h} &= \frac{1}{\mid \vec{R}_{\alpha\beta\gamma}-\vec{r}_{ij}\mid}\left(\vec{R}_{\alpha\beta\gamma}-\vec{r}_{ij}\right)M^T \\
\frac{\partial(\vec{K}_{\alpha\beta\gamma}\cdot\vec{r}_{ij})}{\partial h} &= -2\pi h^{T-1}M\vec{r}_{ij}^T h^T \\
&= -\vec{K}_{\alpha\beta\gamma}(h^T\vec{r}_{ij})^T
\end{aligned}$$

Then

$$\begin{aligned}
f_h &= -\sum_i\sum_{j\le i} z_i z_j e^2 {\sum_{\alpha\beta\gamma}}' \Big\{c_{\alpha\beta\gamma}^{(h)} cos(\vec{K}_{\alpha\beta\gamma}\cdot\vec{r}_{ij} \\
&\quad +c_{\alpha\beta\gamma}\vec{K}_{\alpha\beta\gamma}\vec{r}_{ij}^T h^{T-1} sin(\vec{K}_{\alpha\beta\gamma}\cdot\vec{r}_{ij}) \\
&\quad -g(\mid \vec{R}_{\alpha\beta\gamma}-\vec{r}_{ij}\mid)(\vec{R}_{\alpha\beta\gamma}-\vec{r}_{ij})M^T\Big\}(1-\frac{1}{2}\delta_{ij})
\end{aligned}$$

Appendix D

Multipole Summations

D-1 Derivation of the Multipole Expansion

In terms of the unnormalized spherical harmonics, the usual multipole expansion is

$$\begin{aligned}\frac{1}{\mid \vec{r}_i - \vec{R} - \vec{r}_j \mid} &\equiv \frac{1}{\mid \vec{R}_i - \vec{r}_j \mid} \\ &= \sum_{l=0}^{\infty} \sum_{m=-l}^{l} \frac{(l-m)!}{(l+m)!} r_j^l Y_{lm}^*(\hat{r}_j) \frac{Y_{lm}(\hat{R}_i)}{R_i^{l+1}} \qquad r_j < R_i \\ Y_{lm}(\hat{r}) &\equiv P_l^{|m|}(\cos\theta) e^{im\phi}\end{aligned}$$

According to the well-known differentiation formula for the spherical harmonics, the last term is

$$\begin{aligned}\frac{Y_{lm}(\hat{R}_i)}{R_i^{l+1}} &= \frac{(-1)^{l-\frac{1}{2}m(1+sgn(m))}}{(l-m)!} \left(\frac{\partial}{\partial X_i} + i\, sgn(m) \frac{\partial}{\partial Y_i}\right)^{|m|} \left(\frac{\partial}{\partial Z_i}\right)^{l-|m|} \left(\frac{1}{R_i}\right) \\ &= \frac{(-1)^{l-\frac{1}{2}m(1+sgn(m))}}{(l-m)!} (-1)^l \left(\frac{\partial}{\partial X} + i\, sgn(m) \frac{\partial}{\partial Y}\right)^{|m|} \left(\frac{\partial}{\partial Z}\right)^{l-|m|} \left(\frac{1}{R_i}\right)\end{aligned}$$

The upper sign is for $m \geq 0$, the lower for $m \leq 0$. With

$$\begin{aligned}\frac{1}{R_i} &= \frac{1}{\mid \vec{r}_i - \vec{R} \mid} \\ &= \sum_{k=0}^{\infty} \sum_{n=-k}^{k} \frac{(k-n)!}{(k+n)!} r_i^k Y_{kn}^*(\hat{r}_i) \frac{Y_{kn}(\hat{R})}{R^{k+1}} \qquad r_i < R \\ &= \sum_{k=0}^{\infty} \sum_{n=-k}^{k} \frac{(k-n)!}{(k+n)!} r_i^k Y_{kn}^*(\hat{r}_i) \frac{(-1)^{k-\frac{1}{2}n(1+sgn(n))}}{(k-n)!} \left(\frac{\partial}{\partial X} + i\, sgn(n) \frac{\partial}{\partial Y}\right)^{|n|} \\ &\qquad \left(\frac{\partial}{\partial Z}\right)^{k-|n|} \left(\frac{1}{R}\right)\end{aligned}$$

When this expression is substituted into the previous equation,

$$\frac{Y_{lm}(\hat{R}_i)}{R_i^{l+1}} = \sum_{k=0}^{\infty} \sum_{n=-k}^{k} \frac{1}{(k+n)!(l-m)!} r_i^k Y_{kn}^*(\hat{r}_i) F_{kn;lm}(\hat{R})$$

$$F_{kn;lm}(\hat{R}) = (-1)^{k-\frac{1}{2}m(1+sgn(m))-\frac{1}{2}n(1+sgn(n))}\left(\frac{\partial}{\partial X}+i\,sgn(m)\frac{\partial}{\partial Y}\right)^{|m|}$$
$$\left(\frac{\partial}{\partial X}+i\,sgn(n)\frac{\partial}{\partial Y}\right)^{|n|}\left(\frac{\partial}{\partial Z}\right)^{l+k-|m|-|n|}\left(\frac{1}{R}\right)$$

Using

$$\left(\frac{\partial}{\partial x}+i\frac{\partial}{\partial y}\right)\left(\frac{\partial}{\partial x}-i\frac{\partial}{\partial y}\right)\left(\frac{1}{r}\right) = \nabla^2-\left(\frac{\partial}{\partial z}\right)^2\left(\frac{1}{r}\right)$$
$$= -\frac{\partial^2}{\partial^2 z}\left(\frac{1}{r}\right)$$

and keeping track of the signs,

$$F_{kn;lm}(\hat{R}) = (-1)^{k-\frac{1}{2}(m+n)(1+sgn(m+n))}\left(\frac{\partial}{\partial X}+i\,sgn(n+m)\frac{\partial}{\partial Y}\right)^{|n+m|}$$
$$\left(\frac{\partial}{\partial Z}\right)^{k+l-|m+n|}\left(\frac{1}{R}\right)$$
$$= (-1)^l(k+l-m-n)!\frac{Y_{k+l,n+m}(\hat{R})}{R^{k+l+1}}$$

Inserting these results into the original multipole expansion gives

$$\frac{1}{\mid \vec{r}_i-\vec{R}-\vec{r}_j \mid} = \sum_{l=0}^{\infty}\sum_{m=-l}^{l}\frac{(l-m)!}{(l+m)!}r_j^l Y_{lm}^*(\hat{r}_j)$$
$$\sum_{k=0}^{\infty}\sum_{n=-k}^{k}\frac{1}{(k+n)!(l-m)!}r_i^k Y_{kn}^*(\hat{r}_i)(-1)^l(k+l-m-n)!\frac{Y_{k+l,n+m}(\hat{R})}{R^{k+l+1}}$$
$$= \sum_{l=0}^{\infty}\sum_{m=-l}^{l}\sum_{k=0}^{\infty}\sum_{n=-k}^{k}\frac{(-1)^l(k+l-m-n)!}{(k+n!)(l+m)!}r_j^l Y_{lm}^*(\hat{r}_j)r_i^k Y_{kn}^*(\hat{r}_i)\frac{Y_{k+l,n+m}(\hat{R})}{R^{k+l+1}}$$

D-2 Coulomb Energy and Force Summations

The energy per unit cell of a collection of N charged particles subject to periodic boundary conditions is expressed as

$$U^{(mp)} = E_{nn}+\tilde{E}_{nn}+E_{mp}$$

The first two terms are contributions to the energy from particles in near neighbor unit cells, that is, unit cells displaced by lattice vectors $\vec{R}_{\alpha\beta\gamma}$ with $R_{\alpha\beta\gamma} < r_0$. The constant r_0 can be, in

principle, any length greater than twice the unit cell diagonal. The first term is the interparticle energy, and the second is the energy from the interaction of the particles with the compensating charges.

$$\begin{aligned} E_{nn} &= \frac{1}{2}\sum_{i=1}^{N}\sum_{j=1}^{N} q_i q_j \sum_{nn}{}' \frac{1}{\mid \vec{r}_i - \vec{R}_{\alpha\beta\gamma} - \vec{r}_j \mid} \\ &= \frac{1}{2}\sum_{i}\sum_{nn\prime} \frac{q_i^2}{R_{\alpha\beta\gamma}} + \sum_{i=1}^{N}\sum_{j<1}^{N} q_i q_j \sum_{nn} \frac{1}{\mid \vec{r}_i - \vec{R}_{\alpha\beta\gamma} - \vec{r}_j \mid} \end{aligned}$$

The prime on the summation index indicates that the near neighbor at the origin is excluded.

The forces on the particles are

$$\begin{aligned} \vec{f}_i^{(nn)} &= -\frac{\partial E_{nn}}{\partial \vec{r}_i} \\ &= q_i \sum_{j\neq i} q_j \sum_{nn} \frac{(\vec{r}_i - \vec{R}_{\alpha\beta\gamma} - \vec{r}_j)}{\mid \vec{r}_i - \vec{R}_{\alpha\beta\gamma} - \vec{r}_j \mid^3} \end{aligned}$$

The 'virtual' forces are defined as

$$\begin{aligned} (f_h)_{ij} &\equiv -\frac{\partial E_{nn}}{\partial h_{ij}} \\ h &= \begin{pmatrix} a_x & b_x & c_x \\ 0 & b_y & c_y \\ 0 & 0 & c_z \end{pmatrix} \end{aligned}$$

so that

$$f_h^{(nn)} = \frac{1}{2}\sum_{i}\sum_{j}\sum_{nn\prime} q_i q_j \frac{(\vec{r}_i - \vec{R}_{\alpha\beta\gamma} - \vec{r}_j)}{\mid \vec{r}_i - \vec{R}_{\alpha\beta\gamma} - \vec{r}_j \mid^3} \begin{pmatrix} \alpha \\ \beta \\ \gamma \end{pmatrix}^T$$

The second term in the energy is

$$\tilde{E}_{nn} = \frac{1}{2}\sum_{i} q_i \sum_{nn} \sum_{j=a,b,c} \tilde{q}_j \left(\frac{1}{\mid \vec{r}_i - \vec{R}_{\alpha\beta\gamma} - \frac{1}{2}\vec{j} \mid} - \frac{1}{\mid \vec{r}_i - \vec{R}_{\alpha\beta\gamma} + \frac{1}{2}\vec{j} \mid} \right)$$

It is not necessary to sum over all of the lattice points, since the compensating charges $\tilde{q}$ cancel inside the near neighbor volume. The lattice points which give non-zero contributions for the first term in the parentheses are denoted collectively as 'nna','nnb',and 'nnc' for $\tilde{q}_a$,$\tilde{q}_b$,and $\tilde{q}_c$, respectively. The contributing lattice points for the second term in the parentheses are found by

inversion, since the near-neighbor surface has the inversion symmetry of the Bravais lattice. The sum is then

$$\tilde{E}_{nn} = \frac{1}{2}\sum_i q_i \sum_{j=a,b,c}\sum_{nnj} \tilde{q}_j \left(\frac{1}{\mid \vec{r}_i - \vec{R}_{nnj} \mid} - \frac{1}{\mid \vec{r}_i + \vec{R}_{nnj} \mid} \right)$$

$$\vec{R}_{nnj} \equiv \vec{R}_{\alpha\beta\gamma} + \frac{1}{2}\vec{j}$$

The forces from the compensating charges are

$$\begin{aligned}
\vec{f}_i^{(c)} &= -\frac{\partial \tilde{E}_{nn}}{\partial \vec{r}_i} \\
&= \frac{1}{2} q_i \sum_{j=a,b,c} \tilde{q}_j \sum_{nnj} \left[\frac{(\vec{r}_i - \vec{R}_{nnj})}{\mid \vec{r}_i - \vec{R}_{nnj} \mid^3} - \frac{(\vec{r}_i + \vec{R}_{nnj})}{\mid \vec{r}_i + \vec{R}_{nnj} \mid^3} \right] \\
&\quad + \frac{1}{2} q_i \sum_{j=a,b,c} \vec{h}_j^{-1} S_j \\
S_j &\equiv \sum_k q_k \sum_{nnj} \left[\frac{1}{\mid \vec{r}_k - \vec{R}_{nnj} \mid} - \frac{1}{\mid \vec{r}_k + \vec{R}_{nnj} \mid} \right] \\
(h_j^{-1})_k &\equiv h_{jk}^{-1}
\end{aligned}$$

In the last definition the subscripts j of the inverse matrix elements are 1,2, and 3 for j=a,b,and c respectively. The 'virtual' forces are

$$\begin{aligned}
f_h^{(c)} &= -\frac{\partial \tilde{E}_{nn}}{\partial h} \\
&= -\frac{1}{2} q_i \sum_{j=a,b,c} \tilde{q}_j \sum_{nnj} \left[\frac{(\vec{r}_i - \vec{R}_{nnj})}{\mid \vec{r}_i - \vec{R}_{nnj} \mid^3} - \frac{(\vec{r}_i + \vec{R}_{nnj})}{\mid \vec{r}_i + \vec{R}_{nnj} \mid^3} \right] \begin{pmatrix} \alpha + \frac{1}{2}\delta_{ja} \\ \beta + \frac{1}{2}\delta_{jb} \\ \gamma + \frac{1}{2}\delta_{jc} \end{pmatrix}^T \\
&\quad + h^{T-1} \begin{pmatrix} S_a \\ S_b \\ S_c \end{pmatrix} (\tilde{q}_a \quad \tilde{q}_b \quad \tilde{q}_c)
\end{aligned}$$

The long-range Coulomb energy is

$$E_{mp} = \frac{1}{2} \sum_{knlm} c_{kn;lm} Q_{kn}^* (Q_{lm}^* + \tilde{Q}_{lm}^*) \sum_{\alpha\beta\gamma \neq nn} \frac{Y_{k+l,n+m}(\vec{R}_{\alpha\beta\gamma})}{R_{\alpha\beta\gamma}^{k+l+1}}$$

$$Q_{lm}^* = \sum_i q_i r_i^l Y_{lm}^*(\hat{r}_i)$$

$$\tilde{Q}^*_{lm} = \sum_{j=a,b,c} \tilde{q}_j (\frac{1}{2} j)^l (Y^*_{lm}(\hat{j}) - Y^*_{lm}(-\hat{j}))$$

$$c_{kn;lm} = (-1)^k \frac{(k+l-n-m)!}{(k+n)!(l+m)!}$$

The lattice sum is calculated with the planewise summation method, which gives the multipole sums over all lattice points except the origin. Defining

$$PSM^{(0)}_{lm} \equiv {\sum_{\alpha\beta\gamma}}' \frac{Y_{lm}(\vec{R}_{\alpha\beta\gamma})}{R^{l+1}_{\alpha\beta\gamma}}$$

$$S^{(0)}_{lm} \equiv {\sum_{nn}}' \frac{Y_{lm}(\vec{R}_{\alpha\beta\gamma})}{R^{l+1}_{\alpha\beta\gamma}}$$

and excluding multipoles with indices greater than a maximum index μ, the energy is

$$E_{mp} = \frac{1}{2} \sum_{k=1}^{\mu-1} \sum_{n=-k}^{k} \sum_{l=1}^{\mu-k} \sum_{n=-l}^{l} c_{kn;lm} Q^*_{kn} (Q^*_{lm} + \tilde{Q}^*_{lm}) (PSM - S)^{(0)}_{k+l,n+m}$$

All of the terms with k+l=odd are zero, because of the inversion symmetry in the lattice sums.

Long-range forces on the particles are

$$\begin{aligned} \vec{f}^{(lr)}_i &= -\frac{\partial E_{mp}}{\partial \vec{r}_i} \\ &= -\frac{1}{2} q_i \sum_{kn} \frac{\partial}{\partial \vec{r}_i} (r^k_i Y^*_{kn}(\hat{r}_i)) \sum_{lm} c_{kn;lm} (2Q^*_{lm} + \tilde{Q}^*_{lm}) (PSM - S)^{(0)}_{k+l,n+m} \\ &\quad + \frac{1}{2} q_i \sum_{knlm} c_{kn;lm} Q^*_{kn} \sum_{j=a,b,c} \vec{h}_j^{-1} (\frac{1}{2} j)^l (Y^*_{lm}(\hat{j}) - Y^*_{lm}(-\hat{j})) (PSM - S)^{(0)}_{k+l,n+m} \end{aligned}$$

The derivatives of the spherical harmonics are calculated with the following expressions:

$$\begin{aligned} \frac{\partial}{\partial x}[r^l Y^*_{lm}(\hat{r})] &= \frac{1}{2}[r^{l-1} Y^*_{l-1,m+1}(\hat{r}) - (l+m)(l+m-1) r^{l-1} Y^*_{l-l,m-1}(\hat{r})] \\ \frac{\partial}{\partial y}[r^l Y^*_{lm}(\hat{r})] &= -\frac{i}{2}[r^{l-1} Y^*_{l-1,m+1}(\hat{r}) + (l+m)(l+m-1) r^{l-1} Y^*_{l-l,m-1}(\hat{r})] \\ \frac{\partial}{\partial z}[r^l Y^*_{lm}(\hat{r})] &= (l+m) r^{l-1} Y^*_{l-1,m}(\hat{r}) \end{aligned}$$

The long-range 'virtual' forces are

$$
\begin{aligned}
f_h^{(lr)} &= -\frac{\partial E_{mp}}{\partial h} \\
&= -\frac{1}{2}\sum_{k=1}^{\mu-1}\sum_{n}\sum_{l=1}^{\mu-k}\sum_{m} c_{kn;lm} Q_{kn}^{*}(Q_{lm}^{*}+\tilde{Q}_{lm}^{*})(PSM-S)_{k+l,n+m}^{(h)} \\
&\quad -\frac{1}{2}\sum_{k=1}^{\mu-1}\sum_{n}\sum_{l=1}^{\mu-k}\sum_{m} c_{kn;lm} Q_{kn}^{*}\frac{\partial \tilde{Q}_{lm}^{*}}{\partial h}(PSM-S)_{k+l,n+m}^{(0)} \\
S_{lm}^{(h)} &= \frac{\partial}{\partial h}\sum_{nn'}\frac{Y_{lm}(R_{\alpha\beta\gamma})}{R_{\alpha\beta\gamma}^{l+1}} \\
&= \sum_{nn'}\frac{\partial}{\partial \vec{R}_{\alpha\beta\gamma}}\left(\frac{Y_{lm}(R_{\alpha\beta\gamma})}{R_{\alpha\beta\gamma}^{l+1}}\right)(\alpha \quad \beta \quad \gamma) \\
PSM_{lm}^{(h)} &= \frac{\partial}{\partial h}{\sum_{\alpha\beta\gamma}}'\frac{Y_{lm}(R_{\alpha\beta\gamma})}{R_{\alpha\beta\gamma}^{l+1}} \\
\left(\frac{\partial \tilde{Q}_{lm}}{\partial h}\right)_{ij} &= \frac{\partial \tilde{Q}_{lm}}{\partial h_{ij}} \\
&= \tilde{q}_j\left(\frac{\partial}{\partial r_i}+\sum_k h_{ki}^{-1}\right)q_{lm}^{(j)} \\
q_{lm}^{(j)} &\equiv \left(\frac{1}{2}\right)^l Y_{lm}(\hat{j}) \qquad j=a,b,c
\end{aligned}
$$

The derivatives of the spherical harmonics are obtained from the differentiation formula:

$$
\begin{aligned}
\frac{\partial}{\partial x}\left[\frac{Y_{lm}^{*}(\hat{r})}{r^{l+1}}\right] &= \frac{1}{2}\left[\frac{Y_{l+1,m+1}^{*}(\hat{r})}{r^{l+2}}-(l-m+2)(l-m+1)\frac{Y_{l+l,m-1}^{*}(\hat{r})}{r^{l+2}}\right] \\
\frac{\partial}{\partial y}\left[\frac{Y_{lm}^{*}(\hat{r})}{r^{l+1}}\right] &= -\frac{i}{2}\left[\frac{Y_{l+1,m+1}^{*}(\hat{r})}{r^{l+2}}+(l-m+2)(l-m+1)\frac{Y_{l+l,m-1}^{*}(\hat{r})}{r^{l+2}}\right] \\
\frac{\partial}{\partial z}\left[\frac{Y_{lm}^{*}(\hat{r})}{r^{l+1}}\right] &= -(l-m+1)\frac{Y_{l+l,m}^{*}(\hat{r})}{r^{l+2}}
\end{aligned}
$$

Expressions for the components of $PSM_{lm}^{(h)}$ are given in the next section.

D-3 Planewise Summations

The equations used to implement the planewise summation method are adapted from the formula of Massidda[65] for a general triclinic lattice. The equations used here are as follows:

$$
\begin{aligned}
\sum_{\alpha\beta\gamma}{}' \frac{Y_{\mu\nu}(\hat{R}_{\alpha\beta\gamma})}{R_{\alpha\beta\gamma}^{\mu+1}} &\equiv PSM_{\mu\nu}^{(0)} \\
&= S_{\mu\nu}^{(0)} + S_{\mu\nu}^{(1)} + S_{\mu\nu}^{(2)} \\
S_{\mu\nu}^{(0)} &= (-1)^{\frac{\mu}{2}} (\frac{\sqrt{\pi}}{a_x})^{\mu} \frac{2}{(\frac{\mu}{2})!} (\frac{1}{(\mu-1)b_y} - \frac{1}{(\mu+1)a_x}) \delta_{\nu 0} \\
S_{\mu\nu}^{(1)} &= \frac{2}{a_x^{\mu} b_y} \frac{(2\pi)^{\mu}}{(\mu-\nu)!} \sum_{\alpha\beta}{}' l i^{\nu} e^{i\nu\theta_{\alpha\beta}} h_{\alpha\beta}^{\mu-1} c_{\alpha\beta} c_{\alpha\beta l} \\
\theta_{\alpha\beta} &= tan^{-1}(\frac{\vec{h}_{\alpha\beta} \cdot \hat{y}}{\vec{h}_{\alpha\beta} \cdot \hat{x}}) \equiv tan^{-1} \frac{h_{\alpha\beta,y}}{h_{\alpha\beta,x}} \\
\vec{h}_{\alpha\beta} &= \alpha\hat{x} + \frac{1}{b_y}(\beta a_x - \alpha b_x)\hat{y} \\
c_{\alpha\beta} &= \frac{e^{-H_{\alpha\beta}}}{1 - e^{-H_{\alpha\beta}}(2cosX_{\alpha\beta} - e^{-H_{\alpha\beta}})} \\
H_{\alpha\beta} &= 2\pi \frac{c_z}{a_x} h_{\alpha\beta} \\
X_{\alpha\beta} &= 2\pi(\frac{\alpha}{a_x}(c_x - \frac{c_y b_x}{b_y}) + \frac{\beta c_y}{b_y}) \\
c_{\alpha\beta l} &= \begin{cases} cosX_{\alpha\beta} - e^{-H_{\alpha\beta}} & \nu = even \\ sinX_{\alpha\beta} & \nu = odd \end{cases} \\
S_{\mu\nu}^{(2)} &= \frac{2^{\nu}(-1)^{\frac{1}{2}(\mu+\nu)}}{\sqrt{\pi}[\frac{1}{2}(\mu-\nu)]!} (\sum_{\alpha\beta}{}' \frac{e^{i\nu\phi_{\alpha\beta}} \Gamma[\frac{1}{2}(\mu+\nu+1), \pi\sigma_{\alpha\beta}^2]}{(a_x \sigma_{\alpha\beta})^{\mu+1}} \\
&\quad + \frac{\pi^{\mu}}{a_x^{\mu} b_y} \sum_{\alpha\beta}{}' l i^{\nu} e^{i\nu\theta_{\alpha\beta}} h_{\alpha\beta}^{\mu-1} \Gamma[\frac{1}{2}(-\mu+\nu+1), \pi h_{\alpha\beta}^2]) \\
\vec{\sigma}_{\alpha\beta} &= (\alpha + \frac{\beta b_x}{a_x})\hat{x} + \frac{\beta b_y}{a_x}\hat{y} \\
\phi_{\alpha\beta} &= tan^{-1}(\frac{\vec{\sigma}_{\alpha\beta} \cdot \hat{y}}{\vec{\sigma}_{\alpha\beta} \cdot \hat{x}}) \equiv tan^{-1} \frac{\sigma_{\alpha\beta,y}}{\sigma_{\alpha\beta,x}} \\
\Gamma(a,x) &= \int_x^{\infty} e^{-t} t^{(a-1)} dt
\end{aligned}
$$

The incomplete gamma function $\Gamma(a,x)$ is calculated for $a = \frac{1}{2}, x = \pi h_{\alpha\beta}^2$ and $a = \frac{3}{2}$, $x = \pi\sigma_{\alpha\beta}^2$. For other values of a, the recurrence relation is used:

$$\Gamma(a+1,x) = a\Gamma(a,x) + x^a e^{-x}$$

The derivatives with respect to the components of the matrix h are

$$PSM_{\mu\nu}^{(h)} = \frac{\partial S_{\mu\nu}^{(0)}}{\partial h} + \frac{\partial S_{\mu\nu}^{(1)}}{\partial h} + \frac{\partial S_{\mu\nu}^{(2)}}{\partial h}$$

The non-zero derivatives of $S_{\mu\nu}^{(0)}$ are

$$\begin{aligned} c_{\mu}^{(0)} &\equiv (-1)^{\frac{\mu}{2}} \left(\frac{\sqrt{\pi}}{a_x}\right)^{\mu} \frac{2}{(\frac{1}{2}\mu)!} \\ \frac{\partial S_{\mu\nu}^{(0)}}{\partial a_x} &= -\frac{c_{\mu}^{(0)}}{a_x}\left[\frac{\mu}{(\mu-1)b_y} - \frac{1}{a_x}\right] \\ \frac{\partial S_{\mu\nu}^{(0)}}{\partial b_y} &= -\frac{c_{\mu}^{(0)}}{(\mu-1)b_y^2} \end{aligned}$$

Derivatives of $S_{\mu\nu}^{(1)}$ are:

$$\begin{aligned} c_{\mu\nu}^{(1)} &\equiv \frac{2(2\pi)^{\mu}}{(\mu-\nu)!} \\ \frac{\partial S_{\mu\nu}^{(1)}}{\partial h} &= \frac{c_{\mu\nu}^{(1)}}{a_x^{\mu} b_y} {\sum_{\alpha\beta}}' i^{\nu} e^{i\nu\theta_{\alpha\beta}} h_{\alpha\beta}^{\mu-2} c_{\alpha\beta} c_{\alpha\beta'} \left\{ \frac{i\nu h_{\alpha\beta,x} + (\mu-1)h_{\alpha\beta,y}}{h_{\alpha\beta}} \frac{\partial h_{\alpha\beta,y}}{\partial h} \right. \\ &\quad \left. -h_{\alpha\beta}c_{\alpha\beta}(\sinh H_{\alpha\beta}\frac{\partial H_{\alpha\beta}}{\partial h} + \sin X_{\alpha\beta}\frac{\partial X_{\alpha\beta}}{\partial h}) + \frac{h_{\alpha\beta}}{c_{\alpha\beta'}}\frac{\partial c_{\alpha\beta'}}{\partial h} \right\} \\ &\quad + \frac{\partial (a_x^{\mu} b_y)^{-1}}{\partial h} c_{\mu\nu}^{(1)} {\sum_{\alpha\beta}}' i^{\nu} e^{i\nu\theta_{\alpha\beta}} h_{\alpha\beta}^{\mu-1} c_{\alpha\beta} c_{\alpha\beta'} \\ \frac{\partial c_{\alpha\beta'}}{\partial h} &= \begin{cases} -\sin X_{\alpha\beta}\frac{\partial X_{\alpha\beta}}{\partial h} + e^{-H_{\alpha\beta}}\frac{\partial H_{\alpha\beta}}{\partial h} & \nu = even \\ \cos X_{\alpha\beta}\frac{\partial X_{\alpha\beta}}{\partial h} & \nu = odd \end{cases} \\ \frac{\partial h_{\alpha\beta,y}}{\partial h} &= -\frac{1}{b_y}\begin{pmatrix} -\beta & \alpha & 0 \\ 0 & h_{\alpha\beta,y} & 0 \\ 0 & 0 & 0 \end{pmatrix} \\ \frac{\partial H_{\alpha\beta}}{\partial h} &= H_{\alpha\beta}\begin{pmatrix} -\frac{1}{a_x} & 0 & 0 \\ 0 & 0 & 0 \\ 0 & 0 & \frac{1}{c_z} \end{pmatrix} + H_{\alpha\beta}\frac{h_{\alpha\beta,y}}{h_{\alpha\beta}^2}\begin{pmatrix} \beta & -\alpha & 0 \\ 0 & -h_{\alpha\beta,y} & 0 \\ 0 & 0 & 0 \end{pmatrix} \\ \frac{\partial X_{\alpha\beta}}{\partial h} &= 2\pi\begin{pmatrix} -\frac{\alpha}{a_x^2}(c_x - \frac{c_y b_x}{b_y}) & -\frac{\alpha c_y}{a_x b_y} & \frac{\alpha}{a_x} \\ 0 & \frac{1}{b_y^2}(\frac{\alpha c_y b_x}{a_x} - \beta c_y) & -\frac{\alpha b_x}{a_x b_y} \\ 0 & 0 & 0 \end{pmatrix} \\ \frac{\partial (a_x^{\mu} b_y)^{-1}}{\partial h} &= -\frac{1}{a_x^{\mu} b_y}\begin{pmatrix} \frac{\mu}{a_x} & 0 & 0 \\ 0 & \frac{1}{b_y} & 0 \\ 0 & 0 & 0 \end{pmatrix} \end{aligned}$$

Finally, the derivatives of $S^{(2)}_{\mu\nu}$ are:

$$
\begin{aligned}
c^{(2)}_{\mu\nu} &= \frac{(-1)^{\mu}2^{\nu}}{\sqrt{\pi}(\frac{1}{2}[\mu-\nu]!)} \\
\frac{\partial S^{(2)}_{\mu\nu}}{\partial h} &= c^{(2)}_{\mu\nu}{\sum_{\alpha\beta}}' \frac{e^{i\nu\phi_{\alpha\beta}}\Gamma[\frac{1}{2}(\mu+\nu+1),\pi\sigma^2_{\alpha\beta}]}{(a_x\sigma_{\alpha\beta})^{\mu+1}} \\
&\quad * \left\{ \frac{i\nu}{\sigma^2_{\alpha\beta}}(\sigma_{\alpha\beta,x}\frac{\partial\sigma_{\alpha\beta,y}}{\partial h} - \sigma_{\alpha\beta,y}\frac{\partial\sigma_{\alpha\beta,x}}{\partial h}) - \frac{(\mu+1)}{a_x\sigma^2_{\alpha\beta}}\vec{\sigma}_{\alpha\beta}(\alpha \quad \beta \quad 0) \right\} \\
&\quad -2\pi^{\frac{1}{2}(\mu+\nu+1)}c^{(2)}_{\mu\nu}{\sum_{\alpha\beta}}' \frac{e^{i\nu\phi_{\alpha\beta}}}{(a_x\sigma_{\alpha\beta})^{\mu+1}}e^{-\pi\sigma^2_{\alpha\beta}}\sigma^{(\mu+\nu-1)}_{\alpha\beta}(\sigma_{\alpha\beta,x}\frac{\partial\sigma_{\alpha\beta,x}}{\partial h} + \sigma_{\alpha\beta,y}\frac{\partial\sigma_{\alpha\beta,y}}{\partial h}) \\
&\quad + \frac{\partial(a^{\mu}_x b_y)^{-1}}{\partial h}c^{(2)}_{\mu\nu}\pi^{\mu}i^{\nu}{\sum_{\alpha\beta}} \prime e^{i\nu\theta_{\alpha\beta}}h^{\mu-1}_{\alpha\beta}\Gamma[\frac{1}{2}(-\mu+\nu+1),\pi h^2_{\alpha\beta}]) \\
&\quad + c^{(2)}_{\mu\nu}\frac{\pi^{\mu}}{a^{\mu}_x b_y}{\sum_{\alpha\beta}} \prime i^{\nu}e^{i\nu\theta_{\alpha\beta}}h^{\mu-3}_{\alpha\beta}\Gamma[\frac{1}{2}(-\mu+\nu+1),\pi h^2_{\alpha\beta}] \\
&\quad * (i\nu h_{\alpha\beta,x} + (\mu-1)h_{\alpha\beta,y})\frac{\partial h_{\alpha\beta,y}}{\partial h} \\
&\quad -2c^{(2)}_{\mu\nu}\frac{\pi^{\frac{1}{2}(\mu+\nu+1)}}{a^{\mu}_x b_y}{\sum_{\alpha\beta}}' i^{\nu}e^{i\nu\theta_{\alpha\beta}}e^{-\pi h^2_{\alpha\beta}}h^{\nu-2}_{\alpha\beta}\frac{\partial h_{\alpha\beta,y}}{\partial h} \\
\frac{\partial\sigma_{\alpha\beta,x}}{\partial h} &= \frac{\beta}{a_x}\begin{pmatrix} -\frac{b_x}{a_x} & 1 & 0 \\ 0 & 0 & 0 \\ 0 & 0 & 0 \end{pmatrix} \\
\frac{\partial\sigma_{\alpha\beta,y}}{\partial h} &= \frac{\beta}{a_x}\begin{pmatrix} -\frac{b_y}{a_x} & 0 & 0 \\ 0 & 1 & 0 \\ 0 & 0 & 0 \end{pmatrix}
\end{aligned}
$$

Appendix E

Planewise Sums for r^{-4} and r^{-6}

The evaluation of lattice sums with the form

$$U^n(\vec{r},h) \equiv \frac{1}{2}\sum_{ij} c_{ij} \sum_{\alpha\beta\gamma}{}' \frac{1}{\mid \vec{R}_{\alpha\beta\gamma} - \vec{r}_{ij} \mid^{\frac{n}{2}}}$$

is performed here for n=4 and n=6. The method generally follows that of Scholl[68], including planewise summation over the lattice. The prime on the sum indicates exclusion of the self-energy term.

The terms with $\vec{r}_{ij} = 0$ are separated from the total, and the two sums are evaluated separately:

$$U^n(\vec{r},h) = \frac{1}{2}\sum_i \sum_{j\neq i} c_{ij} S_1^{(n)}(\vec{r},h) + \frac{1}{2}\sum_i c_{ii} S_0^{(n)}(h)$$

$$S_1^{(n)} = \sum_{\alpha\beta\gamma} \frac{1}{\mid \vec{R}_{\alpha\beta\gamma} - \vec{r} \mid^n}$$

$$S_0^{(n)} = \sum_{\alpha\beta\gamma}{}' \frac{1}{R^n_{\alpha\beta\gamma}}$$

In these expressions

$$\begin{aligned}
\vec{R}_{\alpha\beta\gamma} &= \alpha\vec{a} + \beta\vec{b} + \gamma\vec{c} \\
&= (\alpha a_x + \beta b_x + \gamma c_x)\hat{x} + (\beta b_y + \gamma c_y)\hat{y} + (\gamma c_z)\hat{z} \\
\vec{r} &= \vec{r}_{ij} \\
&= \xi\vec{a} + \eta\vec{b} + \zeta\vec{c}
\end{aligned}$$

With the following definitions

$$\begin{aligned}
\vec{\sigma}_{\alpha\beta} &= \alpha\vec{a} + \beta\vec{b} \\
\vec{\sigma}_{\gamma} &= \gamma(c_x\hat{x} + c_y\hat{y}) \\
&= \gamma\left(\frac{b_y c_x - c_y b_x}{a_x b_y}\vec{a} + \frac{c_y}{b_y}\vec{b}\right) \\
\vec{\sigma}_{r} &= \xi\vec{a} + \eta\vec{b} \\
k &= \mid \gamma - \zeta \mid c_z
\end{aligned}$$

then

$$S_1^{(n)} = \sum_\gamma \sum_{\alpha\beta} \frac{1}{(\mid \vec{\sigma}_{\alpha\beta} + \vec{\sigma}_\gamma - \vec{\sigma}_r \mid^2 + k^2)^{\frac{n}{2}}}$$

The sum over α and β is done by applying the two-dimensional version of Poisson's rule:

$$\sum_{\alpha\beta} f(\vec{\sigma}_{\alpha\beta}) = \frac{1}{\omega} \sum_{\mu\nu} F(\vec{s}_{\mu\nu})$$

where

$$\begin{aligned}
\vec{s}_{\mu\nu} &= \mu\vec{s}_a + \nu\vec{s}_b \\
\vec{s}_i \cdot \vec{j} &= \delta_{ij} \quad i,j = a,b \\
\omega &= \vec{a} \times \vec{b} \\
F(\vec{s}) &= \int d^2\sigma \frac{e^{i2\pi\vec{\sigma}\cdot\vec{s}}}{(\mid \vec{\sigma} + \vec{\sigma}_\gamma - \vec{\sigma}_r \mid^2 + k^2)^{\frac{n}{2}}} \\
&= e^{-i2\pi(\vec{\sigma}_\gamma - \vec{\sigma}_r)\cdot\vec{s}} \int d^2\sigma \frac{e^{i2\pi\vec{\sigma}\cdot\vec{s}}}{(\sigma^2 + k^2)^{\frac{n}{2}}}
\end{aligned}$$

The angular integral is

$$\int_{\theta=0}^{2\pi} d\theta e^{i2\pi s\sigma cos(\theta)} = 2\pi J_0(2\pi s\sigma)$$

The complete integral is[73]:

$$\begin{aligned}
\int d^2\sigma \frac{e^{i2\pi\vec{\sigma}\cdot\vec{s}}}{(\sigma^2 + k^2)^{\frac{n}{2}}} &= \int_0^\infty d\sigma \frac{\sigma}{(\sigma^2 + k^2)^{\frac{n}{2}}} 2\pi J_0(2\pi s\sigma) \\
&= 2\pi \frac{k^{1-\frac{n}{2}}(2\pi s)^{\frac{n}{2}-1}}{2^{\frac{n}{2}-1}\Gamma(\frac{n}{2})} K_{-\frac{n}{2}-1}(2\pi sk)
\end{aligned}$$

For n=4 and n=6, this becomes

$$\begin{aligned}
S_1^{(4)} &= \sum_\gamma \frac{\pi}{\omega} \sum_{\mu\nu} e^{-i2\pi(\vec{\sigma}_\gamma - \vec{\sigma}_r)\cdot\vec{s}_{\mu\nu}} \frac{2\pi s_{\mu\nu}}{k} K_{-1}(2\pi s_{\mu\nu}k) \\
S_1^{(6)} &= \sum_\gamma \frac{\pi}{\omega} \sum_{\mu\nu} e^{-i2\pi(\vec{\sigma}_\gamma - \vec{\sigma}_r)\cdot\vec{s}_{\mu\nu}} \frac{\pi^2 s_{\mu\nu}^2}{k^2} K_{-2}(2\pi s_{\mu\nu}k)
\end{aligned}$$

The modified Bessel functions can be replaced with the integral expression

$$K_{-n}(z) = \frac{\sqrt{\pi}(\frac{1}{2}z)^n}{\Gamma(n + \frac{1}{2})} \int_1^\infty e^{-zt}(t^2 - 1)^{n-\frac{1}{2}} dt$$

With the change of variables $x = 2\pi s_{\mu\nu}t$, the sums are then

$$
\begin{aligned}
S_1^{(4)} &= \frac{\pi}{\omega}\sum_{\mu\nu} e^{-i2\pi(\vec{\sigma}_\gamma-\vec{\sigma}_r)\cdot\vec{s}_{\mu\nu}} \int_{2\pi s_{\mu\nu}}^{\infty} dx(x^2-(2\pi s_{\mu\nu})^2)^{\frac{1}{2}} \sum_{\gamma} e^{-|\gamma-\zeta|c_z x} e^{-i\gamma c_{\mu\nu}} \\
S_1^{(6)} &= \frac{\pi}{12\omega}\sum_{\mu\nu} e^{-i2\pi(\vec{\sigma}_\gamma-\vec{\sigma}_r)\cdot\vec{s}_{\mu\nu}} \int_{2\pi s_{\mu\nu}}^{\infty} dx(x^2-(2\pi s_{\mu\nu})^2)^{\frac{3}{2}} \sum_{\gamma} e^{-|\gamma-\zeta|c_z x} e^{-i\gamma c_{\mu\nu}} \\
c_{\mu\nu} &\equiv 2\pi\vec{\sigma}_\gamma\cdot\vec{s}_{\mu\nu}
\end{aligned}
$$

The sum over γ can now be done analytically, yielding

$$
\begin{aligned}
\sum_{\gamma} e^{-|\gamma-\zeta|c_z x} e^{-i\gamma c_{\mu\nu}} &= \frac{\sinh((1+\zeta)c_z x)+e^{ic_{\mu\nu}}\sinh(\zeta c_z x)}{\cosh(c_z x)-\cos(c_{\mu\nu})} \qquad \zeta \le 0 \\
&= \frac{\sinh((1-\zeta)c_z x)+e^{-ic_{\mu\nu}}\sinh(\zeta c_z x)}{\cosh(c_z x)-cos(c_{\mu\nu})} \qquad \zeta \ge 0
\end{aligned}
$$

Inserting the expression for the sum over γ into $S_1^{(4)}$ and $S_1^{(6)}$ makes the integral rather complicated. Without an analytic expression for this integral, it would be simpler computationally to use the three-dimensional sums with the modified Bessel functions $K_1(z)$ and $K_2(z)$. These functions decrease asymptotically as $z^{-\frac{1}{2}}e^{-z}$, so convergence should be fairly rapid.

The second part of the lattice sum is

$$
\begin{aligned}
S_0^{(n)} &= {\sum_{\alpha\beta\gamma}}' \frac{1}{R_{\alpha\beta\gamma}^n} \\
&= \sum_{\gamma\neq 0}\sum_{\alpha\beta} \frac{1}{R_{\alpha\beta\gamma}^n} + {\sum_{\alpha\beta}}' \frac{1}{R_{\alpha\beta 0}^n} \\
&\equiv S_{0a}^{(n)} + S_{0b}^{(n)}
\end{aligned}
$$

The first term, with $\gamma \neq 0$, can be evaluated by the same method used for $S_1^{(n)}$. The resulting expressions are

$$
\begin{aligned}
S_{0a}^{(4)} &= \sum_{\gamma\neq 0}\frac{\pi}{\omega}\sum_{\mu\nu} e^{-i2\pi(\vec{\sigma}_\gamma-\vec{\sigma}_r)\cdot\vec{s}_{\mu\nu}} \frac{2\pi s_{\mu\nu}}{|\gamma|c_z} K_{-1}(2\pi s_{\mu\nu}c_z\,|\,\gamma\,|) \\
S_{0a}^{(6)} &= \sum_{\gamma\neq 0}\frac{\pi}{\omega}\sum_{\mu\nu} e^{-i2\pi(\vec{\sigma}_\gamma-\vec{\sigma}_r)\cdot\vec{s}_{\mu\nu}} \frac{\pi^2 s_{\mu\nu}^2}{|\gamma|^2 c_z^2} K_{-2}(2\pi s_{\mu\nu}c_z\,|\,\gamma\,|)
\end{aligned}
$$

The sum over γ can again be performed within the integral representations of the modified Bessel function:

$$
\sum_{\gamma\neq 0} e^{-|\gamma|c_z x} e^{-i\gamma c_{\mu\nu}} = \frac{\cos(c_{\mu\nu})-e^{-c_z x}}{\cosh(c_z x)-\cos(c_{\mu\nu})}
$$

The term $S_{0b}^{(n)}$ can be partly evaluated by line-wise summation:

$$\begin{aligned}
\sum_{\alpha\beta}{}' \frac{1}{R_{\alpha\beta 0}^n} &= \sum_{\alpha\beta}{}' \frac{1}{((\alpha a_x+\beta b_x)^2+(\beta b_y)^2)^{\frac{n}{2}}} \\
&\equiv \sum_{\beta\neq 0}\sum_{\alpha} f_\beta^{(n)}(\alpha)+\sum_{\alpha\neq 0}\frac{1}{(\alpha a_x)^n} \\
f_\beta^{(n)}(x) &= \frac{1}{((xa_x+\beta b_x)^2+(\beta b_y)^2)^{\frac{n}{2}}}
\end{aligned}$$

The one-dimensional Poisson rule is applied to the first lattice sum, giving, for n=4,

$$\begin{aligned}
\sum_\alpha f_\beta^{(4)}(\alpha) &= \sum_\mu F_\beta^{(4)}(\mu) \\
F_\beta^{(4)}(\mu) &= \int_{-\infty}^{\infty} e^{-i2\pi\mu x} f_\beta^{(4)}(x)dx \\
&= \frac{\pi}{2a_x}\left(\frac{a_x}{2\pi b_y \mid \beta \mid}\right)^3 (1+\frac{2\pi b_y \mid \beta \mid}{a_x} \mid \mu \mid) e^{-\frac{2\pi|\beta|}{a_x}(b_y|\mu|-b_x\mu)}
\end{aligned}$$

This expression can be summed in two dimensions, with convergence going as $\beta^{-3}e^{-|\beta|}$. The complete expression for n=4 is

$$\begin{aligned}
S_{0b}^{(4)} &= \frac{1}{2}\left(\frac{a_x}{2\pi}\right)^2 \sum_{\beta=1}^{\infty}\frac{1}{(\beta b_y)^3}\left\{1+2\sum_{\mu=1}^{\infty}(1+2\pi\frac{b_y}{a_x}\beta\mu)e^{-2\pi\frac{b_y}{a_x}\beta\mu}\cos(2\pi\frac{b_x}{a_x}\beta\mu)\right\} \\
&\quad +\sum_{\beta\neq 0}\frac{1}{(\beta a_x)^4}
\end{aligned}$$

With the sum over μ done analytically, this becomes

$$\begin{aligned}
S_{0b}^{(4)} &= \frac{1}{2}\left(\frac{a_x}{2\pi}\right)^2 \sum_{\beta=1}^{\infty}\frac{1}{(\beta b_y)^3}\left\{\frac{e^{2\pi\frac{b_y}{a_x}\beta}-\cos(2\pi\frac{b_x}{a_x}\beta)}{\cosh(2\pi\frac{b_y}{a_x}\beta)-cos(2\pi\frac{b_x}{a_x}\beta)}\right. \\
&\quad \left. +\frac{2\pi b_y\beta}{a_x}\frac{cosh(2\pi\frac{b_y}{a_x}\beta)\cos(2\pi\frac{b_x}{a_x}\beta)-1}{(\cosh(2\pi\frac{b_y}{a_x}\beta)-\cos(2\pi\frac{b_x}{a_x}\beta))^2}\right\} \\
&\quad +\sum_{\beta\neq 0}\frac{1}{(\beta a_x)^4}
\end{aligned}$$

Although the lattice sums in this expression are only one-dimensional, the first sum converges as β^{-3} and the second as β^{-4}. Neither can be said to converge quickly. A preferable method might be to apply an extended Ewald method to the two-dimensional sums obtained for $\vec{r}=0$ and $\gamma=0$.

Complete expressions for the lattice sums with $\vec{r}_{ij} = 0$ are

$$
\begin{aligned}
S_0^{(4)} &= \sum_{\gamma\neq 0}\frac{\pi}{\omega}\sum_{\mu\nu} e^{-i2\pi(\vec{\sigma}_\gamma-\vec{\sigma}_\tau)\cdot\vec{s}_{\mu\nu}}\frac{2\pi s_{\mu\nu}}{|\,\gamma\,|\,c_z}K_{-1}(2\pi s_{\mu\nu}c_z\,|\,\gamma\,|) \\
&\quad +\frac{1}{2}\left(\frac{a_x}{2\pi}\right)^2\sum_{\beta=1}^{\infty}\frac{1}{(\beta b_y)^3}\left\{1+2\sum_{\mu=1}^{\infty}(1+2\pi\frac{b_y}{a_x}\beta\mu)e^{-2\pi\frac{b_y}{a_x}\beta\mu}\cos(2\pi\frac{b_x}{a_x}\beta\mu)\right\} \\
&\quad +\sum_{\beta\neq 0}\frac{1}{(\beta a_x)^4} \\
S_0^{(6)} &= \sum_{\gamma\neq 0}\frac{\pi}{\omega}\sum_{\mu\nu} e^{-i2\pi(\vec{\sigma}_\gamma-\vec{\sigma}_\tau)\cdot\vec{s}_{\mu\nu}}\frac{\pi^2 s_{\mu\nu}^2}{|\,\gamma\,|^2\,c_z^2}K_{-2}(2\pi s_{\mu\nu}c_z\,|\,\gamma\,|) \\
&\quad +\frac{1}{8}\left(\frac{a_x}{2\pi}\right)^2\sum_{\beta=1}^{\infty}\frac{b_y}{(\beta b_y)^5}\left\{-\frac{3\beta}{b_y}+2\sum_{\mu=1}^{\infty}\left[-\frac{3\beta}{b_y}(1+2\pi\frac{b_y}{a_x}\beta\mu)\right.\right. \\
&\quad \left.\left.+\frac{2\pi\beta\mu}{a_x}(1-\frac{2\pi\beta\mu}{a_x})\right]e^{-2\pi\frac{b_y}{a_x}\beta\mu}\cos(2\pi\frac{b_x}{a_x}\beta\mu)\right\} \\
&\quad +\sum_{\beta\neq 0}\frac{1}{(\beta a_x)^6}
\end{aligned}
$$

The expression for n=6 was obtained with the use of the relation

$$F_\beta^{(6)}(\mu) = -\frac{1}{4\beta^2 b_y}\frac{\partial F_\beta^{(4)}}{\partial b_y}$$

Appendix F

Error Approximations for Numerical Calculations

F-1 Short-range Energy

The truncation error for the short-range energy is defined as

$$\begin{aligned}
\delta E^{(sr)} &= E^{(sr)} - E^{(sr)}_{calc} \\
&= \frac{1}{2}\sum_{ij} c_{ij} \left\{ \sum_{\alpha\beta\gamma=-\infty}^{\infty} \frac{1}{\mid \vec{r}_i - \vec{R}_{\alpha\beta\gamma} - \vec{r}_j \mid^n} - \sum_{\alpha\beta\gamma=nn} \frac{1}{\mid \vec{r}_i - \vec{R}_{\alpha\beta\gamma} - \vec{r}_j \mid^n} \right\} \\
&\equiv \frac{1}{2}\sum_{ij} c_{ij} \sum_{\alpha\beta\gamma\neq nn} \frac{1}{\mid \vec{R}_{\alpha\beta\gamma} - \vec{r}_{ij} \mid^n}
\end{aligned}$$

If the lattice sums are truncated by deleting any terms with the absolute value of the lattice indices α, β, or γ greater than a given positive integer M, then the error can be characterized as a function of M.

The number of lattice points with the absolute value of any one or more of the lattice indices equal to M and having no index with absolute value greater than M (abbreviated as $\alpha\beta\gamma \in M$) is

$$m_M = 24M^2 + 2$$

Then

$$\begin{aligned}
\delta E^{(sr)} &= \frac{1}{2}\sum_{ij} c_{ij} \sum_{\mu=M+1}^{\infty} \sum_{\alpha\beta\gamma\in\mu} \frac{1}{\mid \vec{R}_{\alpha\beta\gamma} - \vec{r}_{ij} \mid^n} \\
&\leq \frac{1}{2}\sum_{ij} c_{ij} \sum_{\mu=M+1}^{\infty} \frac{24\mu^2 + 2}{[(\mu-1)a]^n} \\
&\approx \frac{1}{2}\sum_{ij} c_{ij} \int_{\mu=M}^{\infty} d\mu \frac{24}{a^n \mu^{n-2}} \\
&= \frac{12}{a^n (n-3) M^{n-3}} \sum_{ij} c_{ij}
\end{aligned}$$

In these equations the quantity a is an average lattice vector length. The total short-range energy is approximated by calculating the energy in the unit cell with a separation between particles of half of the lattice vector length:

$$E^{(sr)} \approx \frac{1}{2}\sum_{ij} c_{ij} \left(\frac{2}{a}\right)^n$$

Then

$$\begin{aligned} \epsilon_M^{(sr)} &\equiv \frac{\delta E^{(sr)}}{E^{(sr)}} \\ &\approx \frac{24}{2^n}\frac{1}{(n-3)M^{n-3}} \end{aligned}$$

If the sums are truncated instead by including only terms with $R_{\alpha\beta\gamma} \leq R_{co}$, then the truncation error is

$$\begin{aligned} \delta E^{(sr)} &\approx \frac{1}{2}\sum_{ij}\sum_{\mu=\frac{R_{co}}{a}}^{\infty}\sum_{\mu a \leq R_{\alpha\beta\gamma} \leq (\mu+1)a} \frac{1}{\mid \vec{R}_{\alpha\beta\gamma} - \vec{r}_{ij} \mid^n} \\ &\approx \frac{1}{2}\sum_{ij} c_{ij} \sum_{\mu=\frac{R}{a}}^{\infty} \frac{4\pi\mu^2}{(\mu a)^n} \\ &\leq \frac{2\pi}{a^n}\sum_{ij} c_{ij} \int_{\frac{R}{a}}^{\infty} \frac{d\mu}{\mu^{n-2}} \\ &= \frac{2\pi}{a^n}\frac{1}{(n-3)}(\frac{a}{R})^{n-3}\sum_{ij} c_{ij} \end{aligned}$$

Then

$$\begin{aligned} \epsilon_R^{(sr)} &\equiv \frac{\delta E^{(sr)}}{E^{(sr)}} \\ &\approx \frac{4\pi}{2^n}\frac{1}{(n-3)}(\frac{a}{R})^{n-3} \end{aligned}$$

F-2 Ewald Energy Sums

The Ewald energy contains sums over reciprocal space as well as a direct lattice sum. If the free parameter ϵ is chosen so that the two sums converge at the same rate, then the total truncation error will be twice that calculated for either sum alone. This is assumed to be the case, so the truncation error is calculated for by considering only the reciprocal space sum. The value used for ϵ is $\frac{\sqrt{\pi}}{a}$, where a is the length of a unit cell vector. The truncation error is estimated as

$$\begin{aligned} \delta E_M^{(ew)} &\approx 2 \cdot \frac{1}{2}\frac{4\pi}{\Omega}\sum_{\mu=M+1}^{\infty}\sum_{\alpha\beta\gamma\in\mu}\frac{e^{-\frac{K^2_{\alpha\beta\gamma}}{4\epsilon^2}}}{K^2_{\alpha\beta\gamma}}\sum_{ij} q_i q_j e^{-i\vec{K}_{\alpha\beta\gamma}\cdot\vec{r}_{ij}} \\ &\leq \frac{4\pi}{\Omega}\sum_{\mu=M+1}^{\infty}\sum_{\alpha\beta\gamma\in\mu}\frac{e^{-\frac{K^2_{\alpha\beta\gamma}}{4\epsilon^2}}}{K^2_{\alpha\beta\gamma}}\sum_{ij} \mid q_i q_j \mid \end{aligned}$$

$$
\begin{aligned}
&\approx \frac{4\pi}{a^3}\sum_{\mu=M+1}^{\infty} 4\pi\mu^2 \frac{e^{-(\frac{2\pi}{a})^2(\frac{a^2}{4\pi})\mu^2}}{(\frac{2\pi}{a})^2\mu^2}\sum_{ij} \mid q_i q_j \mid \\
&\approx \frac{4}{a}\sum_{\mu=M+1}^{\infty} e^{-\pi\mu^2}\sum_{ij} \mid q_i q_j \mid \\
&\approx \frac{4}{a}e^{-\pi(M+1)^2}\sum_{ij} \mid q_i q_j \mid \\
\epsilon_M^{(ew)} &= \frac{\delta E_M^{(ew)}}{E^{(ew)}} \\
&\approx \frac{\delta E_1^{(ew)}}{\delta E_0^{(ew)}}\cdot\frac{\delta E_2^{(ew)}}{\delta E_1^{(ew)}}\cdot\cdots\cdot\frac{\delta E_M^{(ew)}}{\delta E_{M-1}^{(ew)}} \\
&= e^{-3\pi}e^{-5\pi}\cdots e^{-(2M+1)\pi} \\
&= e^{-\pi(3+5+\cdots+(2M+1))}
\end{aligned}
$$

In the expressions for the relative error, $\delta E_0^{(ew)}$ is taken to be equal to the total Ewald energy since the origin ($M = 0$) is excluded from the lattice sum. If the length of a second lattice vector $\vec{b}$ is greater than that of $\vec{a}$, then

$$
\begin{aligned}
\delta E_M^{(ew)} &\approx \frac{4}{a}e^{-\pi(\frac{a}{b})^2(M+1)^2} \\
\epsilon_M^{(ew)} &\approx e^{-\pi(\frac{a}{b})^2)(3+5+\cdots+(2M+1))}
\end{aligned}
$$

This expression is defined for $M \geq 1$, and is a maximum if a is the smallest lattice vector length and b is the largest.

F-3 Multipole Expansions

The multipole energy is defined in terms of the unnormalized spherical harmonics as

$$
\begin{aligned}
E^{(mp)} &= \frac{1}{\mid \vec{r}_i - \vec{R} - \vec{r}_j \mid} \\
&= \sum_{k=0}^{\infty}\sum_{n=-k}^{k}\sum_{l=0}^{\infty}\sum_{m=-l}^{l}\frac{(-1)^l(k+l-m-n)!}{(k+n)!(l+m)!} r_i^l Y_{lm}^*(\hat{r}_i) r_j^k Y_{kn}^*(\hat{r}_j)\frac{Y_{k+l,m+n}(\hat{R})}{R^{k+l+1}}
\end{aligned}
$$

If the multipole terms are calculated only up to a maximum index μ, then

$$
\begin{aligned}
E^{(mp)} &= \sum_{k=0}^{\mu}\sum_{n=-k}^{k}\sum_{l=0}^{\mu-k}\sum_{m=-l}^{l}\frac{(-1)^l(k+l-m-n)!}{(k+n)!(l+m)!} r_i^l Y_{lm}^*(\hat{r}_i) r_j^k Y_{kn}^*(\hat{r}_j)\frac{Y_{k+l,m+n}(\hat{R})}{R^{k+l+1}} \\
&\quad +\delta E_1^{(mp)} + \delta E_2^{(mp)}
\end{aligned}
$$

$$
\begin{aligned}
\delta E_1^{(mp)} &= \sum_{k=\mu+1}^{\infty}\sum_{n=-k}^{k}\sum_{l=0}^{\infty}\sum_{m=-l}^{l}\frac{(-1)^l(k+l-m-n)!}{(k+n)!(l+m)!}r_i^l Y_{lm}^*(\hat{r}_i)r_j^k Y_{kn}^*(\hat{r}_j)\frac{Y_{k+l,m+n}(\hat{R})}{R^{k+l+1}} \\
&= \sum_{k=\mu+1}^{\infty}\sum_{n=-k}^{k}\frac{(k-n)!}{(k+n)!}r_j^k Y_{kn}^*(\hat{r}_j)\frac{Y_{kn}(\hat{R}_i)}{R_i^{k+1}} \\
&\equiv \sum_{k=\mu+1}^{\infty}\sum_{n=-k}^{k}\frac{1}{(2k+1)}\frac{r_j^k}{R_i^{k+1}} \qquad \vec{R}_i \equiv \vec{r}_i - \vec{R} \\
&= \frac{1}{R_i}(\frac{r_j}{R_i})^{\mu+1}\sum_{l=0}^{\infty}(\frac{r_j}{R_i})^l \\
&\equiv \frac{1}{R_i}\frac{r_1^{\mu+1}}{(1-r_1)} \qquad r_1 \equiv \frac{r_j}{R_i} \\
\delta E_2^{(mp)} &= \sum_{k=0}^{\mu}\sum_{n=-k}^{k}\sum_{l=\mu-k+1}^{\infty}\sum_{m=-l}^{l}\frac{(-1)^l(k+l-m-n)!}{(k+n)!(l+m)!}r_i^l Y_{lm}^*(\hat{r}_i)r_j^k Y_{kn}^*(\hat{r}_j)\frac{Y_{k+l,m+n}(\hat{R})}{R^{k+l+1}} \\
&\approx \sum_{k=0}^{\mu}\sum_{n=-k}^{k}\sum_{l=\mu-k+1}^{\infty}\sum_{m=-l}^{l}\left[\frac{(k+l-m-n)!}{(2l+1)(2k+1)(2k+2l+1)}\right]^{\frac{1}{2}} \\
&\quad * \left[\frac{(k+l+m+n)!}{(l-m)!(l+m)!(k-n)!(k+n)!}\right]^{\frac{1}{2}}\frac{r_i^l r_j^k}{R^{k+l+1}} \\
&\approx \sum_{k=0}^{\mu}\sum_{l=\mu-k+1}^{\infty}\frac{(k+l)!}{k!l!}\frac{r_i^l r_j^k}{R^{k+l+1}} \\
&= \sum_{k=0}^{\mu}\sum_{l=\mu+1}^{\infty}\frac{l!}{k!(l-k)!}\frac{r_i^{l-k}r_j^k}{R^{l+1}} \\
&= \sum_{l=\mu+1}^{\infty}\frac{1}{R^{l+1}}\sum_{k=0}^{\mu}\frac{l!}{k!(l-k)!}r_i^{l-k}r_j^k \\
&\leq \sum_{l=\mu+1}^{\infty}\frac{1}{R^{l+1}}\sum_{k=0}^{l}\frac{l!}{k!(l-k)!}r_i^{l-k}r_j^k \\
&= \sum_{l=\mu+1}^{\infty}\frac{1}{R^{l+1}}(r_i+rj)^l \\
&= \frac{1}{R}(\frac{(r_i+rj)}{R})^{\mu+1}\sum_{l=0}^{\infty}(\frac{r_i+rj}{R})^l \\
&= \frac{1}{R}\frac{r_2^{\mu+1}}{(1-r_2)} \qquad r_2 \equiv \frac{r_i+r_j}{R}
\end{aligned}
$$

The approximations for the spherical harmonics are made by converting the unnormalized expressions to normalized form and replacing each normalized spherical harmonic with an average value of $(4\pi)^{-\frac{1}{2}}$.

If D is the length of the longest cell diagonal and the smallest lattice vector is n times the

length of the diagonal, then

$$\begin{aligned} r_i &\leq \frac{D}{2} \\ r_j &\leq \frac{D}{2} \\ R &\geq nD \quad n > 1 \end{aligned}$$

Then

$$\begin{aligned} r_1 &\leq \frac{\frac{1}{2}D}{nD - \frac{1}{2}D} \\ &= \frac{1}{2n-1} \\ r_2 &\leq \frac{\frac{1}{2}D + \frac{1}{2}D}{nD} \\ &= \frac{1}{n} \\ E^{(mp)} &\geq \frac{1}{nD + \frac{1}{2}D + \frac{1}{2}D} \\ &= \frac{1}{D}\frac{1}{(n+1)} \\ \delta E_1^{(mp)} &\leq \frac{1}{(nD - \frac{1}{2}D)}\left(\frac{1}{2n-1}\right)^{\mu+1}\left(\frac{1}{1-\frac{1}{2n-1}}\right) \\ &\leq \frac{1}{D}\left(\frac{1}{2n-1}\right)^{\mu+1}\left(\frac{1}{n-1}\right) \\ \epsilon_1^{(mp)} &= \frac{\delta E_1^{(mp)}}{E^{(mp)}} \\ &\leq \frac{(n+1)}{(n-1)}\left(\frac{1}{(2n-1)}\right)^{\mu+1} \\ \delta E_2^{(mp)} &\leq \frac{1}{nD}\left(\frac{1}{n}\right)^{\mu+1}\left(\frac{1}{1-\frac{1}{n}}\right) \\ &\leq \frac{1}{D}\left(\frac{1}{n}\right)^{\mu+1}\left(\frac{1}{n-1}\right) \\ \epsilon_2^{(mp)} &= \frac{\delta E_2^{(mp)}}{E^{(mp)}} \\ &\leq \frac{(n+1)}{(n-1)}\left(\frac{1}{n}\right)^{\mu+1} \end{aligned}$$

Since $\epsilon_1^{(mp)}$ is less than $\epsilon_2^{(mp)}$ for $n > 1$,

$$\epsilon(mp) \approx \frac{(n+1)}{(n-1)} n^{-(\mu+1)}$$

F-4 Planewise Summation

The truncation error for the planewise summation is found to be almost entirely due to the sum over lattice planes which excludes the plane at $z = 0$. The sum over terms for $z = 0$ is calculated with the use of incomplete gamma functions, which converge very rapidly with increasing lattice indices. The lattice sum for $z \neq 0$ is

$$
\begin{aligned}
S_{\mu\nu}^{(1)} &= \sum_{\gamma\neq 0}\sum_{\alpha\beta}{}' \frac{Y_{\mu\nu}(\hat{R}_{\alpha\beta\gamma})}{R_{\alpha\beta\gamma}^{\mu+1}} \\
&= \frac{2}{a_x^\mu b_y}\frac{(2\pi)^\mu}{(\mu-\nu)!} i^\nu \sum_{\alpha\beta}{}' \frac{e^{i\nu\theta_{\alpha\beta}} h_{\alpha\beta}^{\mu-1}}{\cosh H_{\alpha\beta} - \cos X_{\alpha\beta}} \begin{cases} \cos X_{\alpha\beta} - e^{-H_{\alpha\beta}} & \nu = even \\ \sin X_{\alpha\beta} & \nu = odd \end{cases} \\
\delta S_{\mu\nu}^{(1)} &= \frac{2}{a_x^\mu b_y}\frac{(2\pi)^\mu}{(\mu-\nu)!} i^\nu \sum_{k=M+1}^{\infty}\sum_{\alpha\beta\in k} \frac{e^{i\nu\theta_{\alpha\beta}} h_{\alpha\beta}^{\mu-1}}{\cosh H_{\alpha\beta} - \cos X_{\alpha\beta}} \begin{cases} \cos X_{\alpha\beta} - e^{-H_{\alpha\beta}} & \nu = even \\ \sin X_{\alpha\beta} & \nu = odd \end{cases} \\
&\approx \frac{2}{a_x^\mu b_y}\frac{(2\pi)^\mu}{(\mu-\nu)!} \sum_{k=M+1}^{\infty}\sum_{\alpha\beta\in k} \frac{h_{\alpha\beta}^{\mu-1}}{e^{H_{\alpha\beta}} + e^{-H_{\alpha\beta}} - 2\cos X_{\alpha\beta}} \\
&\approx \frac{2}{a_x^\mu b_y}\frac{(2\pi)^\mu}{(\mu-\nu)!} \sum_{k=M+1}^{\infty}\sum_{\alpha\beta\in k} h_{\alpha\beta}^{\mu-1} e^{-H_{\alpha\beta}} \\
&\approx \frac{2}{a^{\mu+1}}\frac{(2\pi)^\mu}{(\mu-\nu)!} \sum_{k=M+1}^{\infty} 8k\cdot k^{\mu-1} e^{-2\pi k\frac{c_z}{a_x}} \\
&\approx \frac{2}{a^{\mu+1}}\frac{(2\pi)^\mu}{(\mu-\nu)!} 8(M+1)^\mu e^{-2\pi(M+1)\frac{c_z}{a_x}} \\
S_{\mu\nu}^{(1)} &\approx \sum_{\alpha\beta\gamma}{}' \left[\frac{4\pi}{(2\mu+1)}\frac{(\mu+\nu)!}{(\mu-\nu)!}\right]^{\frac{1}{2}} \frac{1}{\sqrt{4\pi}}\frac{1}{R_{\alpha\beta\gamma}^{\mu+1}} \\
&\approx \left[\frac{(\mu+\nu)!}{(2\mu+1)(\mu-\nu)!}\right]^{\frac{1}{2}} \sum_{k=1}^{\infty} 8k\frac{1}{(ka)^{\mu+1}} \\
&\approx \left[\frac{(\mu+\nu)!}{(2\mu+1)(\mu-\nu)!}\right]^{\frac{1}{2}} \frac{8}{a^{\mu+1}}\sum_{k=1}^{\infty}\frac{1}{k^\mu} \\
&\approx \left[\frac{(\mu+\nu)!}{(2\mu+1)(\mu-\nu)!}\right]^{\frac{1}{2}} \frac{8}{a^{\mu+1}} \\
\epsilon_M^{(\mu)} &= \frac{\delta S_{\mu\nu}^{(1)}}{S_{\mu\nu}^{(1)}} \\
&\approx 2(2\pi)^\mu \frac{(2\mu+1)^{\frac{1}{2}}}{\mu!}(M+1)^\mu e^{-2\pi(M+1)\frac{c_z}{a_x}}
\end{aligned}
$$

Appendix G

Short Range Energy and Forces

The expression used to calculate the short range energy is

$$E^{(sr)} = \frac{c^{(sr)}}{2} \sum_{i=0}^{N-1} \sum_{j=0}^{N-1} \sum_{\alpha\beta\gamma}{}' \sum_{k=1}^{t_{ij}} \frac{f_{ijk}}{\mid \vec{R}_{\alpha\beta\gamma} - \vec{r}_{ij} \mid^{n_{ijk}}}$$

In this expression, i and j refer to atomic species, $c^{(sr)}$ and f_{ijk} are constants, n_{ijk} is a positive integer and $\vec{r}_{ij} = \vec{r}_j - \vec{r}_i$. The prime on the lattice sum indicates exclusion of the self-energy terms. For calculation of the forces, $E^{(sr)}$ is written

$$\begin{aligned} E^{(sr)} &= \frac{c^{(sr)}}{2} \sum_{i=0}^{N-1} \sum_{\alpha\beta\gamma}{}' \sum_{k=1}^{t_{ii}} \frac{f_{iik}}{R_{\alpha\beta\gamma}^{n_{ijk}}} \\ &\quad + c^{(sr)} \sum_{i=0}^{N-1} \sum_{j=0}^{i-1} \sum_{\alpha\beta\gamma} \sum_{k=1}^{t_{ij}} \frac{f_{ijk}}{\mid \vec{R}_{\alpha\beta\gamma} - \vec{r}_{ij} \mid^{n_{ijk}}} \end{aligned}$$

The short range forces on the particles are

$$\begin{aligned} \vec{f}_i &= -\frac{\partial E^{(sr)}}{\partial \vec{r}_i} \\ &= c^{(sr)} \sum_{j \neq i} \sum_{\alpha\beta\gamma} (\vec{R}_{\alpha\beta\gamma} - \vec{r}_{ij}) \sum_{k=1}^{t_{ij}} \frac{n_{ijk} f_{ijk}}{\mid \vec{R}_{\alpha\beta\gamma} - \vec{r}_{ij} \mid^{n_{ijk}+2}} \end{aligned}$$

The 'virtual' forces are defined as

$$\begin{aligned} (f_h)_{\mu\nu} &= \left(-\frac{\partial E^{(sr)}}{\partial h} \right)_{\mu\nu} \\ &= -\frac{\partial E^{(sr)}}{\partial h_{\mu\nu}} \\ h &\equiv \begin{pmatrix} a_x & b_x & c_x \\ 0 & b_y & c_y \\ 0 & 0 & c_z \end{pmatrix} \end{aligned}$$

With these definitions,

$$f_h = c^{(sr)} \sum_{i=0}^{N-1} \sum_{j=0}^{i} (1 - \frac{1}{2}\delta_{ij}) \sum_{\alpha\beta\gamma}{}' (\vec{R}_{\alpha\beta\gamma} - \vec{r}_{ij}) \begin{pmatrix} \alpha \\ \beta \\ \gamma \end{pmatrix}^T \sum_{k=1}^{t_{ij}} \frac{n_{ijk} f_{ijk}}{| \vec{R}_{\alpha\beta\gamma} - \vec{r}_{ij} |^{n_{ijk}+2}}$$